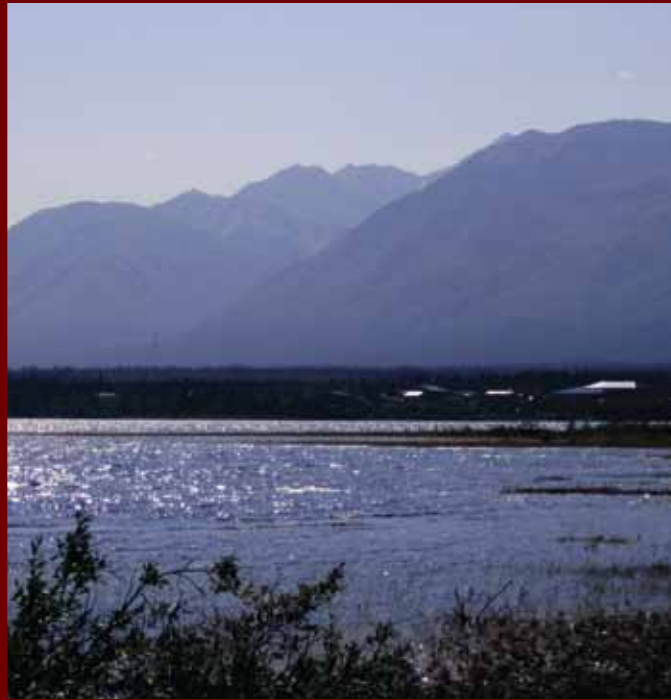


Community Adaptation Project



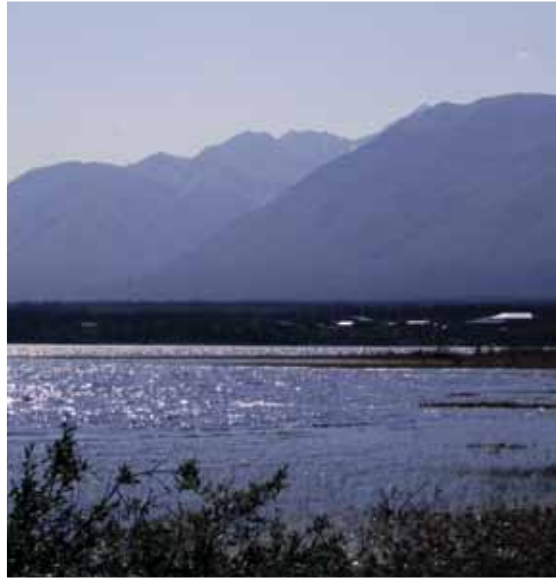
BURWASH LANDING AND DESTRUCTION BAY LANDSCAPE HAZARDS: GEOLOGICAL MAPPING FOR CLIMATE CHANGE ADAPTATION PLANNING

April 2013



Northern Climate Exchange
YUKON RESEARCH CENTRE • Yukon College

COMMUNITY ADAPTATION PROJECT



BURWASH LANDING AND DESTRUCTION BAY LANDSCAPE HAZARDS: GEOLOGICAL MAPPING FOR CLIMATE CHANGE ADAPTATION PLANNING

April 2013



Affaires autochtones et
Développement du Nord Canada

Aboriginal Affairs and
Northern Development Canada



Université 
de Montréal



uOttawa



Northern Climate ExChange
YUKON RESEARCH CENTRE • Yukon College

Printed in Whitehorse, Yukon, 2013 by Integraphics Ltd, 411D Strickland St.

This publication may be obtained from:

Northern Climate ExChange
c/o Yukon Research Centre, Yukon College
500 College Drive
PO Box 2799
Whitehorse, YT
Y1A 5K4

Supporting research documents that were not published with this report may also be obtained from the above address.

Recommended citation:

Northern Climate ExChange, 2013. Burwash Landing and Destruction Bay Landscape Hazards: Geological Mapping for Climate Change Adaptation Planning. Yukon Research Centre, Yukon College, 111 p. and 2 maps.

Production by Leyla Weston, Whitehorse, Yukon.

Front cover photograph: Burwash Landing, with Kluane Lake in the foreground and the Kluane Range in the background; view is looking southeast from Dalan campground. Photo courtesy of Northern Climate ExChange

FOREWORD

The Kluane First Nation is made up of strong and inspired people, who have lived in their Traditional Territory since time immemorial. Their Territory spans an area between the White River to the north, and the Slims River to the south; and from the St. Elias Mountains to the west, to the Ruby Ranges to the east. We have seen many changes on the land and in our community - from the establishment of the Alaska Highway, to the inception of the Kluane First Nation Government; all the while, we remain present with the land. Today, we are witnessing changes in our climate that are reflected on the land, and so we must take action to address the needs of our future generations.

Climate change poses a great threat to our community and our lifestyles. The Kluane area is a diverse and rugged geographic region. The land formations here are constantly changing and so we must plan for a dynamic landscape and a changing climate and learn to adapt in order to thrive and succeed into the future. The Yukon Research Centre, Yukon Geological Survey, University of Montreal, University of Ottawa, Laval University, and Kluane First Nation have joined together to develop a Landscape Hazards project which compiles geoscience data from various field studies, scientific reviews and traditional knowledge. The data collected by the project team identifies landscape hazards between the villages of Burwash Landing and Destruction Bay. This data was used to create a map of landscape hazards that delineate low, moderate, and high-risk areas in the Kluane region.

The Hazards Mapping Project has increased our understanding of how landscape characteristics may change in the Kluane area as regional climate conditions change. This information will be utilized in the adaptation planning process to provide the basis for evaluating how community infrastructure, security and well-being may be influenced and how the community might take action to respond.



Colin Wright

Environment Officer, Kluane First Nation



Lead Authors on the Report

Bronwyn Benkert	Northern Climate ExChange, Yukon Research Centre, Yukon College
Daniel Fortier	Université de Montréal
Kristen Kennedy	Yukon Geological Survey, Government of Yukon
Antoni Lewkowicz	University of Ottawa

Contributors

Philip Bonnaventure	Queen's University
Isabelle de Grandpré	Université de Montréal
Katerine Grandmont	Université de Montréal
Sarah Laxton	Yukon Geological Survey, Government of Yukon
Erin Light	Northern Climate ExChange, Yukon Research Centre, Yukon College
Michel Sliger	Université de Montréal
Graham Pope	Queen's University

Technical Advisors

Jeff Bond	Yukon Geological Survey, Government of Yukon
Guy Doré	Université Laval
Lacia Kinnear	Northern Climate ExChange, Yukon Research Centre, Yukon College
Colin Wright	Kluane First Nation

Technical Editing and Production

Leyla Weston, private consultant, Whitehorse

Acknowledgements

The project team would like to thank all the participants in this project for their enthusiasm and commitment. We would like to express our appreciation to the Yukon Geological Survey, Yukon Research Centre, Université de Montréal, University of Ottawa, Université Laval, Government of Yukon, and all those noted above for their support.

We would especially like to thank the communities of Burwash Landing and Destruction Bay, and Kluane First Nation, for supporting this project and welcoming us on their lands and within the Traditional Territory of Kluane First Nation. We appreciate the support and cooperation of Colin Wright (Kluane First Nation), and fruitful conversations with JP Pinaré (JP Pinaré Consulting) and Kai Peetoom (KP Environmental).

Thank you to the many field assistants involved in the project, including several of our contributing authors, as well as Louis-Philippe Roy, Manuel Versplat, Sabine Veuille, Chelsea Raley and Julia Quigley. We are especially grateful to Leyla Weston for technical editing and layout of this report, and to Samantha Darling for GIS contributions.

Funding for this project was provided by Aboriginal Affairs and Northern Development, Government of Canada. Project management was conducted by the Northern Climate ExChange, part of the Yukon Research Centre at Yukon College.

TABLE OF CONTENTS

INTRODUCTION	1
BURWASH LANDING AND DESTRUCTION BAY	1
Physiography	3
Vegetation	4
Contemporary Climate	4
Past Climate Trends	5
Hydrology	6
<i>Kluane Lake</i>	6
<i>Kaskawulsh Glacier</i>	7
<i>Slims River</i>	7
APPROACH AND METHODS	8
Surficial Geology	8
Permafrost	8
<i>Ground Penetrating Radar</i>	8
<i>Electrical Resistivity</i>	8
<i>Geotechnical Analysis of Permafrost</i>	10
Fire Disturbance Mapping.....	15
Hazards Classification.....	15
REGIONAL GEOLOGICAL AND PERMAFROST CONDITIONS	16
Surficial Geology	16
<i>Glacial History</i>	16
<i>Surficial Materials</i>	18
<i>Stratigraphy</i>	22
<i>Landslide Processes</i>	23
<i>Neotectonics</i>	25
Permafrost	25
<i>Regional Characteristics</i>	25
<i>Geotechnical Properties</i>	25
<i>Contemporary Permafrost Probability</i>	30
CASE STUDY INVESTIGATIONS	32
Burwash Landing Townsite.....	32
<i>Fire Break Location</i>	33
<i>Baseball Diamond Location</i>	35
<i>Empty Lot Location</i>	37
Copper Joe Subdivision	38
<i>Copper Joe Phase 1</i>	38
<i>Copper Joe Phase 2</i>	40

Kluane First Nation Wind Energy Project Site	42
Destruction Bay Townsite.....	46
PERMAFROST SENSITIVITY TO ENVIRONMENTAL CHANGE	48
Sensitivity of Local Permafrost Soil Types	49
<i>Organic Cover</i>	49
<i>Units 1 and 2</i>	49
<i>Unit 3</i>	49
Implications for Permafrost in the Study Area	50
Projected Climate Changes in the Study Area.....	52
Projected Climate Change Implications for Surficial Geology	52
Projected Climate Change Implications for Permafrost	53
HAZARDS CLASSIFICATION	57
GENERATING ACTION FROM SCIENCE	61
REFERENCES.....	63
APPENDIX A - BOREHOLE LOG DESCRIPTIONS	69
APPENDIX B - TEXTURE RESULTS FOR SURFICIAL DEPOSITS	77
APPENDIX C - GRAIN SIZE ANALYSIS OF PERMAFROST BOREHOLE SAMPLES	83
APPENDIX D - CLIMATE PROJECTIONS	85
APPENDIX E - HAZARDS MAP POLYGON DESCRIPTIONS	93
APPENDIX F - SAFE HOME CONSTRUCTION ON PERMAFROST	99

INTRODUCTION

Climate change is a significant challenge for northern communities, where the impacts of a warming climate are already having considerable effects (Huntington and Weller, 2005). Many people living in small, isolated communities in northern Yukon are concerned about climate-related risks in their regions. Because adverse impacts are a reality, it is important to implement measures to reduce or moderate the negative effects of climate change – in other words, to implement climate change adaptation strategies.

The development of adaptation strategies offers tangible ways in which the impacts of climate change can be reduced (Ford, 2008). Increasingly, programs aimed at identifying adaptation needs start with an assessment of vulnerability (Ford and Smit, 2004). Here, a community's climate-related vulnerability is a function of its exposure to risk, while its adaptive capacity refers to its ability to address, plan for, or adapt to risk. By developing a synthesis of current levels of vulnerability, a baseline from which to identify future adaptation approaches can be created, and a first step can be taken towards understanding the implications of climate change (Thomalla et al., 2006; Ford et al., 2008).

A useful tool in the assessment of landscape-scale vulnerability to climate change involves the development of hazard classification maps, which create simplified representations of biophysical vulnerability (Cutter, 1996). Hazards classification maps integrate science into decision-making processes by amalgamating and classifying geoscience data to create an easily interpretable ranked representation of current and future hazard potential. Such approaches have been used successfully in Yukon (NCE, 2011; Benkert et al., in prep) and Nunavik, Quebec (Grandmont et al., 2012), and serve as valuable tools for integrating scientific knowledge into the adaptation planning process.

This project investigates contemporary landscape hazards related to permafrost degradation in Burwash Landing and Destruction Bay, Yukon. It also considers potential impacts of a changing climate on the local landscape. The work is accomplished by conducting surficial geological mapping and gathering geoscience data, including landscape metrics, permafrost conditions and hydrology. Projections of future climate variability (e.g., temperature and precipitation) for the region are used to identify potential future trajectories of change. Based on these data, landscape hazards are ranked in four categories, varying from no risk to high risk, and are represented graphically (in stoplight colours) on maps covering the study area. By incorporating projections of future climate variability, landscape hazards classification reflects both contemporary and potential future conditions.

Landscape hazards maps are intended to be used as an adaptation planning tool, to assist with municipal planning activities aimed at addressing local concerns about permafrost thaw. It is important to note that this report is prepared as a guide, rather than as a document upon which to base planning decisions. It should not be used as a basis for development site selection, but rather treated as a tool for use in identifying areas that may require additional engineering or technical studies, should development be desired.

BURWASH LANDING AND DESTRUCTION BAY

Burwash Landing (61.35°N, 138.98°W) and Destruction Bay (61.25°N, 138.80°W) are both located on the Alaska Highway, at Historic Mileposts 1093 and 1083, respectively (Figure 1). Destruction Bay is 106 km north of Haines Junction, and Burwash Landing is 17 km north of Destruction Bay.

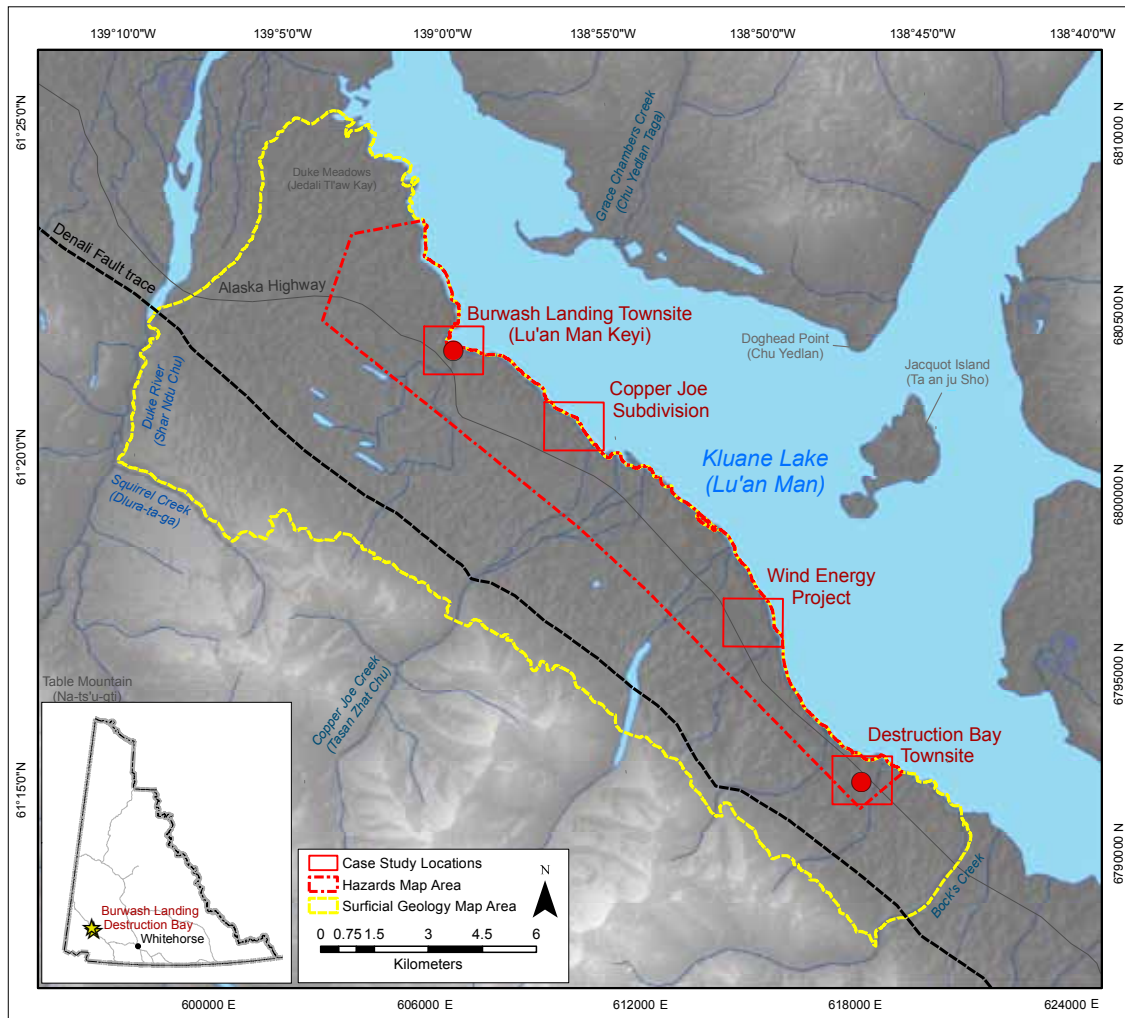


Figure 1. Location of study area, illustrating the surficial geology and hazards map footprints, and case study site locations.

Destruction Bay was established as an Alaska Highway construction camp and continues to serve as a local centre for government services, including highway maintenance, healthcare and education. Burwash Landing is located at the site of a traditional Southern Tutchone summer camp, where a trading post was later built by the Jacquot brothers in the early 1900s. Construction of the trading post prompted more formalized settlement of local First Nation people, leading to a permanent settlement. Burwash Landing celebrated its 100th anniversary in 2004, and acts as the administrative hub for Kluane First Nation.

Burwash Landing and Destruction Bay both fall within the Traditional Territory of Kluane First Nation. The majority of Kluane First Nation is made up of Southern Tutchone people who have occupied the region for generations. However, ancestral members of the First Nation also identify themselves as Tlingit, Upper Tanana and Northern Tutchone. Kluane First Nation signed Final and Self-Government agreements that came into effect in February 2004, establishing a governance structure through its Constitution. At that time, the First Nation had a membership of 206, and over half of the KFN citizens were living in other Yukon communities (Yukon Community Profiles, 2004).

As of June 2012, the total population of Burwash Landing was 97, while the total population of Destruction Bay was 51 (YBS, 2012). In Burwash Landing in 2006, 55 census survey respondents were identified as Aboriginal, while 10 from Destruction Bay were identified as such (YBS, 2008).

There were 41 occupied private dwellings in Burwash Landing in 2006, and 24 in Destruction Bay (YBS, 2007). The median value of a single detached house in Destruction Bay at that time was \$124,928 (comparable data for Burwash Landing is not available; YBS, 2009). In addition to administration buildings, Burwash Landing has a community centre, library, fire hall and daycare, while Destruction Bay hosts a volunteer library and emergency health services from its health centre.

Employment in both communities is composed in part of seasonal occupations, including commercial services aimed at tourism. In Destruction Bay, the Highways and Public Works maintenance camp offers year-round employment, as does the school and health centre. In Burwash Landing, the majority of employment is related to Kluane First Nation administration. Traditional subsistence economies are also important in the region, and provide a substantial portion of food resources for local residents.

PHYSIOGRAPHY

Burwash Landing and Destruction Bay are located on the northwest shore of Kluane Lake, near the lake's outlet, at ~807 and 823 m a.s.l., respectively. The surficial geology of the region reflects its physiographic setting, underlying bedrock geology, repeated cycles of glaciation during the Quaternary Period, and modern landscape processes actively modifying the landscape through fluvial, eolian and permafrost processes.

The study area is situated within a northwest-trending valley in a broad physiographic region known as the Shakwak Trench. The Shakwak Trench is a structurally controlled longitudinal valley and represents the surface expression of the Denali Fault, which runs from Haines, Alaska, to the south end of Kluane Lake, and on to eastern Alaska. The trench is oriented in a northwest direction and is ~65 km long, an average of 4 km wide, and up to 78 m deep (Rampton, 1981). It separates the tectonically active rugged Kluane Range to the west from the lower Ruby Range mountains and broad valleys east of the fault (Campbell and Dodds, 1982; Wahl et al., 1987). The Kluane Range, which form part of the St. Elias Mountains, rise steeply above the Shakwak Trench as a narrow band of glaciated peaks. Topographic relief in the Kluane Range is in excess of 1600 m and the mountain front to the west of the study area has an average slope of about 30-40 degrees. The west side of Kluane Lake is partly bordered by glacial drift from the Kluane Glaciation as well as colluvial and alluvial fans that were issued from the Kluane Range (Clague et al., 2006). Late Pleistocene drift comprises glaciolacustrine and glaciofluvial sediments that form beaches bordering parts of the lake. On the opposing valley side, the topography and relief of the western Yukon Plateau is much more subdued than that of the Kluane Range. Local relief rarely exceeds 1750 m a.s.l. and rock faces are rare except along Kluane Lake.

The Kluane Range is characterized by Late Paleozoic volcanic and sedimentary rocks, unconformably overlain by a thick sequence of Mesozoic volcanic rocks, carbonates and turbidites. These rocks were deformed in the Late Mesozoic into regional folds cut by northeast-verging thrust faults. Dextral strike-slip faulting along the Denali fault and associated structures, overprints earlier formed structures and coincided with late Paleogene terrestrial basin development. The whole region was uplifted during a recurrence of northeast-directed faulting and was accompanied by deposition of a thick sequence of Miocene to Pliocene volcanic and sedimentary rock. Deformation is ongoing resulting in numerous small-scale and rarer large-scale earthquakes along the Duke River and Denali fault systems (Cobbett, 2011).

The study area for this project includes the floor of the Shakwak Valley from the western shores of Kluane Lake, up a gently inclined pediment, to the mountain front of the Kluane Range. The southern limit of the study area is Bock’s Creek, while the northern boundary is located along the Duke River (see Figure 1).

VEGETATION

Burwash Landing and Destruction Bay are located in the Boreal Cordillera ecozone, on the western limit of the Ruby Ranges ecoregion (Smith et al., 2004). In areas of lower elevation within the study area, such as around communities, vegetation is dominated by northern boreal forest consisting of white spruce (*Picea glauca*), black spruce (*Picea mariana*), willow (*Salix sp.*), birch (*Betula papyrifera*), lodgepole pine (*Picea contorta*) and heath shrubs. As altitude increases, forests thin. In southwest parts of the Ruby Ranges ecoregion, there are pockets of grasslands as a result of low precipitation.

CONTEMPORARY CLIMATE

Burwash Landing and Destruction Bay are located in the Upper Yukon Stikine Basin climate zone (Wahl et al., 1987). This area typically has a continental climate and is characterized by long, cold winters and short, warm summers. High elevations in the region result in less extreme values of both maximum and minimum temperatures when compared to other Yukon climate zones. Based on 30-year (1971-2000) climate normal data collected from the Burwash Airport meteorological monitoring station (61°22’N, 139°03’W; Environment Canada, 2013), average January and July temperatures are -22.0°C and 12.8°C, respectively. A notable climatological feature of the Yukon Stikine Basin climate zone is low precipitation, which results from the rain shadow effect of the St. Elias-Coast Mountain barrier (Wahl et al., 1987). The most arid area in this climate zone is within the vicinity of Kluane Lake. At Burwash Airport, 30-year (1971-2000) average precipitation is 279.7 mm (Environment Canada, 2013). Of this, approximately one-third falls as snow during the winter season. Month-by-month climate normal temperature and precipitation data are summarized in Figure 2.

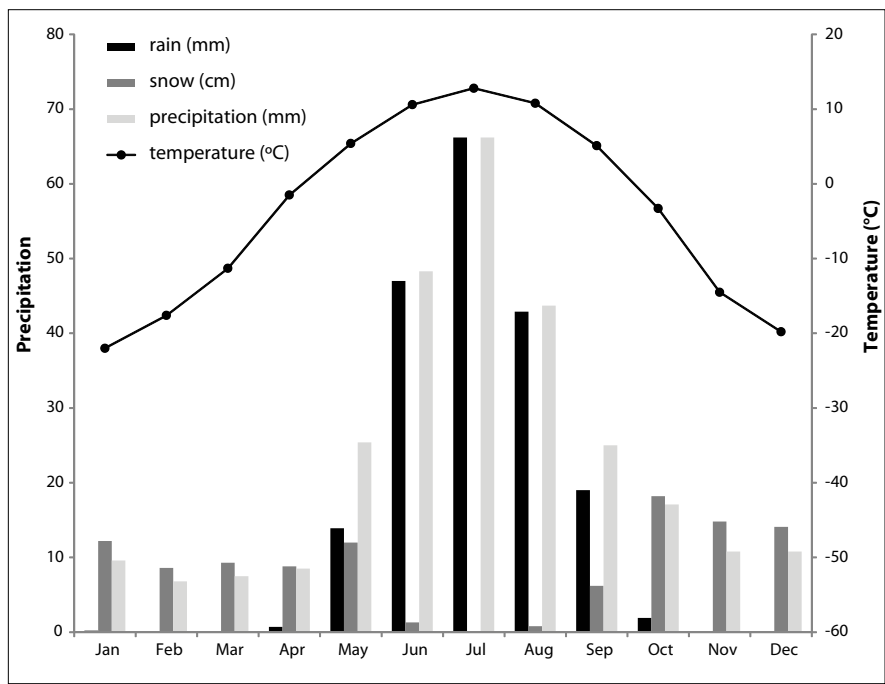


Figure 2. Climate normal (1961-1990) temperature and precipitation data for the Burwash Airport meteorological monitoring station (Environment Canada, 2013). To calculate total precipitation in millimetres, snowfall was converted to snow water equivalent (SWE) and summed with rainfall.

PAST CLIMATE TRENDS

To examine past climate trends, meteorological data from the Burwash Airport meteorological monitoring station was acquired from Environment Canada (2013). Temperature data is available for the period 1967-2010 (Figure 3), while precipitation data is available to 2007 (Figure 4). Linear regressions were superimposed on the data in order to assess trends over the period of record.

Increases in temperature are evident over the period of record summarized in Figure 3. The greatest increases in temperature are apparent in winter, while summer temperature increases are less pronounced. Trends in total annual precipitation in Burwash Landing are not apparent, based on the data presented here. However, Berg and Henry (2003) note decreases in total precipitation over the same period.

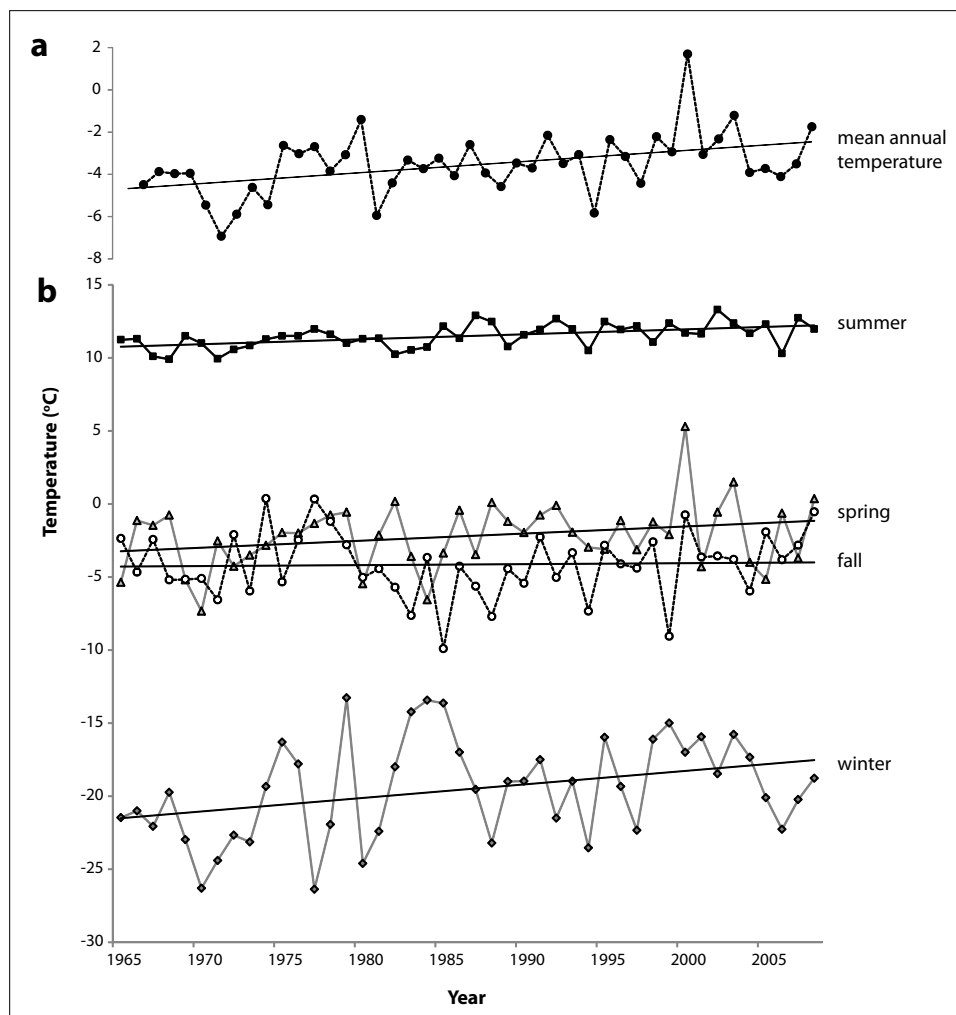


Figure 3. (a) Mean annual temperature (1967-2010) for the Burwash Landing Airport meteorological monitoring station, and (b) average temperatures for spring (MAM), summer (JJA), fall (SON) and winter (DJF; Environment Canada, 2013).

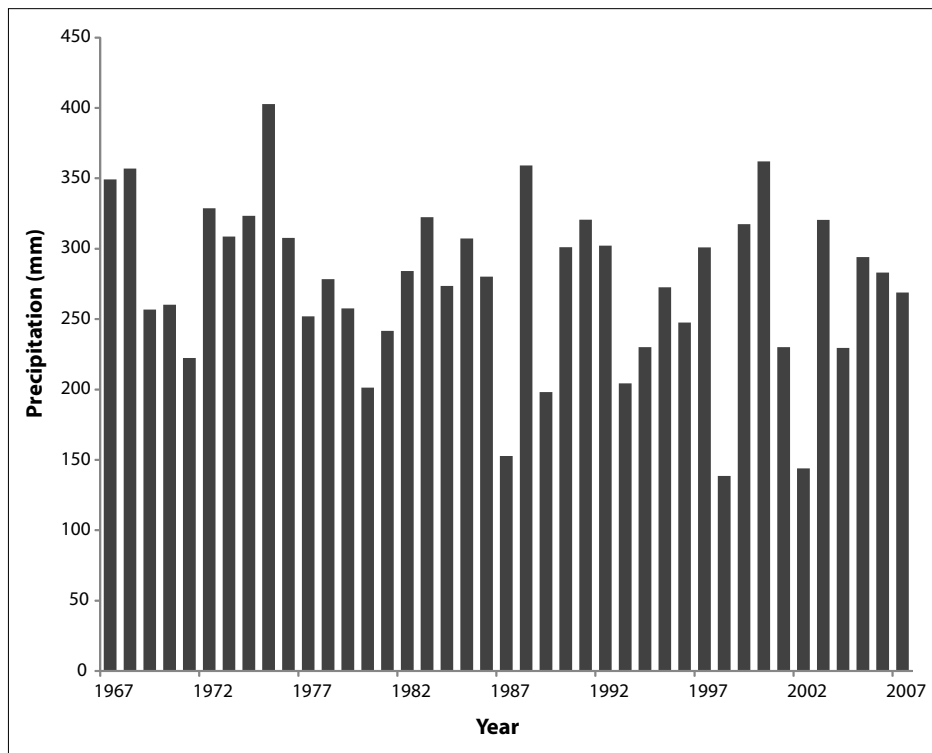


Figure 4. Total annual precipitation in Burwash Landing (1967-2007; Environment Canada, 2013). To calculate total precipitation in millimetres, snowfall was converted to snow water equivalent (SWE) and summed with rainfall.

HYDROLOGY

KLUANE LAKE

Burwash Landing and Destruction Bay are located on the floodplain of Kluane Lake, the longest lake in Yukon. Kluane Lake has a surface area of 409 km² and a maximum depth of ~78 m (Clague et al., 2006). The lake is fed predominantly by runoff from the Kaskawulsh Glacier via the Slims River, although it also receives runoff from many other small streams in its catchment, as well as contributions from direct precipitation, rainfall and snowmelt runoff, and groundwater (Brahney et al., 2010). Kluane Lake’s present-day outlet is at the head of Brook’s Arm, on the north end of the lake, via the Kluane River. The Kluane River ultimately feeds the Yukon River via discharge to the Donjek and White rivers. The Yukon River watershed covers 54% (~260 000 km²) of Yukon (Janowicz, 2008).

The western shore of Kluane Lake, which borders the study region (see Figure 1), is included in the Western Hydrologic Region. This region encompasses much of the St. Elias and Coast mountains and has the highest mean annual precipitation and temperature in Yukon. As a result, this region also has the highest amount of mean annual runoff and many of its streams are fed by glacial meltwater. Streamflow is characterized by an increase in discharge in spring resulting from snowmelt contributions, followed by peak flow in the mid-summer when glacial meltwater contributions are highest (Smith et al., 2004). Minimum annual discharge typically occurs in March when groundwater contributions are minimal. Flow may cease in winter in small streams relying heavily on groundwater contributions.

KASKAWULSH GLACIER

The isolated glaciers in the Kluane Range comprise cirque and small valley glaciers that are generally situated above 3000 m elevation, and are commonly debris covered. Periglacial features, such as solifluction lobes, patterned ground and rock glaciers are common. The Kaskawulsh Glacier is one of the largest valley glaciers in the St. Elias Mountain Range (Sawada and Johnson, 2000). It originates in the extensive icefields of the St. Elias Mountains and flows northeast ~70 km to the present terminus at 820 m a.s.l. Reports indicate that the Kaskawulsh Glacier has advanced and retreated several times throughout the Holocene (Borns and Goldthwait, 1966; Denton and Stuiver, 1966). Recent data presented by Foy et al. (2011) indicates that the terminus of the Kaskawulsh Glacier retreated by 655 m between 1956 and 2007. Over the last three to four decades, the Kaskawulsh Glacier has generally been decreasing in both area and volume, and thinning has occurred in the ablation zone and thickening in the accumulation zone.

For the last century, the terminus of the Kaskawulsh Glacier has been situated on the drainage divide between the Alsek and Yukon river systems (Reyes et al., 2006), and as such is the headwaters of both the Kaskawulsh and Slims rivers. The Kaskawulsh River flows into the Alsek River and out to the Gulf of Alaska, while the Slims River flows north ~20 km to Kluane Lake and ultimately the Bering Sea.

SLIMS RIVER

The drainage basin of the Slims River is 2456 km², and 55% of the basin is glacierized (Sawada and Johnson, 2000). Slims River water is supplied by both the Kaskawulsh Glacier and several tributaries (including Sheep, Bullion and Vulcan creeks). Variability in Slims River discharge is largely attributed to differences in the amount of meltwater released from the Kaskawulsh Glacier, as meltwater typically comprises ~70-90% of the river's discharge (Sawada and Johnson, 2000). However, meltwater contributions can vary markedly on time scales ranging from hours to years, depending on the terminal position of the Kaskawulsh Glacier and whether it is primarily discharging into the Slims or Kaskawulsh rivers. When most of the meltwater is channelled via the Slims River, peak discharges into Kluane Lake may exceed 3000 m³s⁻¹ (Sawada and Johnson, 2000).

Water level change over the past ~5000 years

Numerous studies indicate that Kluane Lake water levels have varied considerably over the past several centuries (e.g., Bostock, 1969; Rampton and Shearer, 1978; Clague et al., 2006) and millennia (e.g., Brahney et al., 2008a,b, 2010). Changes in Kluane Lake water levels over the past ~5000 years are generally attributed to the advance or retreat of the Kaskawulsh Glacier. Between ~5000 and ~1300 cal yrs BP, Kluane Lake water levels were persistently ~25 m lower than present and Kluane Lake drained in the opposite direction, through the Slims River basin. Between ~1800 and ~1000 cal yrs BP, Kluane Lake water levels were ~14 m below present levels as sediment outwash from the Kaskawulsh Glacier increased outflow blockage. Between ~500 and ~400 cal yrs BP, Kluane Lake water levels were ~12 m above present levels, because the Kaskawulsh Glacier advanced and blocked the southern outlet (Brahney et al., 2008a; Clague et al., 2006). Sustained high-water levels incised into the Duke River fan on the north end of the lake and eventually the present-day Kluane River outlet was created. Continued incision of the Duke River fan lowered Kluane Lake water levels ~200 cal yrs BP to a stage similar to that measured today.

APPROACH AND METHODS

SURFICIAL GEOLOGY

Surficial geological mapping was completed in the study area (outlined on Figure 1) at a scale of 1:20 000 during the summer of 2012. Previous mapping of surficial geology was completed by Rampton (1980a,b) at a scale of 1:100 000. The focus of new mapping was to provide more detailed units and descriptions of geology in and around the developed parts of the study area. Remote predictive mapping was completed using 1:40 000 and 1:20 000-scale digital monochrome aerial photographs with PurView Softcopy viewing software. Field checking of units was completed by documenting anthropogenic and natural exposures of surficial materials and by digging soil pits (~1 m depth) in a broad range of materials and landforms. New data incorporated in the surficial mapping includes textural information for 35 samples in various geological materials, geophysical profiles of the subsurface (using ground penetrating radar and Electrical Resistivity Tomography), shallow boreholes, and logging of natural and anthropogenic exposures.

PERMAFROST

GROUND PENETRATING RADAR

Ground-penetrating radar (GPR), a non-invasive method used to identify subsurface features such as stratigraphic boundaries, permafrost, and other anomalies, was used to gain a two dimensional image of subsurface features. A TerraSIRch Subsurface Interface Radar System 3000® with a shielded 200-MHz antenna (Geophysical Survey Systems, Inc.) was employed for the field investigation. Collection parameters for the SIR-3000 control unit were set to record at 40 scans per metre, with the dielectric constant set at 12. The GPR antenna was hand-towed along the survey line, and transects were situated adjacent to sections of the electrical resistivity tomographic profiles and boreholes. This enabled a correlation and comparison of results from each of the three techniques.

Post-collection data processing was conducted using RADAN™ (Version 7, GSSI) software and applied to all of the profiles. Processing of the GPR data included the following: correction of the initial pulse to time-zero to ensure that the first reflection is from the ground surface and the subsequent reflections are from deeper below the ground surface; FIR boxcar filter to remove background horizontal noise; and range gain adjustments to recover lower-amplitude waves from reflections deeper in the ground (Conyers, 2004). Overall, the processing procedures were employed to reduce signal attenuation with depth, as well as improve the continuity of stratigraphic reflections and the signal-to-noise ratio.

ELECTRICAL RESISTIVITY

Electrical Resistivity Tomography (ERT) profiling is a geophysical technique that measures variations in the ability of the ground to conduct electricity along a transect, producing a two-dimensional image of changes in electrical conductance. In permafrost areas, variations in conductance relate mainly to the occurrence of frozen and thawed ground, because water and ice serve as good and poor conductors of electricity, respectively.

ERT profiling has been used extensively to investigate mountain permafrost in Europe (e.g., Kneisel et al., 2000, 2008; Hauck et al., 2004; Hilbich et al., 2008, 2009) and is growing in importance in North America as a technique for permafrost investigations in both mountains and lowlands (e.g., Lewkowicz et al., 2011; Miceli, 2012). ERT is regarded as one of the best

methods to examine changes in frozen ground conditions over short distances, such as in the discontinuous permafrost around Burwash Landing and Destruction Bay.

Many ERT profiles show very clear differences relating to frozen ground conditions which can be correlated to surface changes in drainage, vegetation cover or land use (Lewkowicz et al., 2011). However, like all geophysical techniques, confidence in the interpretation increases where complementary information is available. The latter can include borehole logs, observations of natural exposures, ground temperature measurements, probing of the active layer or other geophysical techniques such as ground penetrating radar.

There is a major difference in the resistivity of water and ice, but there is not always a sharp line between the phase of water in soil pores (frozen or unfrozen) at temperatures above and below 0°C. Instead, percentages of unfrozen moisture gradually increase in the pores of frozen soils (especially in fine-grained soils such as silts and clays) as their temperatures approach 0°C. Consequently, the difference in the electrical resistivity of frozen and unfrozen soils can be gradational rather than sharp (Lewkowicz et al., 2011). In addition, because there can be differences in the porewater salinity and in the conductance of the soil minerals, it is not possible to identify a single threshold resistivity value below which soils are definitely unfrozen and above which soils are definitely unfrozen. However, values for sites in a given area are often quite stable.

The ERT profiling in this report was undertaken in September 2012 when the active layer (i.e., depth from ground surface to the top of perennial permafrost) was at its thickest. The equipment used was an ABEM Terrameter LS profiling system with the electrode array (stainless steel pins) inserted into the ground in a Wenner configuration. The electricity entering the ground builds up an image of its resistivity along a profile whose depth depends on the spread of the array of electrodes (25 m for an array 160 m in length and 8 m for a 40 m array). The penetration depth remains at 25 m, even if surveys longer than 160 m are created using a roll-along technique. Seven ERT profiles with a total length of 1120 m were completed.

Each ERT site was described in terms of vegetation and other salient features. UTM co-ordinates (relative to the WGS 84 datum) were taken using a hand-held Garmin Etrex Vista GPS. Relative variations in elevation along the individual profiles were measured in the field using an abney level and are expected to have accuracies of ± 1 m.

Resistivity profiles were topographically corrected using the abney level surveys. The actual elevations shown on the surveys are approximate. Measured resistivity data were processed with RES2DINV software (Loke and Barker, 1996) using a robust inversion that can respond to the rapid transitions and high contrasts in resistivity (Loke et al., 2003) that occur between frozen and unfrozen ground. A reversed colour scheme was used to portray the profiles so that blue represents high resistivities (generally indicative of frozen soils) and red represents low resistivities (ice-poor or unfrozen soils). All the resistivity profiles use the same scale to allow for inter-site comparison.

There is no single model that fits the observed resistivities. Instead the modelled results converge by iteration with the measured values. The choice of when to stop iteration in the RES2DINV software is made by the operator. Too few iterations lead to large Root Mean Square (RMS) errors (i.e., the model does not fit the measurements). Too many iterations can result in model 'over-fit' in which the broad patterns are lost. In the present analyses, the 4th iteration was the final one as RMS errors were all very low (less than 5%) by that point. The profiles are presented with a linear depth scale and no vertical exaggeration. ERT profiles were interpreted based on the results of frost probing along the profiles, field descriptions of vegetation,

boreholes and laboratory analyses undertaken by the team from Université de Montréal, and surficial mapping.

GEOTECHNICAL ANALYSIS OF PERMAFROST

Permafrost drilling and sample collection

Permafrost cores were extracted from boreholes during a drill program in September 2012. To ensure maximum success in a variety of subsurface conditions, four different instruments were used for the drill program: two sampling drills (Winkie drill and CD06 Honda drill), one auger drill, and one hand auger.

The Winkie drill is a gas-powered drill with a two-speed transmission made for bedrock drilling. The drill has been modified for permafrost drilling conditions using a gearbox that lowers the speed to ~60 rpm for unconsolidated material. Water can be injected during drilling with a water pump and pipes can be fixed on the drill support. It is one of the lightest shift drills on the market with a potential to go down to 30 m in silty sands (Figure 5). The Winkie drill was used with aluminum rods (0.9 and 1.5 m long; Figure 6) and core barrels 10.8 cm in diameter (Figure 7). When the drill reached a gravel layer the resistance on the core barrel became too high, and a core barrel 8.3 cm in diameter was substituted. Some frozen samples were thawed by friction during the drilling process.



Figure 5. Photograph of the Winkie drill, used for permafrost coring.



Figure 6. Photograph of aluminum rods used with the Winkie drill for permafrost coring.



Figure 7. Photograph of core barrels used with the Winkie drill for permafrost coring.

The CD06 Honda (Figure 8) is a light hand drill (~8 kg, 40 rpm) that can be controlled by one or two people, and is therefore easy to move and easy to use. As with the Winkie drill, this drill was not able to penetrate thick layers of gravel. The rods used for drilling were the same as for the Winkie drill, described above. The CD06 can reach about 1 m with a barrel of 10.8 cm in diameter, 2 m with an 8.3 cm-diameter barrel, and 3 m with a 7.0 cm-diameter barrel. All core barrel sizes were used during the drill program.

The auger drill is equipped with a Honda GXV160 (144 rpm) motor and flight auger extensions with diameters of 5-46 cm (Figure 9). This drill is destructive and is used to pass through the active layer allowing for bulk 'grab' sampling, especially in gravelly soils.



Figure 8. Photograph of the CD06 Honda drill, used for permafrost coring.



Figure 9. Photograph of the auger drill, used for permafrost coring.

The hand auger is used to sample the active layer. It has a 10.2 cm diameter sampling core barrel and three 1 m long extension rods (Figure 10). It is a simple, low-cost solution for sampling fine-grained unfrozen soil (e.g., clay, silt, sand and fine gravel containing pebbles with a maximum diameter of 25 mm).

Using a combination of these drills, one or two boreholes were drilled along ERT profiles in representative areas (e.g., FireSmart zones, deforested areas, firebreak zones, and forests). At each borehole, the site was first described (e.g., environment, vegetation type and density, topography), photos were taken, and locations were



Figure 10. Photograph of the hand auger, used for permafrost coring.

recorded using a handheld GPS. The boreholes were initiated using a hand auger if the ground was soft or an auger drill if the ground was gravelly. As soon as the permafrost table was reached, when drilling became too hard, or when boreholes became too deep, the CD06 Honda drill was used. For specific locations where maximum depth was desired, the Winkie Drill was used.

A sample of every unfrozen layer was collected from each borehole. Each sample was photographed and described *in situ* (e.g., soil type, saturated or unsaturated, presence or absence of organic matter, any particularities). The sample was identified with the borehole name and depth and put in doubled hermetic Ziploc bags for laboratory analyses. Frozen samples were also collected and described in the field (Figure 11). Each core was cleaned to remove drilling mud and photographed.



Figure 11. Photograph of the setup used for *in-field* core descriptions.

Permafrost sample analysis

Laboratory analyses were carried out to quantify geotechnical properties of permafrost samples and some active layer samples, and to evaluate the mechanical behavior of the permafrost upon thawing. Both soil grain characteristics and ice characteristics were evaluated. To evaluate soil grain characteristics, the specific values for grain size, specific gravity, remolded bulk density and porosity were measured for every sample. Additionally, plasticity index and hydraulic and thermal conductivities were measured for representative samples. To evaluate ice characteristics in samples where ice is present, the cryostructure, gravimetric ice content, volumetric ice content and settlement potential were quantified. Each analysis method is described below.

Grain-size analysis

Sieve and hydrometer analysis of grain size were performed following a specifically modified American Standard and Testing Method protocol (ASTM D422-63, 2000). The sieves typically used were 75, 12.5, 4.75, 2, 1, 0.5, 0.25, 0.125, 0.09 and 0.063 mm. A hydrometer test was performed on a 40 g subsample passing through 0.25 mm openings; after sedimentation started, readings were taken after 0.25, 0.50, 0.75, 1, 1.5, 2, 5, 15, 30, 60, 120, 180, 300 and 1440 minutes. Statistics were generated by *Gradistat* software.

Specific gravity

Specific gravity (the ratio of a solid’s grain density to the density of water) was systematically measured for every sample collected following the American Standard and Testing Method (ASTM D854-10, 2000). The results were used to compute the porosity of the soil.

Bulk density

Bulk density and voids in aggregate (ρ_b ; the ratio of dried soil’s mass, including its porosity, to its volume (g/cm³)), was performed following American Standard and Testing Method protocol (ASTM C29 – 09, 2000). Values were generated by weighing a 45 cm³ beaker completely filled with sediment and subtracting the empty beaker weight. The sediment weight was then divided by the beaker volume using

$$\rho_b = \frac{(M_{S+B} - M_B)}{V_B} \quad [1]$$

where M_{S+B} is the weight of the beaker full of compacted sediment, M_B is the weight of the empty beaker, and V_B is the beaker’s internal volume.

Compaction of the sediment in the beaker was ensured by adding a 1 cm-thick soil layer to the top of the beaker and patting it down. Results were used to compute the porosity of the soil. It is important to note that the density measured is only an approximation, and that the density of gravelly soils may be under-estimated because the small volume of the beaker excluded measurement of the coarsest fractions.

Porosity

Porosity (n ; the ratio of void space in the bulk volume of the material) was calculated using

$$n = 1 - \frac{\rho_b}{\rho_s} \quad [2]$$

where ρ_b is bulk density in kg/m³, and $\rho_s = G_s \cdot \rho_w$, where G_s is specific gravity (a dimensionless quantity). Results were used to determine the water/ice content of the soil when saturated and the presence of water/ice in excess of the porosity. The porosity of gravelly soils may be over-estimated due to volume-related uncertainty in bulk density data.

Cryostructure

Cryostructure (the form taken by ice when present in a soil) depends on water availability, a soil’s segregation potential, and the time of freezing, resulting in the development of ice bodies in the soil matrix. Information such as soil genesis, climate conditions at the time of freezing, and ground vulnerability when permafrost degrades can be interpreted from cryostructure and cryofacies analysis.

Because field descriptions are based only on a visual interpretation of the core, the samples were described a second time more thoroughly in the laboratory using a standard terminology (Stephani et al., 2010; Murton and French, 1994). Frozen core samples were warmed to near 0°C and any refrozen mud was scrapped off prior to the description.

Gravimetric ice content

Ice content was calculated using

$$u_i = \frac{(M_i)}{(M_s)} \quad [3]$$

where M_i is ice weight (measured as weight loss after drying (g)) and M_s is soil dry weight (g). Results are expressed as percentages (dimensionless).

Volumetric ice content

The volumetric ice content (θ_i ; the ratio of ice volume to total volume) is calculated using

$$\theta_i = \frac{V_i}{V_T} \quad OR \quad \theta_i = \frac{\left(\frac{M_i}{\rho_i}\right)}{\left(\frac{M_s}{G_s}\right) + \left(\frac{M_i}{\rho_i}\right)} \quad [4]$$

where M_i is ice weight, M_s is oven-dry soil weight, ρ_i is ice density and G_s is specific gravity. The volumetric ice content is expressed as percentages (fundamentally meaning cm^3/cm^3). Direct volume measurements proved to be too inaccurate.

Settlement potential

The thaw settlement potential (SP ; the volume of ice unable to fit into the soil's porosity) is calculated using

$$SP = \frac{V_T - V_s}{V_T} \quad OR \quad SP = \frac{\left(\frac{M_i}{\rho_w \cdot G_s}\right) + \left(\frac{M_i}{\rho_i}\right) - \left(\frac{M_i}{\rho_i}\right)}{\left(\frac{M_s}{\rho_w \cdot G_s}\right) + \left(\frac{M_i}{\rho_i}\right)} \quad [5]$$

where the settlement potential (SP) equals the volume of the frozen core (V_T) minus the volume of the unfrozen core (dry soil weight (M_s) divided by bulk density (ρ_s) divided by the volume of the frozen core (V_T). The settlement potential is given as a percentage of volume loss (fundamentally cm^3/cm^3).

Thermal conductivity

Thermal conductivity (a soil's ability to conduct heat) was measured following the American Standard and Testing Method (ASTM D5334-08, 2000). The measurements were obtained using a heated needle probe (Hukseflux model TP-02) connected to a CR1000 Campbell Scientific data logger.

A representative sample from each major soil type identified in the field (e.g., diamicton, uniform fine sandy silt, graded sand, etc.) was selected. The measurement was repeated on dry soil, drained unsaturated (humid) soil, and saturated soil for each sample type.

Hydraulic conductivity

The hydraulic conductivity (k_s ; a soil's ability to transmit water when submitted to a hydraulic gradient) was calculated following Darcy's law (Darcy, 1856), using a falling head permeameter,

$$k_s = \frac{L}{\Delta t} \frac{a}{A} \ln \frac{h_1}{h_2} \quad [6]$$

where L is the sample length, Δt is the amount of time between beginning and end of flow, a is the diameter of the burette upstream the test tube, A is the test tube diameter, and h_1 and h_2 are the water head before and after flow through the test tube, respectively.

Plastic index

The plastic index (PI ; the range of water content where the soil has a plastic behavior) was measured according to the American Standard and Testing method (ASTM D4318-00, 2000) using

$$PI = LL - PL \quad [7]$$

where LL is the liquid limit and PL is the plastic limit.

Borehole logs

After completion of field and laboratory research activities, a log for each permafrost borehole was created using the *Rockware Log Plot* software. Borehole logs include GPS coordinates, a description of the surrounding environment, the stratigraphy of the sediment, the depth to the water and permafrost tables, the ice structure, the grain size ratio, the specific gravity, the bulk density, the porosity, the volumetric ice content, and the settlement potential (see Appendix A for all borehole log descriptions and data).

FIRE DISTURBANCE MAPPING

The extent of a large forest fire, which occurred over a decade ago, was mapped to account for the considerable disturbance of forest fires in the Burwash Landing and Destruction Bay areas. Using Bing Maps aerial images (dating *ca.* 2010) in the ArcGIS ArcMap interface, the extent of the fire-burned area in study site was delineated by zones of very low vegetation cover, areas covered with fireweed, and dead tree trunks standing or lying on the ground. In order to verify the accuracy of this fire disturbance mapping technique, a comparison was made with a map produced by Geomatics Yukon (2011), which identified large fires that burned in Yukon between 1946 and present day. It is important to note that the area was determined at a landscape, rather than site-specific scale, and therefore contains some patches of denser vegetation and hydrological features.

HAZARDS CLASSIFICATION

Landscape-scale hazard classifications were assigned to polygons in a 45 km² subset of the surficial geology map footprint (see Figure 1) by considering the combined properties of surficial geology, hydrology and permafrost.

The qualitative approach used to produce the hazards classification map consisted of identifying and compiling the key contemporary and potential future geological, permafrost and hydrology-related hazards presenting a risk for future development. Geology-related hazards were evaluated by considering the components and processes shaping the landscape, including landforms, surficial geology, ground properties, and drainage conditions. Various active geological processes were considered at both the landscape and local scales, including erosion,

flooding and water table levels, because these processes can contribute to regional instability. Hydrology-related hazards (e.g., areas of shallow groundwater, potential for flooding and surface ponding) were noted during geology and permafrost-related fieldwork activities. Permafrost-related hazards were assessed by a thorough evaluation of the nature of the geological units and the geotechnical properties of the permafrost core samples. The extent of fire disturbance was also considered. These elements were evaluated in the context of projected changes in climate conditions expected for the coming decades.

Based on the analyses described above, polygons in the hazard map area (outlined on Figure 1) were classified into one of four categories by the authors based on local conditions and the identified processes acting on each unit. Classification categories were coded green, yellow, orange and red, representing increasing levels of hazard severity, respectively. (More details about each classification category are included in *Hazards classification*, below.) The compilation of the hazards classification analyses result in a comprehensive map of the study area ranking landscape hazards, in the context of projected climate change for the region.

REGIONAL GEOLOGICAL AND PERMAFROST CONDITIONS

SURFICIAL GEOLOGY

GLACIAL HISTORY

Several periods of glaciation occurred in the region during the Quaternary Period (*ca.* 2 Ma-10 ka BP), the latest being the Wisconsin Kluane Glaciation (*ca.* 22 ka BP; Denton and Stuiver, 1967). While early and middle Pleistocene glacial and interglacial periods are believed to be preserved in some sediment records in the region (Rampton, 1981), only evidence of the most recent Kluane Glaciation is well-preserved in the study area. Ice flow during the Kluane Glaciation was generally out of ice centres in higher mountainous areas, such as the St. Elias, Coast, and Cassiar mountains, and along major structural trenches and valleys.

During the Kluane Glaciation, ice flowed out of the valleys of the St. Elias Mountains and extended northwest along the Shakwak Trench and into the Ruby Range (Figure 12; Duk-Rodkin, 1999; Rampton, 1980a,b,c,d,e; Rampton and Paradis, 1981a,b). Most of the uplands in the Ruby Range remained ice-free during this glaciation, although glacial features in the southern portion of the range suggest it did support cirque glaciers and local ice caps.

During the waning stages of the Kluane Glaciation, valley glaciers may have been out of synch with glaciers in main tributary valleys, impounding lakes and forming large glaciofluvial complexes in alpine valleys. Major glacial lakes likely also formed within the Shakwak Trench (Rampton, 1981), although little evidence of their existence is preserved.

The onset of the post-glacial period in the map area was marked by widespread landslide activity and loess deposition. Glacially over-steepened slopes and abundant glacial material deposited along valley sides could be readily mobilized into the valley bottom where sparse vegetation cover and local katabatic winds would have created favourable conditions for loess deposition.

Neoglacial advances have occurred numerous times in the past ~2800 years in the Kluane Icefields. The most recent Neoglacial advance likely took place ~450 years ago and was responsible for an advance of the Kaskawulsh Glacier that led to a high stand of Kluane Lake (Rampton, 1981). Repeated variations in the level of Kluane Lake throughout the Neoglacial period have been attributed to changes in base level in the Slims and Kaskawulsh valleys (Bostock, 1969; Clague, 1981).

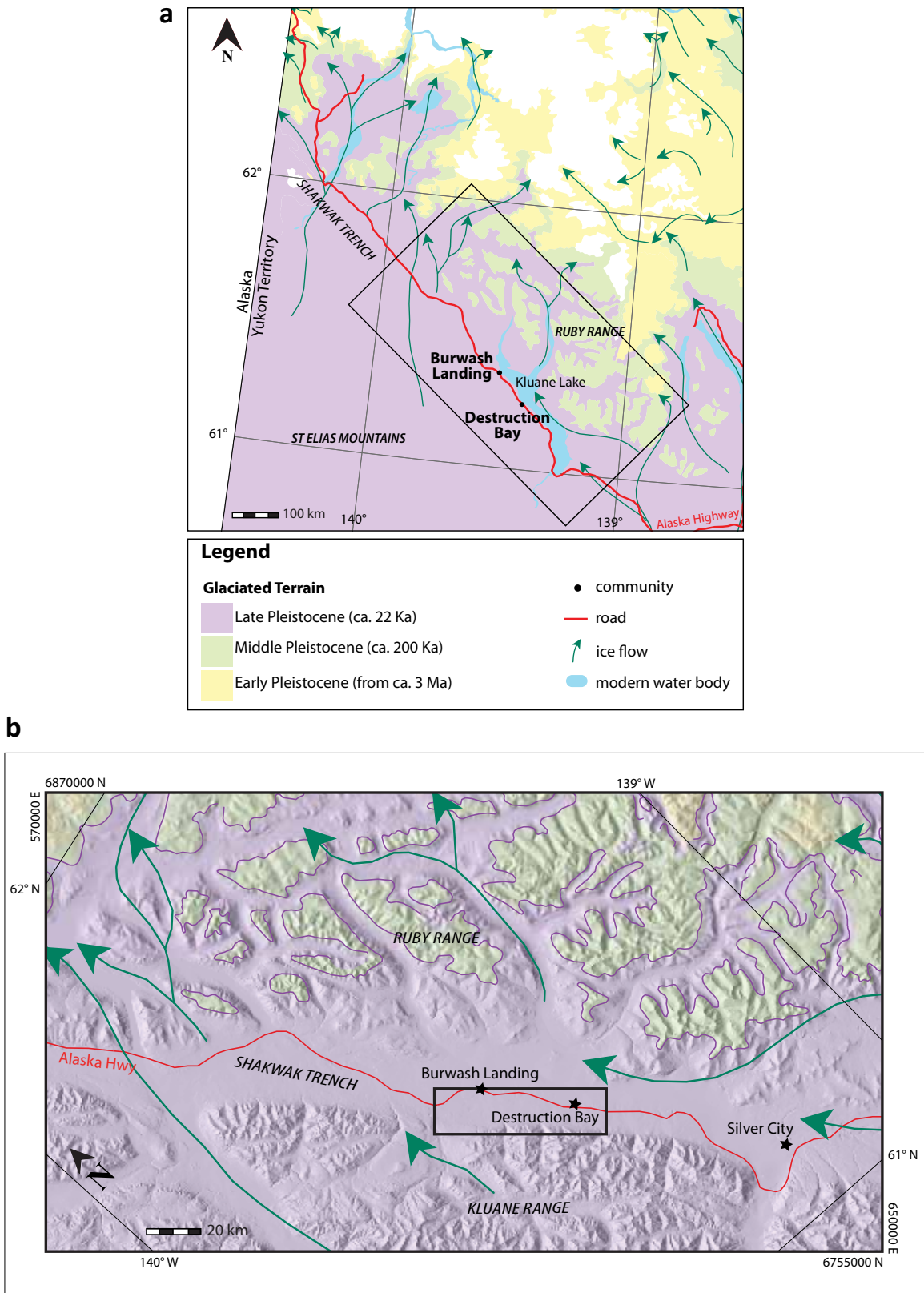


Figure 12. (a) Maximum ice extent in the Shakwak Trench and Ruby Range during the late-Wisconsin Kluane Glaciation (arrows denote ice-flow direction; limits from Duk-Rodkin, 1999). (b) Ice-flow direction in the study area.

SURFICIAL MATERIALS

The Shakwak Valley comprises a gently undulating and glacially fluted floor underlain by thick deposits of till, lacustrine silts and outwash from a number of glaciations, as well as Holocene alluvium and loess (Denton and Stuiver, 1967; Rampton, 1969; Rampton, 1980a,b,c,d,e; Rampton and Paradis, 1981a,b). Along the base of the mountain front of the Kluane and Ruby ranges, colluvial aprons and fans grade into broad alluvial fans and aprons.

Surficial materials in the study area are derived from glacial, fluvial, lacustrine, colluvial, eolian and organic processes. Each process, or combination of processes, forms distinct materials that can be characterized based on the grain size, sorting, structure, and general distribution of the material. Detailed descriptions of the surficial materials found in the study area are located in the map legend (see accompanying map “*Surficial Geology of Burwash Landing and Destruction Bay*”; Kennedy, 2013). Common materials in the study area are those derived from glacial, colluvial, eolian and modern fluvial processes.

Moraine deposits include materials that have been deposited directly by a glacier or ice sheet without modification by any other agent of transportation. Moraine deposits in the study area are characterized by poorly sorted, compacted material lacking stratification and containing a heterogeneous mixture of particle sizes, usually in a matrix of sand, silt and clay (Figure 13). Textures of morainal materials tend to be well-distributed (Figure 14) across particle sizes ranging from gravel to silt and clay. (Results from textural analyses are included in Appendix B.) Moraine deposits are found throughout the map area in a range of deposit types including ridged moraine blankets and loosely consolidated ablation moraine. Moraine deposits occur at surface along the mountain front and on the valley bottom where alluvial deposits are thin. Moraine deposits are also likely present at deeper stratigraphic levels in valley-bottom settings where they are overlain or interbedded with glaciofluvial and non-glacial sediments. Morainal deposits are commonly affected by permafrost in the map area and some moraine deposits may be ice-rich.



Figure 13. Moraine deposits in the study area are commonly poorly sorted, highly compacted material, lacking stratification and containing a heterogeneous mixture of particle sizes.

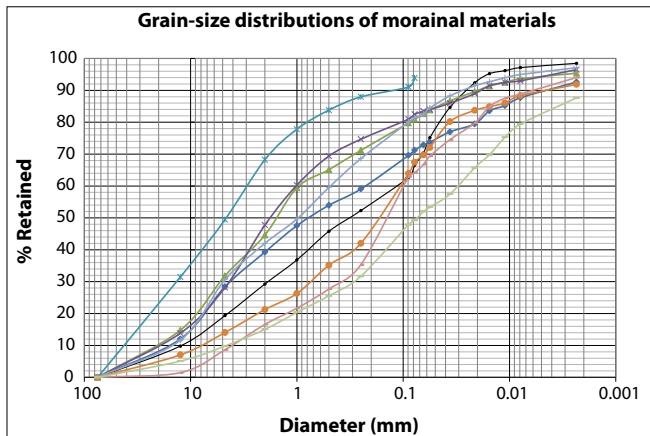


Figure 14. The grain-size distribution of nine samples of morainal material from across the study area. Textures of morainal materials commonly include all grain sizes from silt and clay to cobbles and boulders, and are generally well-distributed across this range.

Moraine deposits in the map area can occur adjacent to, or in a continuum with, glaciofluvial materials deposited at or near a former ice-front. Glaciofluvial deposits include materials that have been deposited by glacial meltwater either directly in front of, or in contact with, glacier ice. Ice-contact glaciofluvial and ice-front moraine deposits have similar characteristic in that they are typically comprised of non-sorted and non-bedded gravel made up of a wide range of particle sizes (see Appendix B), associated with very rapid aggregation at the ice front. Glaciofluvial materials deposited in the ice-marginal environment typically form kettled and hummocky plain surfaces, but are also present as ridged and undulating landforms.

Glaciofluvial materials may contain a smaller fraction of silt and clay-sized particles than morainal materials (Figure 15), but infrequently lack silt and clay fractions to the same degree as non-glacial fluvial materials. Glaciofluvial materials deposited in environments more distal to the former ice-front are typically comprised of moderately to well-sorted, stratified gravel. These deposits are rare in the study area. Glaciofluvial materials may be affected by permafrost but in most cases are ice-poor.

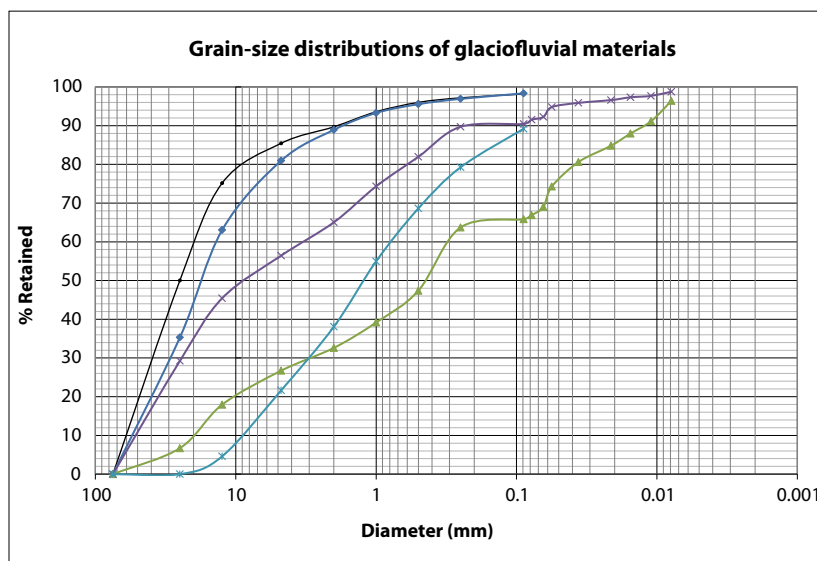


Figure 15. The grain-size distribution of five samples of glaciofluvial material from across the study area. Textures of glaciofluvial material can be variable depending on their proximity to the former ice front, but generally comprise smaller grain-size distributions than morainal materials and contain more silt and sand than fluvial deposits.

Eolian and modern fluvial deposits are the youngest and frequently highest stratigraphic units in the map area. Fluvial deposits are materials that have been transported and deposited by streams and rivers. Fluvial sediments mapped in the study area are predominantly those associated with floodplains, fluvial terraces and channels of the streams draining the Kluane Range (Figure 16). These deposits generally consist of stratified beds of gravel and/or sand with sand and/or silt and/or organic materials (and rarely clay). Gravel deposits contain clasts that are typically rounded and a sandy matrix. Fluvial materials have a characteristic grain-size distribution (Figure 17; Appendix B) defined by the similar stream energy of drainages in the map area. Fine-grained lenses and beds in these fluvial deposits may contain ice, although it may be discontinuous over relatively small areas.

Alluvial fan complexes, located at the break in slope between the steep Kluane Range and the Shawkak valley below (Figure 18), compose the dominant feature on the modern landscape. The fans were largely constructed during, and shortly after, deglaciation and have only been modified to a minor degree in the past 1200 years (Koch et al., *in press*). Modern processes on most of these fans are limited to channel migration (avulsion of new channels and abandonment of old channels) across the fan surfaces (Figure 19).



Figure 16. An example of fluvial sediments deposited by a high-energy stream (the Duke River) draining the Kluane Range.

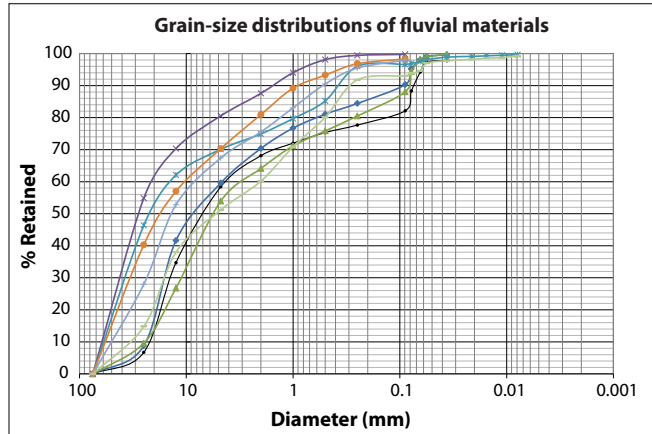


Figure 17. The grain-size distribution of eight samples of fluvial material from across the study area. Textures of fluvial materials are commonly uniform and have abundant sand and gravel, and relatively little silt and clay.

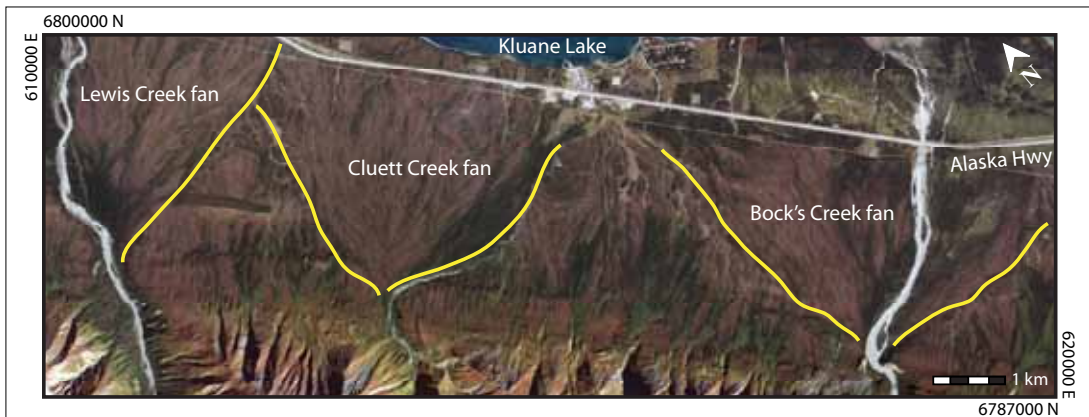


Figure 18. Alluvial fan complexes, located at the break in slope between the Kluane Range and the Shawkak valley, were largely constructed at the end of the last glacial period. Yellow lines on the satellite image outline three prominent fans in the southern part of the study area. Destruction Bay is in the centre top of the figure.



Figure 19. An example of channel migration; note the abandoned channel in the middle ground of the image and the newly incised channel in the foreground.

Eolian deposits include materials transported and deposited by wind. These deposits generally consist of medium to fine sand and coarse silt (Figure 20) that is well-sorted, non-compacted, and may contain internal structures such as cross-bedding (Figure 21) or ripple laminae, or may be massive (Figure 22). Much of the map area is covered with a veneer of wind-deposited silt and fine sand, with less extensive areas of thick eolian deposits. Active landforms such as fluvial channels or colluvial fans are unlikely to have noticeable accumulations of eolian deposits. Modern (active) eolian deposition is limited to isolated deposits of sand and silt along the shores of Kluane Lake (Figure 23). Inactive, silt-rich eolian deposits are commonly affected by permafrost and may be ice-rich.

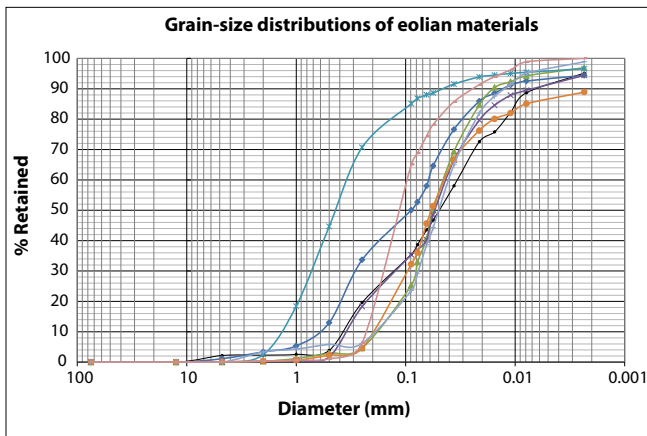


Figure 20. The grain-size distribution of eight samples of eolian material from across the study area. Eolian materials are comprised primarily of silt and sand and minor clay and gravel.



Figure 21. Sandy eolian dune deposits, near the shore of Kluane Lake, contain cross-bedding structures defined by light-coloured tephra deposits.



Figure 22. Massive loess deposits exposed above an exposure of glaciofluvial gravel in the study area.



Figure 23. An example of active cliff-top loess deposition on a high bluff near the shore of Kluane Lake.

Deposition of eolian silt and sand was at its peak during, and immediately following, deglaciation of the study area ~10-12 000 years ago (Denton and Stuvier, 1967). However, it is likely that some of these deposits were reactivated and remobilized briefly following the deposition of the White River tephra (volcanic ash) ~1200 years ago. There is at least one example in the study area of eolian sediments that were active following deposition of the White River tephra, but are inactive today (Figures 21 and 24). In more stable locations, the White River tephra is preserved as a 1-2 cm layer above, and commonly mixed with, eolian deposits (Figure 25).



Figure 24. Sandy dunes formed after the deposition of the White River tephra (white layers are tephra and dark layers are sand).



Figure 25. White River tephra preserved immediately below organic soils and above massive silty loess deposits in the study area.

STRATIGRAPHY

The vertical layering of sediments can be a strong control on landscape stability. Simplified stratigraphy of the Shakwak Trench in the map area is presented in Figure 26. The study area does not contain thick exposures of surface sediments, and no well logs were obtained to characterize the below-surface stratigraphy of unconsolidated sediments in the valley bottom. Thicknesses presented in Figure 26 are hypothetical and actual stratigraphy is certainly more complicated than what is depicted in this figure.

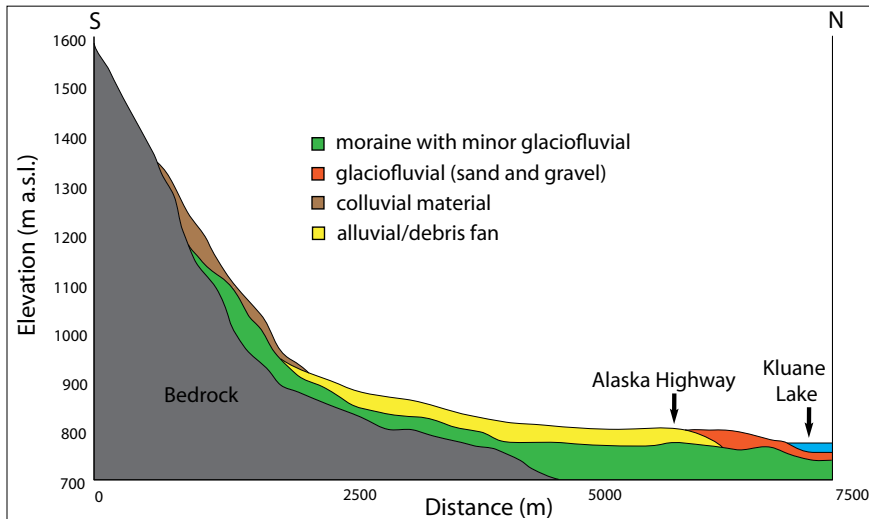


Figure 26. Simplified stratigraphy of the Shakwak Trench in a cross-valley profile looking east toward the Alaska/ Yukon border. Valley-bottom thicknesses of all units are hypothetical.

LANDSLIDE PROCESSES

In a study of landslide processes along the Yukon part of the Alaska Highway Corridor (Huscroft et al., 2004), the Shakwak Trench area was shown to have more landslides than any other region studied. In particular, the rugged slopes, high relief, and intensely faulted and folded rock formations of the Kluane Range are subject to intense landslide activity. Landslide processes are significantly less common downslope in the main Shakwak Valley where the study area is located.

Rock, ice and snow flows/avalanches can be seen in the headwaters of Nines Creek, just south of the map area. These landslides have the potential for very long run-outs (nearly 1 km in the case of Nines Creek) over shallow slopes. Large failures of snow and debris with long run-out distances have not been identified as a potential hazard in the study area but may have implications for hazard analysis and risk if current snow regimes were to change in the future.

Rock slumps and rock fall events do not prove to be a direct threat in the study area; however, they do have the potential to dam creeks that drain into the study area. Breaching and rapid incision of such dams could cause flooding. The probability and magnitude of such events has not been studied for this region, but events could be seismically triggered (Huscroft et al., 2004).

Retrogressive thaw slumps (earth flows) are generally related to thermokarst processes in the study area, particularly where water (lakes and rivers) are actively incising into ice-rich lacustrine sediments. Terrain vulnerable to thaw slumping commonly displays surface evidence of thermokarst activity (Huscroft et al., 2004). No retrogressive thaw slumps were noted in the study area, but landforms containing permafrost are susceptible to these processes.

Debris flows and debris slides are the most common types of mass movements in the Shakwak Valley (Clague, 1981; Huscroft et al., 2004) and are generally triggered by intense rainfall events on steep to moderate, colluvial or till-covered slopes. In general, debris flows and debris slides may be channelized by pre-existing gullies, or occur on open slopes. While there is high debris-flow and debris-slide risk south of the study area from Silver Creek to Congdon Creek (Huscroft et al., 2004), the distance between the mountain front and any infrastructure increases quite markedly north of Congdon Creek and the main hazard becomes water and sediment-laden floods.

In an unpublished study of debris fans along the Alaska Highway corridor in southwest Yukon, Koch et al. (*in press*), document the frequency of debris events on a number of fans within the study area (from south to north; see Figure 27).

- **Bock's Creek:** Three small events recorded in sediments adjacent to the modern channel: the oldest between AD 800 and AD 1100; the second event between AD 1100 and AD 1785; and the most recent event between AD 1785 and the mid-20th century.
- **Cluett Creek:** Occupied different channels in the recent past, but none show evidence of debris flows. Channels interpreted as being formed by high-flow events.
- **Lewis Creek:** Lower fan surface stable since before AD 800; two small events near apex of fan, one before AD 800 and one subsequent to AD 800.

- **Copper Joe Creek:** Two debris flow events recorded near the apex of the fan: the younger event occurred between AD 800 and AD 1810, and the older event occurred prior to AD 800. Neither event reached the distal part of the fan.

The authors conclude that the axial streams of all the fans in the study area have been modified to such a degree by large-diameter culverts, levees and berms (e.g., Figure 28) that any future debris flows will likely be restricted to present stream crossings of the Alaska Highway corridor (Koch et al., *in press*).

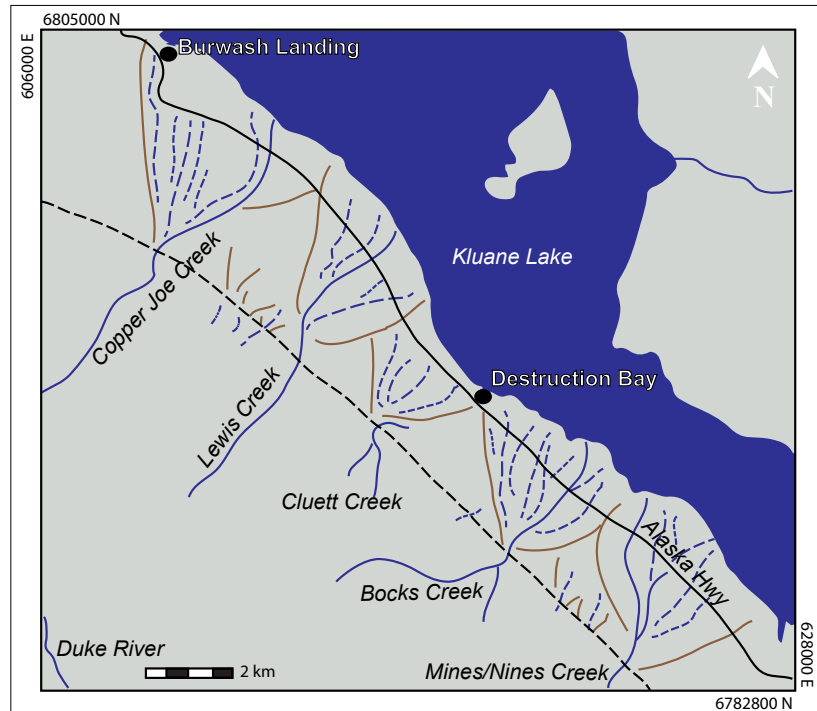


Figure 27. Debris fans documented by Koch et al. (*in press*). The Bock’s Creek, Cluett Creek, Lewis Creek and Copper Joe Creek fans are all within the study area (figure modified from Koch et al., *in press*).



Figure 28. An example of berms on Bock’s Creek that serve to mitigate potential debris floods and flows.

NEOTECTONICS

Neotectonic activity in southwestern Yukon is associated with the convergence of the Yakutat plate into the southern margin of Alaska. Most of the resulting strain is released by earthquakes with displacements along parts of the Denali and Duke River fault systems. Associated seismicity in southwestern Yukon is among the highest in Canada.

Paleoseismic results from a site near Burwash Landing suggest that at least three large magnitude surface-faulting earthquakes have occurred along the Yukon section of the Denali Fault in the past 3800 years, with an average recurrence interval of approximately 1000 years (Seitz et al., 2008). Activity on this fault can include significant ground ruptures (3-4 m displacements) and deformation of surface sediments (Lipovsky et al., 2009). Surface offsets of nearby geomorphic features suggest a late Pleistocene-Holocene slip rate of 2-4 mm/yr along this part of the Denali Fault (Seitz et al., 2008). The slip rate estimate, recurrence data and correlations with Alaskan records suggest that the earthquakes had average displacements in the 3-4 m range and magnitudes of 7.5 Mw or greater (Lipovsky et al., 2009).

PERMAFROST

REGIONAL CHARACTERISTICS

The Permafrost Map of Canada (Heginbottom et al., 1995) depicts the entire area on the southwestern side of Kluane Lake as sporadic discontinuous permafrost (i.e., 10-50% of the area underlain by perennially frozen ground). More detailed mapping of the area was undertaken by Heginbottom and Radburn (1992). They not only used a much larger scale (1: 1 000 000) but added an additional category of *Intermediate discontinuous permafrost* used for areas where about half of the exposed land surface is underlain by permafrost (Figure 29). Their map illustrates the Kluane Range and most of the Ruby Range as being underlain by continuous permafrost. The terrain along the Alaska Highway adjacent to the southwestern shoreline of Kluane Lake is quite variable in terms of permafrost conditions, varying from isolated patches (category 1: <10% of terrain underlain by permafrost) to continuous (category 5: >90% of terrain underlain by permafrost), but is mainly intermediate in nature (category 3: ~50% of terrain underlain by permafrost) around Burwash Landing and Destruction Bay. Ground ice contents are generally described as low to moderate, but some units are shown as varying from low to high. The large fans generated by rivers draining the Kluane Range are described as having isolated patches of permafrost without ground ice.

GEOTECHNICAL PROPERTIES

Soil types

Three distinct soil units were identified based on the geotechnical characteristics of samples gathered during the permafrost drill program, and were classified using the Unified Soil Classification system (USCS) as (1) Sandy Silt (USCS group symbol ML), (2) Silty Sand (USCS group symbol SM) and (3) Silty Sand with Gravel (USCS group symbol SM). These units are hereafter referred to as Units 1-3, respectively. Laboratory analyses indicate that each soil type exhibits specific characteristics related to both composition and ice properties (Tables 1 and 2). There was little variation in specific gravity among soil types. However, the lowest specific gravities values are probably linked to the apparent accumulation of organic matter in sand and silt on top of the active layer. Detailed descriptions of the physical characteristics of each soil type are included below.

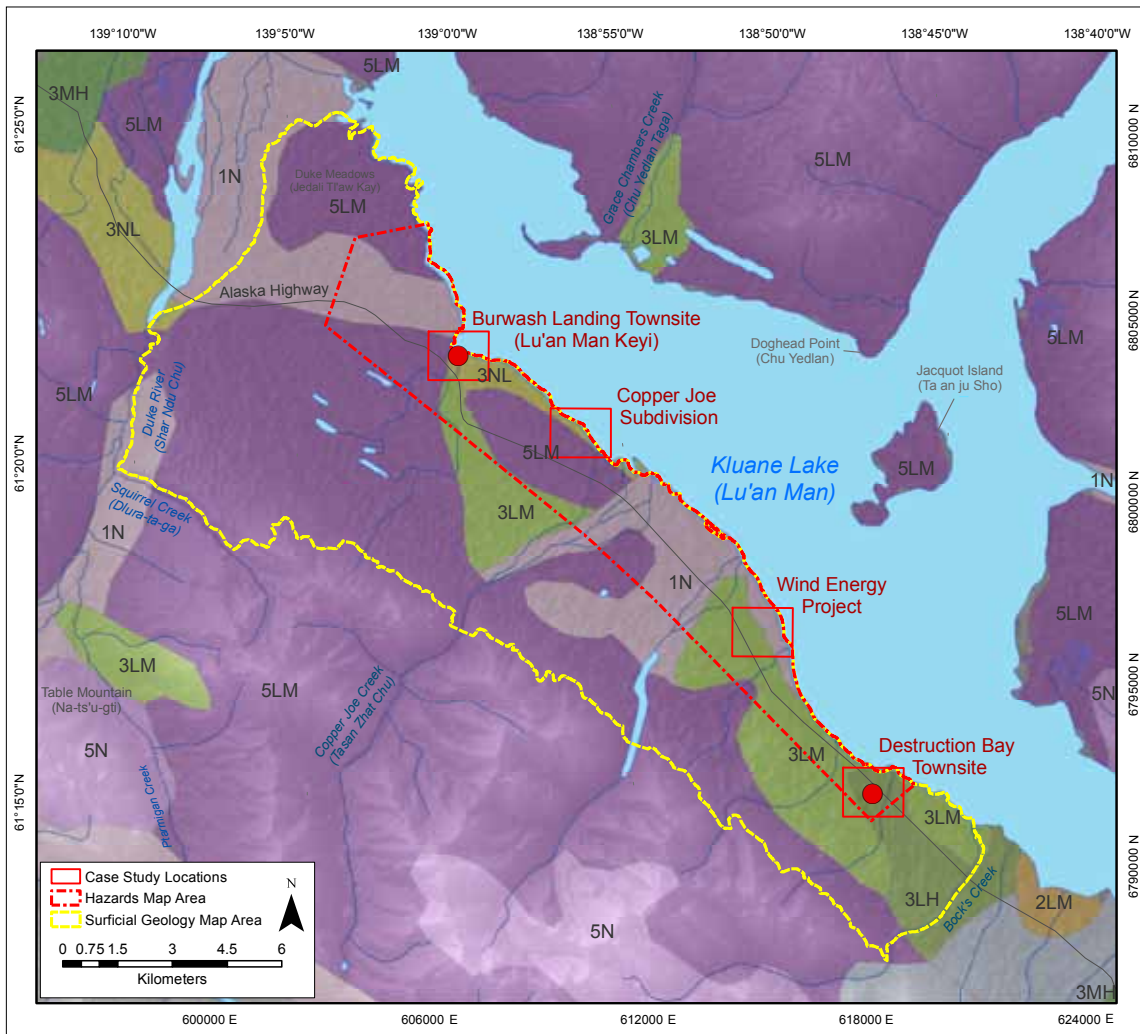


Figure 29. Map of permafrost conditions for the study area (extract from Heginbottom and Radburn, 1992). Permafrost classes are: 5 – continuous (more than 90% of the terrain underlain by permafrost); 4 – extensive discontinuous (>50-90%); 3 – intermediate discontinuous (about 50%); 2 – sporadic discontinuous (10-<50%); 1 – isolated patches (less than 10%). Letters refer to ground ice contents: N – Nil; NL – Nil to Low; LM – Low to Medium; LH – Low to High; MH – Medium to High. Please refer to map legend of Heginbottom and Radburn (1992) for detailed geological descriptions of polygon units.

Unit 1: ML Sandy Silt

Unit 1 is sandy and relatively uniform (Table 1; Figure 30). It was frequently encountered in the first metre of the boreholes, just under the organic cover; no soil of this class was found at a depth greater than 1.25 m. According to the post-glacial geological history of the area (see Surficial materials, above) and borehole locations, this unit may be derived from eolian processes.

When encountered in frozen sections, Unit 1 generally showed a visible cryostructure, meaning that the soil was over-saturated and ice content (Table 2) exceeded porosity (Table 1). However, the excess ice content was variable among Unit 1 samples. Because permafrost temperatures in the study area are generally ~0°C, unfrozen water (or bound water) present in the soil sample

may be relatively high. The clay and organic matter content in Unit 1 was generally low (Table 1), and the soil samples tended to collapse on themselves when thawing.

Table 1. Geotechnical properties of samples collected from Units 1-3 in permafrost boreholes; SD = standard deviation; D50 = median grain size; * denotes values that include clays when unmeasured (if clay = NA).

Soil type		Gravel (%)	Sand (%)	Silt* (%)	Clay (%)	D50 (mm)	Specific gravity (----)	Bulk density (g/cm ³)	Porosity (%)
Unit 1	Average	3%	43%	47%	7%	0.06	2.76	1.31	52%
	SD	5%	7%	5%	3%	0.01	0.05	0.10	3%
Unit 2	Average	2%	76%	18%	4%	0.21	2.77	1.45	48%
	SD	2%	10%	8%	3%	0.10	0.10	0.20	6%
Unit 3	Average	40%	41%	16%	4%	1.21	2.81	1.96	30%
	SD	11%	7%	7%	2%	1.31	0.02	0.11	4%

Table 2. Statistical properties related to ice content measured from Units 1-3 collected from permafrost boreholes; SD = standard deviation

Soil type		Gravimetric ice content (%)	Volumetric ice content (%)	Settlement potential (%)
Unit 1	Average	54%	57%	13%
	SD	38%	13%	22%
Unit 2	Average	35%	51%	11%
	SD	8%	5%	6%
Unit 3	Average	16%	32%	9%
	SD	7%	10%	7%

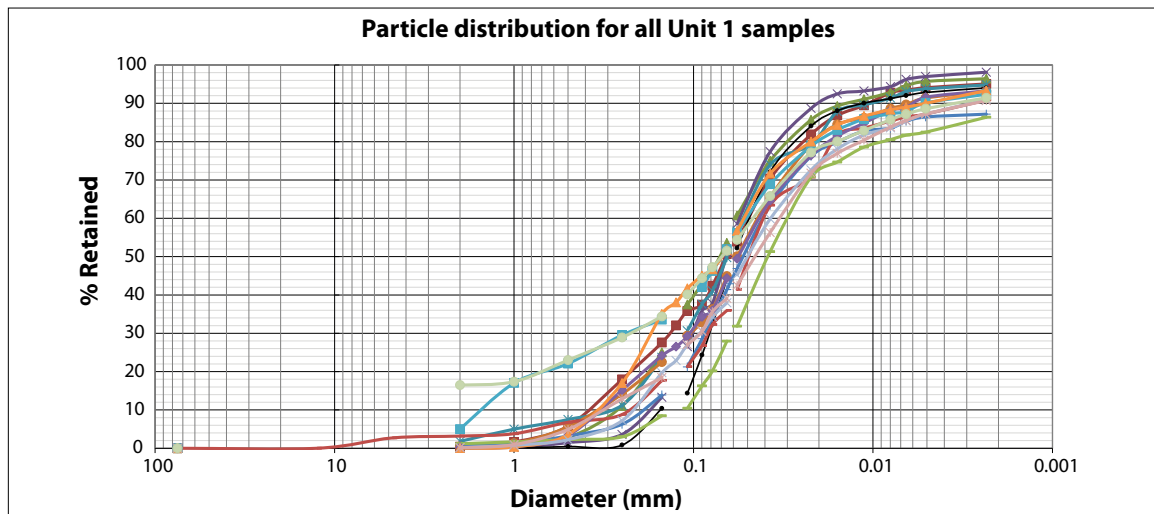


Figure 30. Compilation of cumulative particle distribution analysis for all Unit 1 samples collected from permafrost boreholes.

Unit 2: SM Silty Sand

Unit 2 is fine to medium grained, silty, and moderately sorted (Table 1; Figure 31). This unit is less extensively distributed than unit 2, and is usually found just under the organic cover, although it was found as deep as 2.6 m in some areas. As with Unit 1, Unit 2 is probably of eolian nature.

When frozen, Unit 2 rarely showed a visible cryostructure, and, when it did, it took the form of poorly developed microlenses. Despite the lack of obvious cryostructures, this unit was shown to be over-saturated, and ice content (Table 2) was sometimes found in excess of porosity (Table 1). The plastic state was measurable only when clay and organic contents were notable (and measured ~4 in these cases); otherwise, when thawed and saturated, the samples from this unit tended to collapse on themselves due to a major loss of bearing capacity.

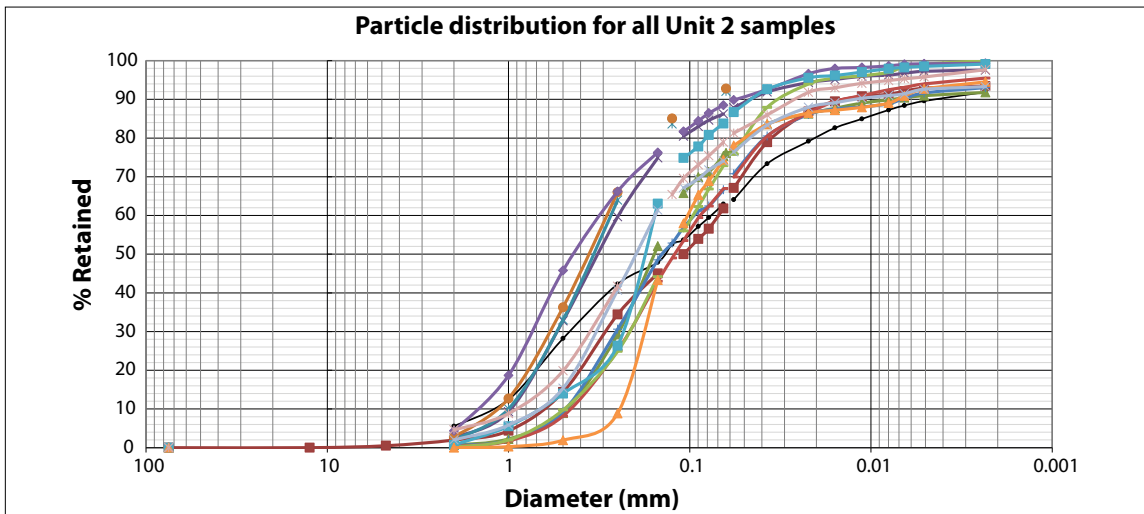


Figure 31. Compilation of cumulative particle distribution analysis for all Unit 2 samples collected from permafrost boreholes.

Unit 3: SM Silty Sand with Gravel

Unit 3 samples collected from the permafrost boreholes in the study area ranges from coarse to fine and is appears to be well graded (Figure 32). However, in some cases, the coarse fraction of the grain-size analysis lacked resolution, and sample sizes may not have been large enough to accurately define sorting level. It is important to note that the silt and finer material proportions of Unit 3 were sometimes greater than 20% (Table 1), which could indicate the potential for ground instability should this unit be over-saturated upon thawing. The angularity of the gravel portion of this unit (>5 mm) ranged from sub-angular to sub-rounded.

Unit 3 may originate from various geological processes. However, the proximity of alluvial fans and drumlins suggest these may be the sources of local Unit 3 deposits. In the study area, Unit 3 was always found under an eolian apron.

All of the frozen core samples collected show microlenses or a crust-like cryostructure. Unit 3 is shown to be over-saturated and ice content (Table 2) is sometimes in excess of porosity (Table 1). The plastic state was measurable only when clay and organic content were notable; otherwise, like Units 1 and 2, Unit 3 samples tended to collapse on themselves when melting due to the loss of bearing capacity.

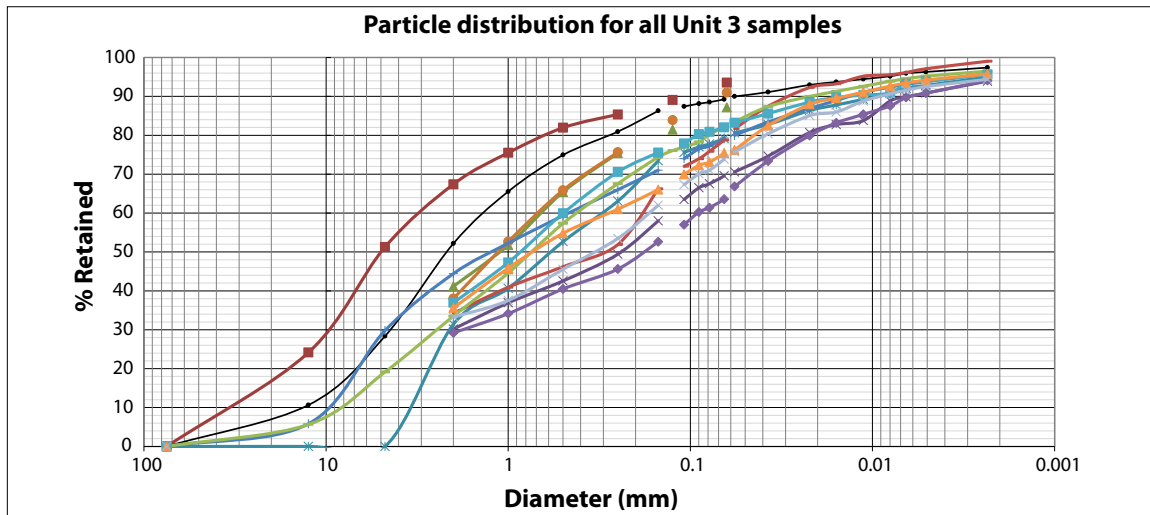


Figure 32. Compilation of cumulative particle distribution analysis for all Unit 3 samples collected from permafrost boreholes.

Hydraulic and thermal conductivities

Hydraulic and thermal conductivities vary notably among the three units of soil analyzed (Table 3). The relatively high hydraulic conductivity of Unit 1 could be explained by sorting, as can the lower hydraulic conductivity of Unit 2, but these values may also be the result of unrepresentative subsamples for the units in question. Typically a soil with larger particles will exhibit a higher hydraulic conductivity than a soil with smaller particles. Further investigation in this regard is warranted.

Table 3. Hydraulic and thermal conductivities of samples collected from Units 1-3 in permafrost boreholes. Thermal conductivities are indicated for representative samples according to gravimetric water content, expressed in the table as percent (%).

Soil type	Hydraulic conductivity cm/s	Thermal conductivity		
		Dry W/(m·°C) - % grav.	Moist W/(m·°C) - % grav.	Saturated W/(m·°C) - % grav.
Fibrous peat	$1.4 \times 10^{-1} - 1.5 \times 10^{-4}$	0.100 - 0%	0.250 - 40%	0.800 - 80%
Unit 1	2.0×10^{-5}	0.155 - 0%	0.562 - 12%	0.900 - 46%
Unit 2	1.1×10^{-5}	0.242 - 0%	0.667 - 05%	1.278 - 21%
Unit 3	2.1×10^{-5}	0.375 - 0%	1.065 - 10%	1.347 - 14%

Thermal conductivity is fairly low for each type of material but increases substantially when water replaces air in the pores (Table 3; Figure 33). In other words, porosity acts against thermal conductivity because of the insulating properties of air-filled pores. Consequently, the coarser the material (and the higher its air content), the stronger the effect of water on thermal conductivity will be.

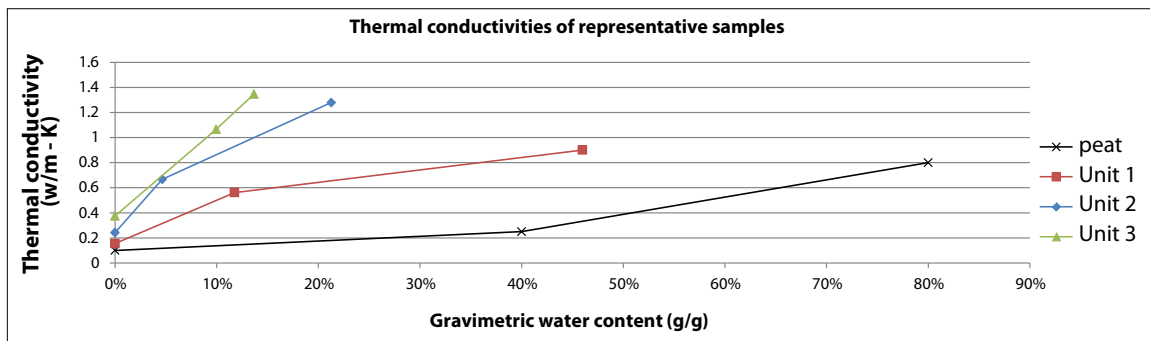


Figure 33. Thermal conductivities for representative samples of peat, and Units 1-3.

To get a more comprehensive indication of hydraulic and thermal conductivity properties of soils in the study area, it is also important to consider organic material. The hydraulic conductivity of low to moderately decomposed organic material (like that found in the study region) is typically higher than that of the three units encountered, while its thermal conductivity is typically lower (Table 3). The presence of water is of particular interest, because soils that are saturated for prolonged periods of time can develop a thicker organic mat. The existence and abundance of organic material is an important aspect in the resilience of permafrost to environmental change.

CONTEMPORARY PERMAFROST PROBABILITY

A high-resolution spatial model of permafrost probability for the discontinuous permafrost zones in the entire southern Yukon was created by Bonnaventure et al. (2012) based on comprehensive field measurements from a number of study sites. The model is essentially climatically based, taking into account of the impacts of air temperature trends with elevation (Lewkowicz and Bonnaventure, 2011) and solar radiation, but not local factors such as snow depth or surficial materials. The calculated probabilities are for typical snow cover conditions and there can be considerable sub-grid cell variability where sites are locally blown clear of snow, resulting in a higher probability of permafrost, or at sites that accumulate early and deep snow covers, resulting in a lower probability of permafrost (Lewkowicz and Ednie, 2004). Results portray the broad spatial trends in permafrost conditions across the landscape but cannot be used for site-specific predictions. For example, if an area is shown as having a probability of 0.5 to 0.6, this means that 50-60% of the grid cells are predicted to be underlain by permafrost, but it does not indicate which of the cells may have permafrost and which may not.

Predictions from the regional model described above have been compared to the following:

- field observations in the Sa Dena Hes area (not used in the derivation of the regional model; Bonnaventure and Lewkowicz, 2011);
- permafrost zone boundaries on the national permafrost map of Canada (Heginbottom et al., 1995);
- a database of Yukon rock glaciers (Page, 2009); and
- a series of temperature measurements in instrumented boreholes (Global Terrestrial Network for Permafrost, 2013).

The results suggest that the model may slightly over-predict permafrost probabilities where they are >0.5 and slightly under-predict at probabilities <0.5. However, the predicted trends reflect observed probability patterns (Bonnaventure et al., 2012).

Model results for the region around Kluane Lake and more specifically for the Burwash Landing and Destruction Bay areas were extracted from the regional model (Figures 34 and 35). Results indicate that permafrost in the area is strongly influenced by elevation but also by aspect. Most of the terrain adjacent to Kluane Lake exhibits permafrost probabilities of 0.5-0.6 (i.e., 50-60% of the terrain predicted to be underlain by permafrost) with some steeper northeast facing slopes in the 0.6-0.7 range and a few south-facing slopes with lower probabilities. Higher elevations in the Kluane Range and the Ruby Range on either side of Kluane Lake and the Shaktwak Trench exhibit continuous permafrost (probability greater than 0.9).

The permafrost probability model is in good agreement with Heginbottom and Radburn's (1992) map (see Figure 29). The level of spatial detail is much higher in the probability map (grid cells are 30 x 30 m), while Heginbottom and Radburn (1992) base mapping on borehole information and take into account geomorphological characteristics and surficial deposits. The concordance lends credence to subsequent modelling that was undertaken to examine the effects of increases in air temperature on permafrost probability (see *Projected climate change implications for permafrost*, below).

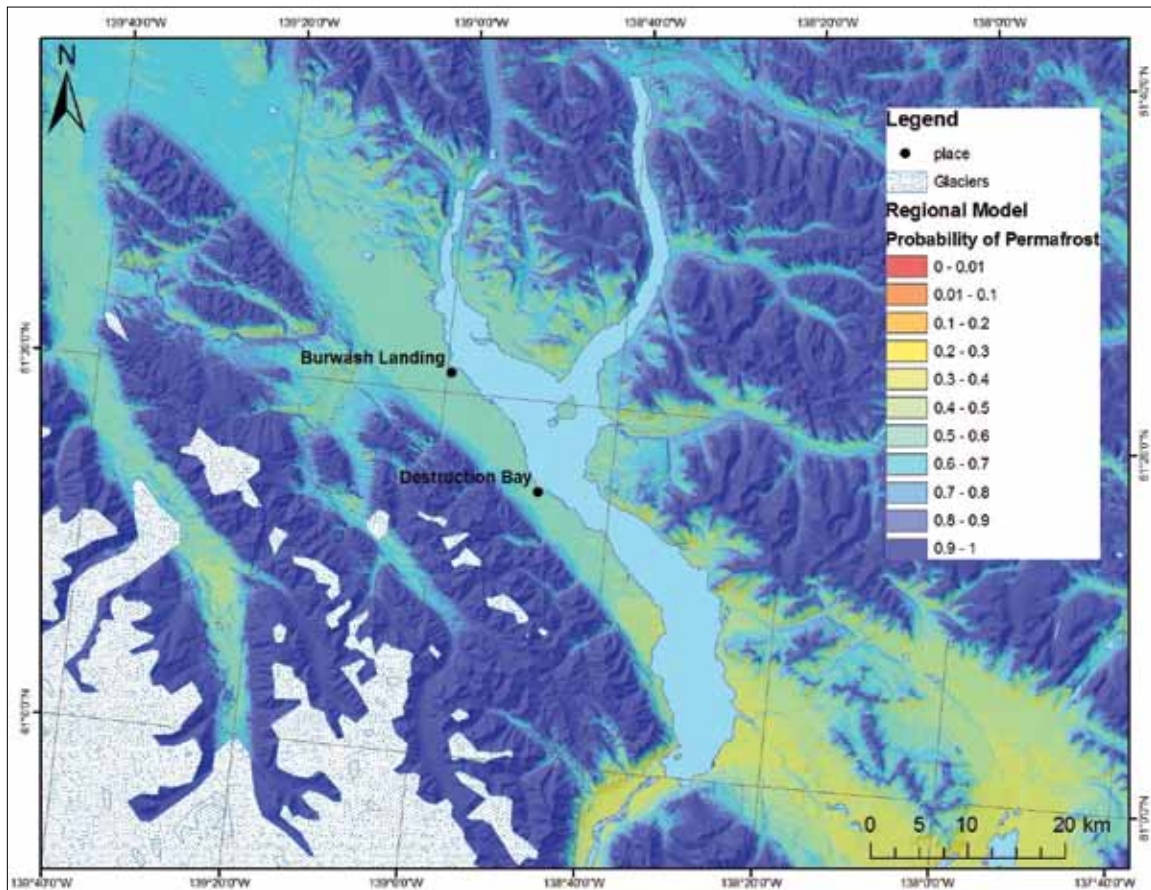


Figure 34. Permafrost probability under current climatic conditions for the Kluane region (from Bonnaventure et al., 2012). Note that glacier extent is highly generalized.

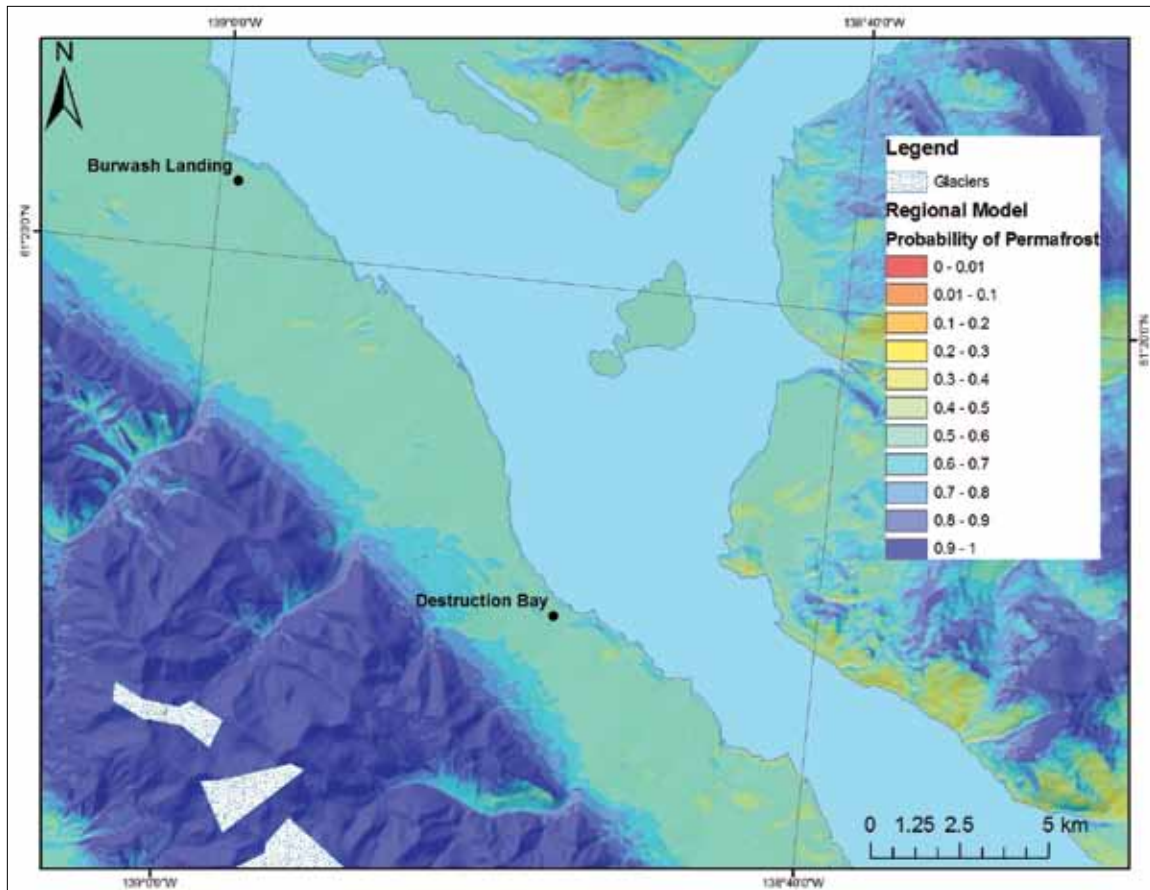


Figure 35. Permafrost probability under current climatic conditions for the study area around Burwash Landing and Destruction Bay (from Bonnaventure et al., 2012). Note that glacier extent is highly generalized.

CASE STUDY INVESTIGATIONS

To develop a more detailed understanding of geological, hydrological and permafrost conditions in the study region, four case study areas were selected for detailed investigations, reflecting local input about potential areas of future development and permafrost areas of concern (see Figure 1 for locations of case study sites). Case study areas chosen were the Burwash Landing townsite, the Copper Joe subdivision, the Kluane First Nation wind energy project site, and the Destruction Bay townsite.

BURWASH LANDING TOWNSITE

The surficial geology around the townsite of Burwash Landing is characterized by glacial diamict and glaciofluvial deposits ranging from well-sorted, pebble-cobble gravel, to poorly-sorted, silt-rich diamict. Much of the surface material in and around the community has been subject to anthropogenic modification at some point over the past ~50 years. Modifications range from simple vegetation clearing and compaction to the excavation and replacement of original geological materials with gravel and other types of fill. However, cut bank sections along the lakeshore, as well as numerous drill and test pit logs from around the community, provide information about original geology and surface materials located at depth. Generally,

the geology beneath the village of Burwash Landing is composed of interbedded fluvial and glaciofluvial gravel, and glacial diamict. Glacial diamict is the dominant material near surface, although a surface veneer or blanket of glaciofluvial gravel is common. As with elsewhere in the map area, loess deposits of sandy silt and silt are the uppermost geological component, but are thin and highly disturbed in this area. Permafrost is present in some borehole logs, but typically at depths >3 m.

ERT and GPR profiles, as well as permafrost boreholes, were done at three locations in the Burwash Landing townsite (Figure 36): (1) across the fire break (ERT profile ERT 1, boreholes *BW_Bh1* and *BW_Bh2*, and GPR profile GPR 33); (2) near the baseball diamond (ERT profile ERT 2, borehole *BW_Bh3*, and GPR profile GPR 34); and (3) at an empty lot near downtown (ERT profile ERT 3 and GPR profile GPR 35). Each location is described in detail below.



Figure 36. Map illustrating locations of detailed site investigations for the Burwash Landing townsite. Refer to Figure 1 for case study location within study area boundary.

FIRE BREAK LOCATION

Heginbottom and Radburn (1992) classify the unit that includes this site as part of the intermediate discontinuous permafrost zone having nil to low ground ice contents (see Figure 29).

A 160 m-long ERT profile (ERT 1) began in the southeast end of the community and covered terrain that included a FireSmart area, a firebreak, a gravel road and forest. ERT 1 (Figure 37) shows a near-surface layer of low resistivities (less than 100 ohm m in places) overlying a higher resistivity layer in the FireSmart area (0-60 m) and in the forest (148-160 m). In the central part

of the profile, corresponding to the firebreak (60-136 m) and a gravel road (136-148 m), the low resistivity surface layer extends to depths of about 8 m. The high resistivity layer (up to 6000 ohm m) extends to the base of the profile throughout.

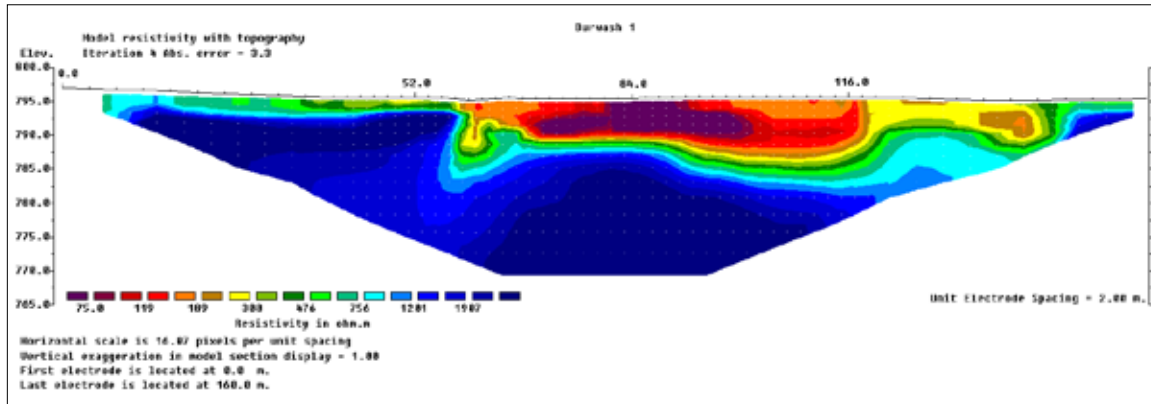


Figure 37. ERT profile 1 from southeast to northwest at Burwash Landing (see Figure 1 and Figure 36 for location). The profile is 160 m long with a maximum penetration depth of 25 m. The boundary between frozen and unfrozen materials is interpreted to be at about 300 ohm m (between the yellow and green shades). *BW_Bh1* was at 40 m along the profile and *BW_Bh2* at 80 m.

The ERT profile is interpreted as representing permafrost more than 25 m thick that has been affected in places by the surface disturbance. The active layer was originally thin, as shown by the permafrost table at *BW_Bh1* (described below), and the impacts of the FireSmart clearing were minimal. The firebreak, on the other hand, disturbed the ground temperature regime sufficiently to result in the formation of a near-surface talik (i.e., an area that is perennially unfrozen) that extends in places to 8 m. (Borehole *BW_Bh2*, described below, stopped at 2.4 m within the talik.) Similarly, the gravel road resulted in a talik to about 6 m. Presumably, the thaw of the top of permafrost resulted in concurrent surface settlement of the terrain.

It is important to note that the modelled resistivities in the active layer at the start and end of the profile are high enough to indicate frozen conditions. Such results are common where the active layer is thin and the model blocks extend across the frozen interface. They can also develop where there is an extreme resistivity contrast between the active layer and the underlying permafrost which cannot be fully accommodated in the model despite the robust inversion used.

Borehole *BW_Bh1* is located at 40 m along ERT 1 in the FireSmart area where the ground is covered by moss, scattered shrubs and spruces at different growth stages. The first 20 cm of the borehole is a mix of organic matter and sandy silt, covering a silty sand layer 65 cm thick, over a diamicton deposit (sand with gravel) to the bottom of the borehole. The water table was encountered at a depth of 55 cm, and the permafrost table at a depth of 65 cm. Here, the permafrost has a high ice content of 78% by volume. At the top of permafrost, where the materials are finer and composed mainly of silt, the profile presents a microlenticular structure. Ice content decreases to a little over 30% by volume below a depth of 90 cm in more sandy and gravelly deposits, and the cryostructure changes to crustal around gravels, and a microlenticular cryostructure in finer sediments. Thaw settlement potential is significant in the top 20 cm of the permafrost (52%), decreasing to about 4% at 1 m depth. Samples extracted from the profile

below 147 cm were not frozen, likely due to heat generated by drilling operations. The complete borehole log is shown in Appendix A1, and grain size analysis results are shown in Appendix C.

Borehole *BW_Bh2* is located at 80 m along the profile, in the fire break area. The area is vegetated by tall grasses (1 to 2 m) and scattered shrubs, and only a thin organic layer is present. The surface layer is composed of silt and sand mixed with organic matter (40 cm thick), covering a layer of silty-sand 50 cm thick, over a diamicton layer (sand and silt with gravel) that extends from a depth of 90 cm to the bottom of the borehole (242 cm). The water table was encountered at a depth of 76 cm. No permafrost was encountered. The complete borehole log is shown in Appendix A2, and grain size analysis results are shown in Appendix C.

GPR profile GPR 33 showed a strong stratigraphic reflection at ~75 cm depth (Figure 38), likely representing the water table and possibly the contact between the silty sand and gravelly sand noted in borehole *BW_Bh2* (Appendix A2). This strong reflection may correspond to the change in resistivity visible on the ERT survey from 80-60 m (see Figure 37).

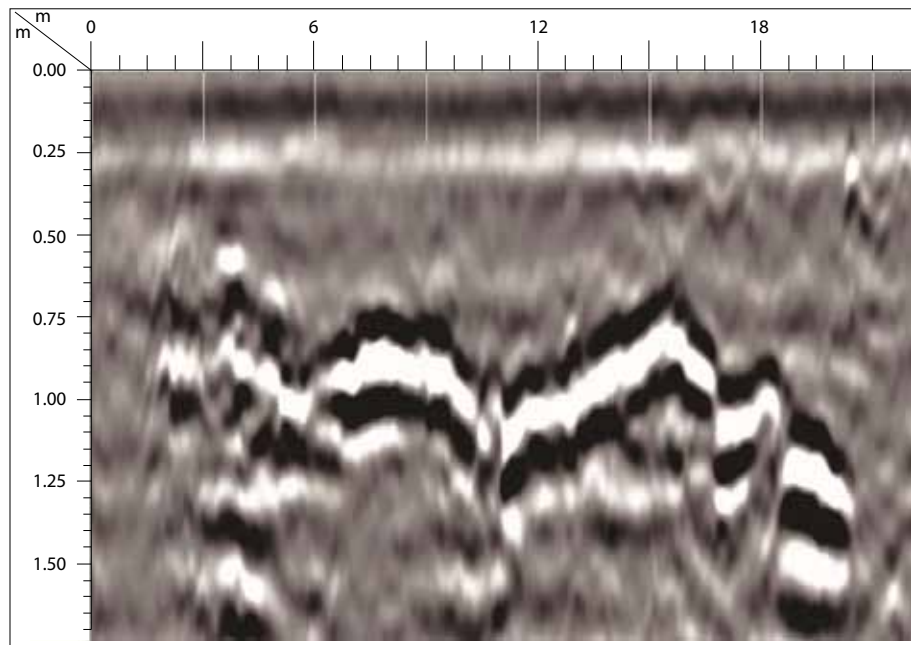


Figure 38. GPR profile from the Burwash Landing fire break, illustrating strong horizontal reflection at 75 cm corresponding to the water table.

Changes to the surface of this site had variable impacts. The FireSmart clearing left the permafrost intact while the greater changes associated with the firebreak and the road caused talik formation, but left permafrost present at depth. This permafrost could be in thermal equilibrium, but more likely, is slowly thawing.

BASEBALL DIAMOND LOCATION

Heginbottom and Radburn (1992) classify the unit that includes this site as part of the intermediate discontinuous permafrost zone having nil to low ground ice contents (see Figure 29).

ERT 2 survey was conducted along a fire break at the western end of the community near the ball diamond, and shows a continuous low resistivity layer (generally less than 100 ohm m) of variable thickness overlying a higher resistivity layer (up to 3000 ohm m) that extends to beyond

the base of the profile at 25 m (Figure 39). The profile is interpreted as representing a talik up to 7 m deep present from 52 m to the end of the profile. This talik overlies permafrost that reaches more than 25 m of depth. From the start of the profile up to 64 m, the results are ambiguous as the low resistivity layer could be a thick active layer (freezing every winter) or may also be a shallower talik extending to 2-3 m depth.

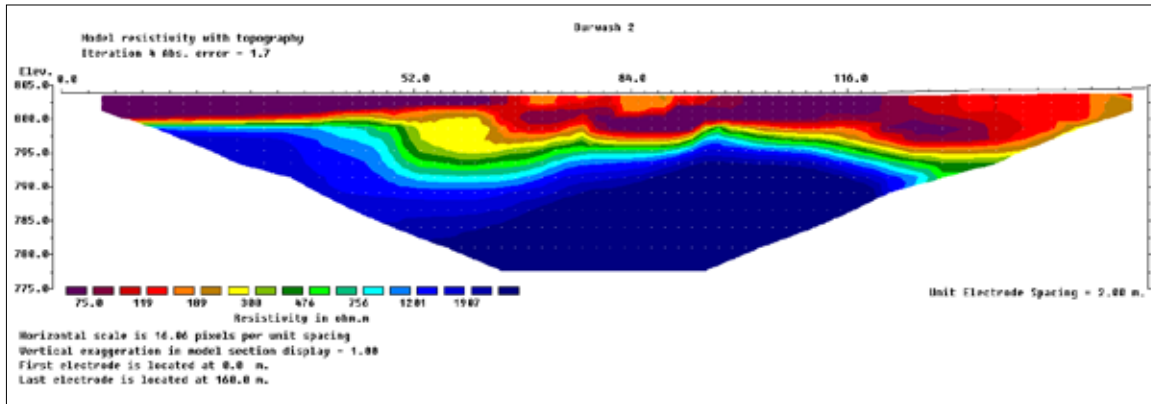


Figure 39. ERT profile 2 from southeast to northwest at Burwash Landing (see Figure 1 and Figure 36 for location). The profile is 160 m long with a maximum penetration depth of 25 m. The boundary between frozen and unfrozen materials is interpreted to be at about 300 ohm m (between the yellow and green shades). BL_Bh3 was at 0 m along the profile.

Borehole *BW_Bh3* is located at 0 m of the ERT 2 profile in an open field covered by grasses. The surface layer is 35 cm thick and composed of sandy silt mixed with organic matter and tephra. The second layer, extending to a depth of 90 cm, is composed of silty sand. The last layer is a diamicton (silty sand with gravel), from a depth of 90 cm to the base of the borehole (117 cm). The water table was measured at a depth of 90 cm. No permafrost was encountered in the borehole. The complete borehole log is shown in Appendix A3, and grain size analysis results are shown in Appendix C.

The water table identified in borehole *BW_Bh3* at a depth of 90 cm (Appendix A3) is not expressed in GPR profile GPR 34 (Figure 40). Attenuation of the GPR signal in the profile at this site is most likely caused by the high dielectric permittivity of the moist sediment.

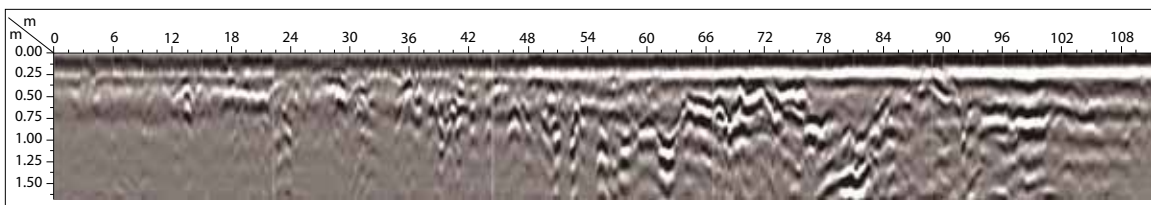


Figure 40. GPR profile from the Burwash Landing ball diamond. The blurring of the image is due to signal attenuation, and is most likely a result of high moisture content in the soil.

The permafrost at this location may be slowly thawing. Like the fire break, results from this site indicate that surface disturbance can have variable impacts, and that the permafrost is sensitive enough that taliks can form near the surface while the permafrost remains intact at depth.

EMPTY LOT LOCATION

Heginbottom and Radburn (1992) classify the unit that includes this site as part of the intermediate discontinuous permafrost zone having nil to low ground ice contents (see Figure 29).

ERT profile ERT 3 was conducted across a gently sloping, undeveloped lot in the community and was restricted in length to 40 m; consequently it penetrated to only 8 m depth. Resistivities generally increase from the surface towards the base of the profile but are generally low, with a maximum of about 1200 ohm m (Figure 41). There is a higher resistivity body at 3-9 m along the profile that extends to a depth of 1 m. This ERT profile can be interpreted in two ways: either the site is entirely unfrozen, or there is a talik extending to a depth of at least 4 m that overlies permafrost. The higher surface resistivities near the start of the profile are probably due to a patch of unfrozen, dry gravel. Given the results from ERT 1 and ERT 2, where disturbance has occurred and resistivities increase towards the base of the profiles, the interpretation of a talik over permafrost is favoured. However, there was no permafrost borehole drilled at this location to provide additional support for this interpretation.

GPR profile GPR 35 shows a strong stratigraphic reflection at a depth of 50 cm (Figure 42). This reflection may correspond to the depth of gravel fill in the empty lot.

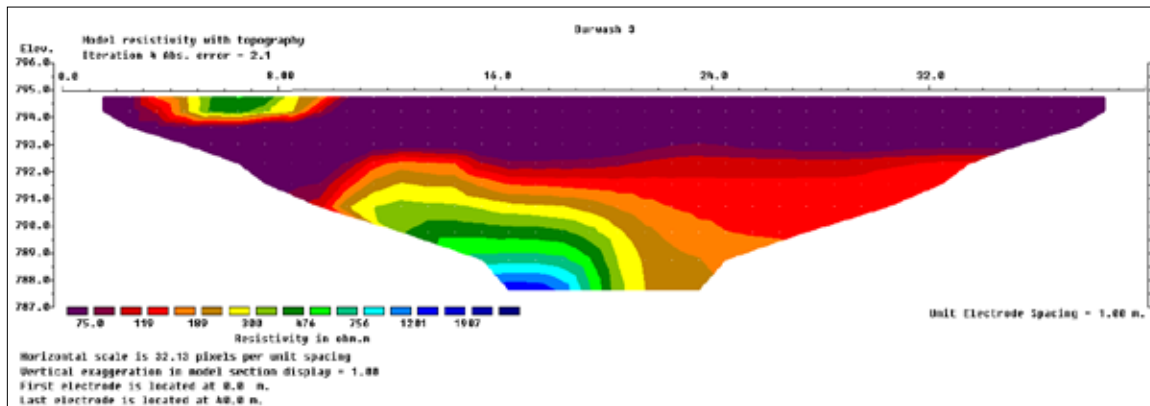


Figure 41. ERT profile 3 across an undeveloped lot in Burwash Landing (see Figures 1 and 36 for location). The profile is 40 m long with a maximum penetration depth of 8 m. The boundary between frozen and unfrozen materials is uncertain but may be at about 300 ohm m (between the yellow and green shades). Either the entire profile is unfrozen, or permafrost may be present near its base.

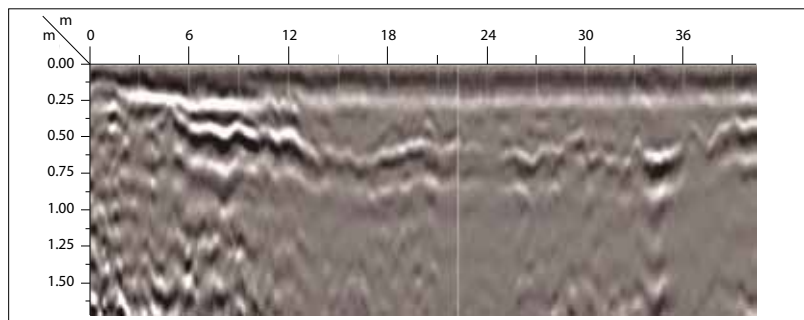


Figure 42. GPR profile from an empty lot in Burwash Landing, illustrating a horizontal reflection at ~50 cm that most likely corresponds to gravel fill.

COPPER JOE SUBDIVISION

Preliminary surficial geology investigations in Copper Joe subdivision suggest the site is located on a complex glaciofluvial landform blanketed in loess. The glaciofluvial unit was likely deposited in a near-ice environment during recession of a valley glacier in the Shakwak Trench. The glaciofluvial/moraine landform is typical of a meltout till and glaciofluvial units that encompass everything from well-washed and sorted gravel, to compact and impermeable till. It is likely that drainage through this unit is good to moderate, but subject to high variability both laterally and vertically. Figure 43 shows local conditions in both developed and undeveloped areas of the subdivision.



Figure 43. Photographs illustrating local site conditions in the Copper Joe subdivision; **(a)** vegetation in the lower Copper Joe subdivision is comprised of sphagnum moss, Labrador tea, black spruce, alder, and various herbs and shrubs; **(b)** saturated clay soils in the Copper Joe subdivision.

Two areas in Copper Joe subdivision were investigated (Figure 44): 1) Phase 1 (the developed portion of the subdivision), near lots 23 and 24 (ERT profile ERT 1, permafrost boreholes *CJ_Bh1* and *CJ_Bh2*, and GPR profile GPR 30); and 2) Phase 2 (the undeveloped portion of the subdivision), near lots 32 and 51 (ERT profile ERT 2, permafrost borehole *CJ_Bh3*, and GPR profile GPR 31).

COPPER JOE PHASE 1

This site falls between the boundary of two units identified by Heginbottom and Radburn (1992). One unit is part of the intermediate discontinuous permafrost zone having nil to low ground ice contents, while the other is continuous permafrost having low to medium ice contents (see Figure 29).

A 160 m-long ERT profile (ERT 1) was completed across a gently climbing site from southwest to northeast, starting in forest, crossing a cleared section (from about 50-85 m) and terminating in forest again. The ERT profile illustrates a two-layer system and has a low resistivity layer (typically about 100 ohm m) overlying a higher resistivity layer (mainly about 2000 ohm m) that extends to the base of the profile (Figure 45). In the centre of the profile, within the cleared zone, the thawed layer appears to be up to about 3 m thick (explaining why borehole *CJ_Bh1*, described below, did not encounter frozen ground). The resistivity values beneath this zone are lower than on either side. This is probably due to the effect of ground warming beneath the cleared zone, causing higher unfrozen moisture contents in the permafrost all the way to the base of

the profile (Lewkowicz et al., 2011). The apparent thaw depths in the centre of the cleared area appear deep enough that a talik is likely present. However, ground temperature measurements would be needed to confirm this interpretation.

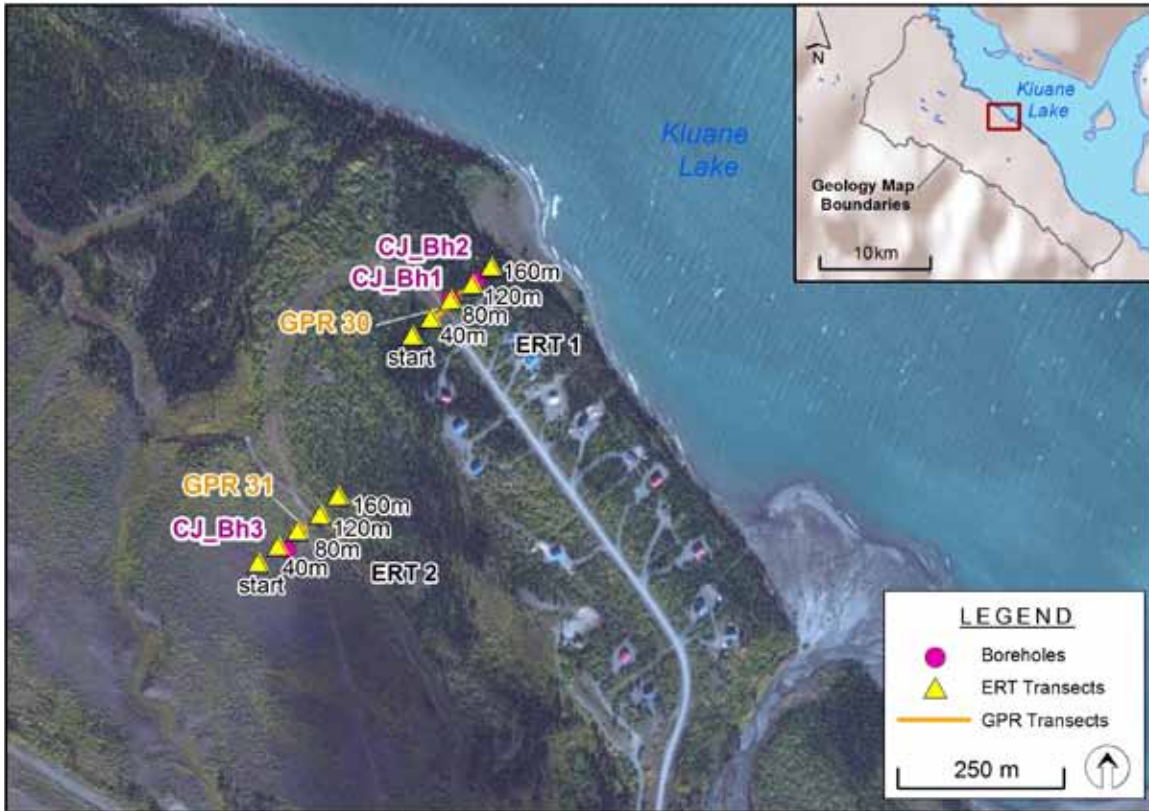


Figure 44. Map illustrating detailed site investigations for the Copper Joe subdivision. Refer to Figure 1 for site location.

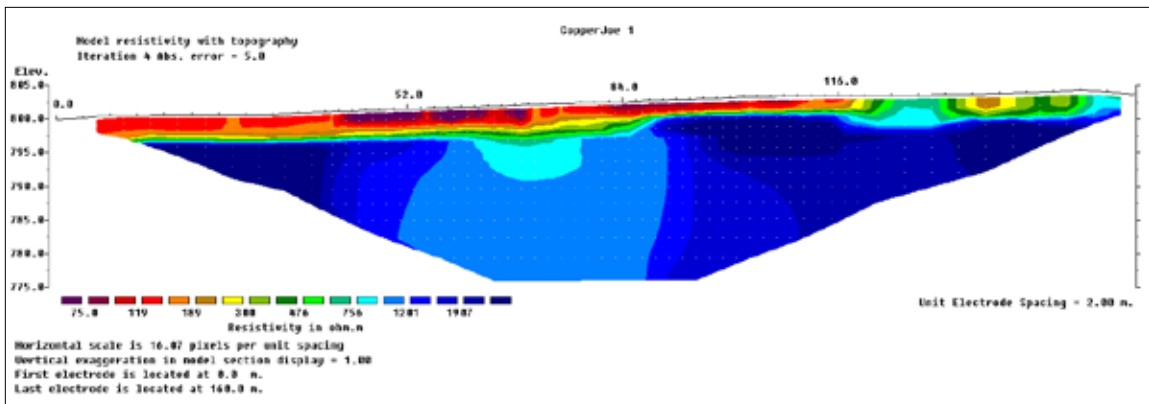


Figure 45. ERT1 profile 1 from southwest to northeast from back of lot 24 into lot 23 at Copper Joe subdivision (see Figures 1 and 44 for location). The profile is 160 m long with a maximum penetration depth of 25 m. The boundary between frozen and unfrozen materials is interpreted to be at about 300 ohm m (between the yellow and green shades). CJ_Bh1 was at 80 m and CJ_Bh2 was 120 m along the profile.

Borehole *CJ_Bh1* was drilled at 80 m along ERT 1 in the cleared section where the ground surface is dominated by shrubs 1 to 2 m tall. The borehole penetrated to 1.1 m without encountering frozen ground. The stratigraphy comprises a thin layer of silty sand mixed with organics and gravel (50 cm thick) over sand and gravel. The complete borehole log is shown in Appendix A4, and grain size analysis results are shown in Appendix C.

Borehole *CJ_Bh2* was drilled at 120 m along ERT 1, in the forest. The borehole was drilled to a depth of 1.4 m, corresponding to 0.6 m below the permafrost table. The water table was observed at a depth of 50 cm. The finer surface layer (silty sand, 80 cm thick) is underlain by sands with gravel and two layers of distinct cryostructure. These are porous invisible in the first 15 cm of the permafrost, and microlenticular over the next 30 cm. Both cryostructures demonstrate low ice contents (about 50% by volume) and virtually no thaw settlement potential. Samples deeper than 120 cm were not frozen, likely due to thawing during coring operations. The complete borehole log is shown in Appendix A5, and grain size analysis results are shown in Appendix C.

GPR transect GPR 30 was completed across the open area under the cleared power line adjacent to borehole *CJ_Bh1*, where no permafrost was noted. There are some strong stratigraphic reflectors at a depth of ~78 cm (Figure 46), corresponding to the permafrost table identified in borehole *CJ_Bh2* (located in the forested area 30 m away from the GPR transect). The GPR transect parallels the ERT survey from 70-20 m.

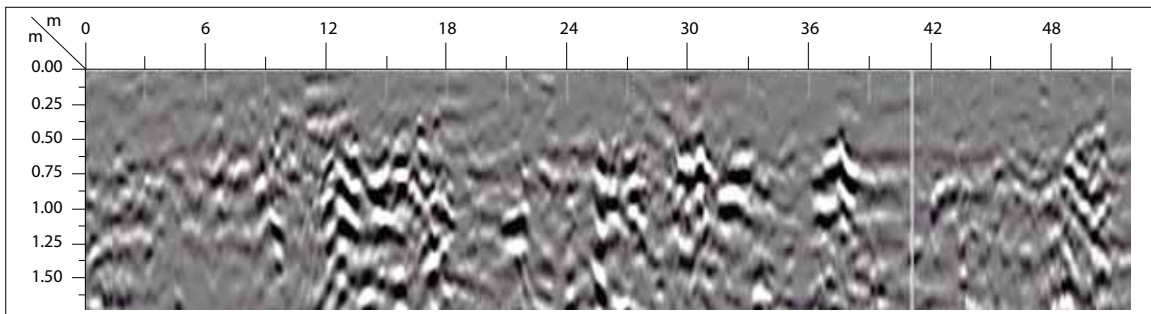


Figure 46. GPR profile from Copper Joe subdivision, illustrating a strong horizontal reflection at ~75 cm corresponding to the water table.

COPPER JOE PHASE 2

Given the scale of Heginbottom and Radburn (1992) permafrost map, the Copper Joe Phase 2 site is assumed to fall between the two permafrost boundaries discussed above for the Copper Joe Phase 1 site (i.e., between the intermediate discontinuous permafrost zone having nil to low ground ice contents, and the continuous permafrost having low to medium ice contents (see Figure 29)).

ERT profile ERT 3 was completed over a length of 160 m across virtually flat terrain comprising lots 51 and 32 in Phase 2 of the Copper Joe subdivision. The surface cover varies from burned forest (0-36 m), unburned shrubs (36-60 m), a partially burned and cleared zone adjacent to two trails (60-120 m; the trails themselves centred at 84 m and 110 m), a less disturbed zone (120-160 m), and terminating at undisturbed forest.

The ERT profile (Figure 47) demonstrates a low resistivity layer (mainly less than 100 ohm m) of variable thickness overlying a high resistivity layer (typically 500-1000 ohm m) that gradually increases in resistivity and extends to the base of the profile at 25 m. The thickness of the low

resistivity layer is proportional to the degree of surface disturbance, and it reaches a maximum depth of 7 m beneath one of the trails in an area that was also burned. Such a depth is too great to freeze annually and so represents a talik. As is described below, borehole log *CJ_Bh3* illustrates that no permafrost is present within 1.7 m of the surface at 80 m along the profile, supporting the interpretation that a talik is present. The fire disturbance (forest fire in 1999) at the start of the profile has led to thaw depths of about 5 m, which are also great enough to support a talik. In fact, an active layer thermally connected to permafrost is unlikely anywhere along the profile. It is probable that the permafrost beneath the talik is slowly degrading as a result of the surface disturbance and, since it has a lower resistivity than ERT 1 where the talik is shallower, the permafrost is probably warmer, and unfrozen moisture contents are consequently higher.

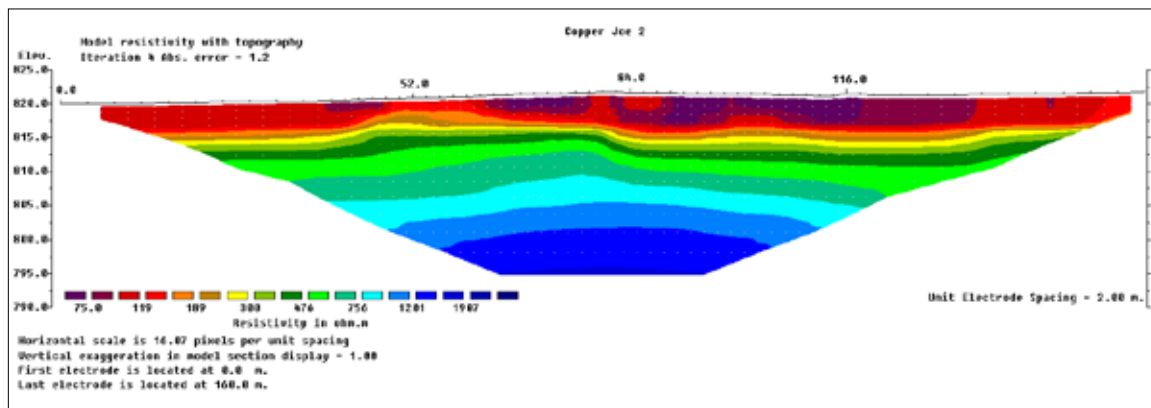


Figure 47. ERT profile 2 from southwest to northeast across lots 51 and 32 at Copper Joe subdivision (see Figures 1 and 44 for location). The profile is 160 m long with a maximum penetration depth of 25 m. The boundary between frozen and unfrozen materials is interpreted to be at about 300 ohm m (between the yellow and green shades). *CJ_Bh3* was at 80 m along the profile.

Permafrost borehole *CJ_Bh3* is located in a forest fire zone at 80 m along ERT 3 profile and penetrated to 173 cm without encountering frozen ground. The stratigraphy consists of a very thin organic layer (20 cm thick) over sandy silt to 70 cm, and sand mixed with gravel to the base of the borehole. The complete borehole log is shown in Appendix A6, and grain size analysis results are shown in Appendix C.

GPR profile GPR 31 exhibits signal attenuation (Figure 48). Signal attenuation in the GPR image is most likely from high soil moisture content. The depth of penetration is shallower than the depth of the water table (168 cm) identified in borehole *CJ_Bh3*.

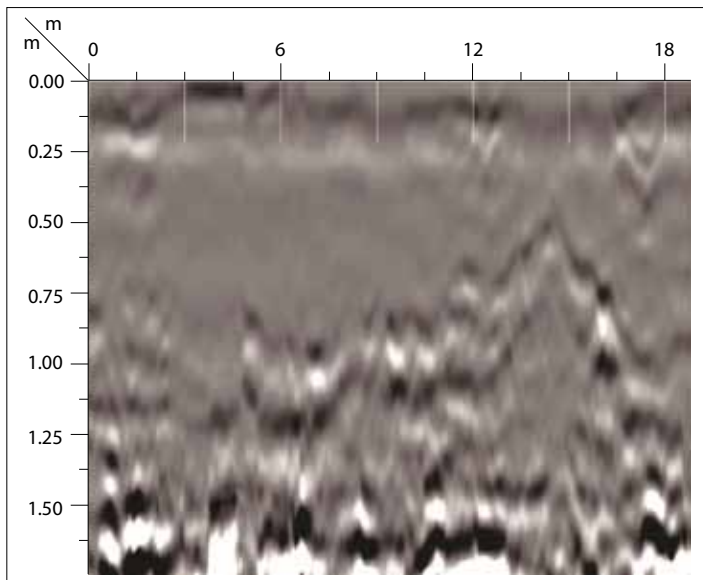


Figure 48. GPR profile from lot 50 of the Copper Joe subdivision, illustrating a weak horizontal reflection at ~80 cm corresponding to the contact between the sandy silt (Unit 2) and sand with gravel (Unit 3).

KLUANE FIRST NATION WIND ENERGY PROJECT SITE

Preliminary surficial geological investigations at the wind energy project site suggest the site is located upon a complex glaciofluvial landform blanketed in loess. The glaciofluvial unit was likely deposited in a near-ice environment during recession of a valley glacier in the Shakwak Trench. The sandy-diamict unit is typical of a meltout till and glaciofluvial units that encompass everything from well-washed and sorted gravel, to compact and impermeable till. It is likely that drainage through this unit is good to moderate, but subject to high variability both laterally and vertically. The thick loess blanket at surface, while well-drained, serves as an insulator over the underlying glaciofluvial unit. Figure 49 illustrates local site conditions at the wind energy project site.

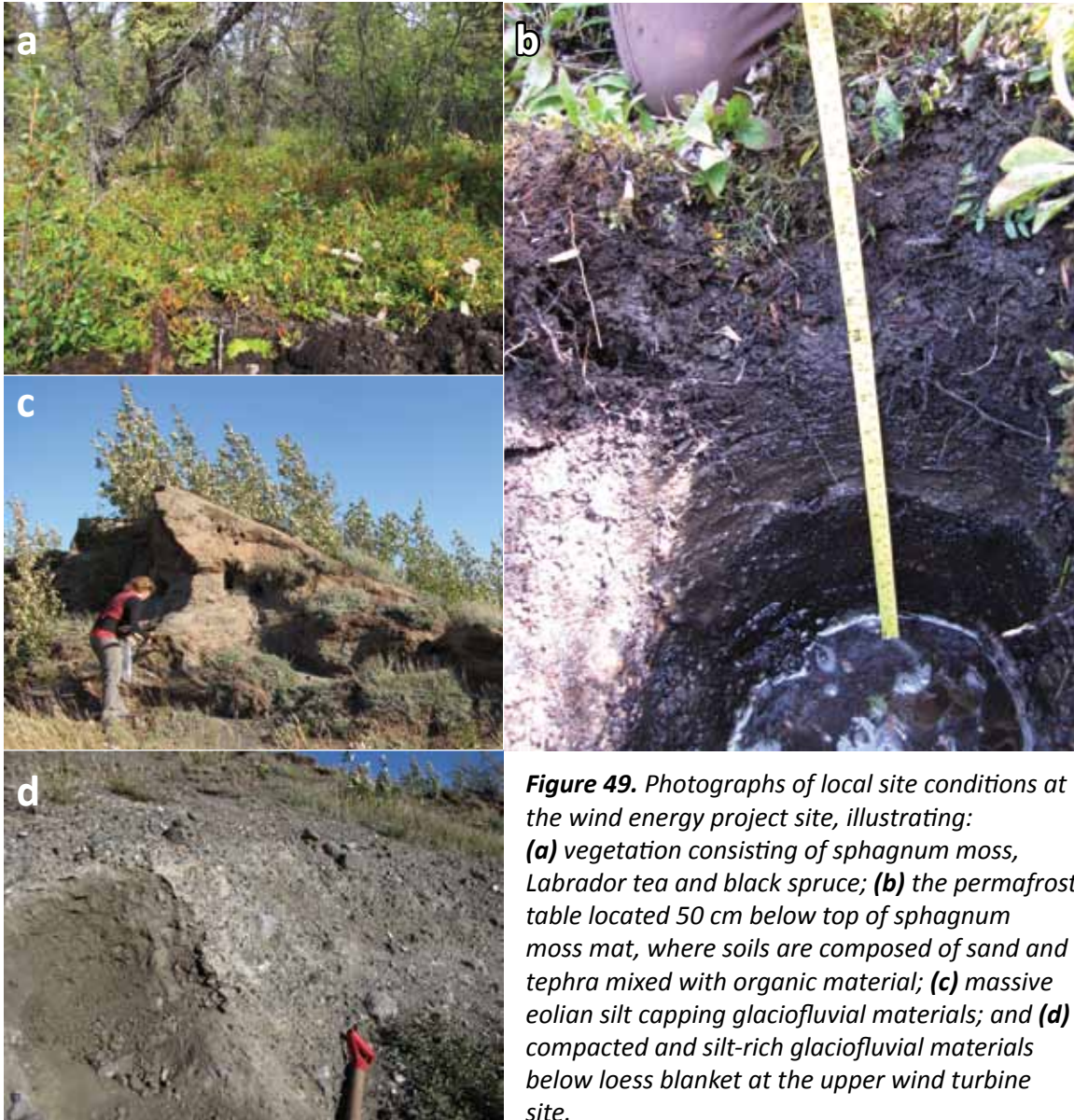
Detailed site investigations included ERT and GPR profiles (ERT 1; GPR 32) and two permafrost boreholes (*WF_Bh1*, *WF_Bh2*). Locations are illustrated on Figure 50.

Heginbottom and Radburn (1992) classify the unit that includes this site as part of the intermediate discontinuous permafrost zone having low to medium ground ice contents (see Figure 29).

Resistivity profiling at the wind energy project site used a roll-along technique to extend the ERT profile to 280 m (Figure 51). The first part of the profile crosses a hill that contains thin, well-drained soil, which changes at about 120 m to an organic surface layer covered by black spruce. ERT 1 demonstrates considerable lateral and vertical variability, and values range from less than 100 ohm m to more than 3000 ohm m. There are two main high resistivity bodies. The first is at a depth of greater than 10 m that occurs between the start of the profile and 70 m. The second is located at 105 m along the profile and extends to the end of the profile; it is expressed from shallow depths and continues to the base, and includes several centres of higher resistivity. A third small body, having moderate resistivities, is present between 36 and 50 m along the profile at depths of 2-5 m and connects into other areas with resistivities of about 300 ohm m as well as the higher resistivity body beneath.

For that part of the profile between 105 m and 280 m, interpretation is relatively straightforward. A single body of permafrost, whose presence is supported by the frozen sediments encountered in *WF_Bh1* (described below), extends close, if not all the way to the

base of the profile beneath an active layer. Even though the active layer was unfrozen, its ERT values were not always low enough to indicate unfrozen conditions due to the extreme contrast and a shallow permafrost table. Two particularly resistive bodies, from 180-190 m and 205-280 m along the profile, likely represent permafrost with a higher ice content, or at a slightly lower temperature, resulting in a lower unfrozen moisture content (see Lewkowicz et al., 2011).



The resistive body at depth, which is visible between 30 and 70 m along the profile, cannot be unambiguously interpreted. The deeper end of any ERT profile may be subject to anomalous values, so the validity of this body is uncertain. If it is legitimate, it most likely represents degrading permafrost, but it may also indicate the presence of electrically resistive bedrock. The small body with higher resistivities (observed at 36-50 m along the profile) may represent part of an area of permafrost that formerly extended across the first part of the profile but now

has degraded to depths of up to 10 m and having taliks present from 0 to 34 m and 52 to 88 m along the profile. This interpretation depends on the threshold used to delineate permafrost, as a slightly higher resistivity threshold would lead to classification of the majority of this zone as unfrozen.



Figure 50. Map illustrating detailed site investigations for the wind energy project site. Refer to Figure 1 for site location.

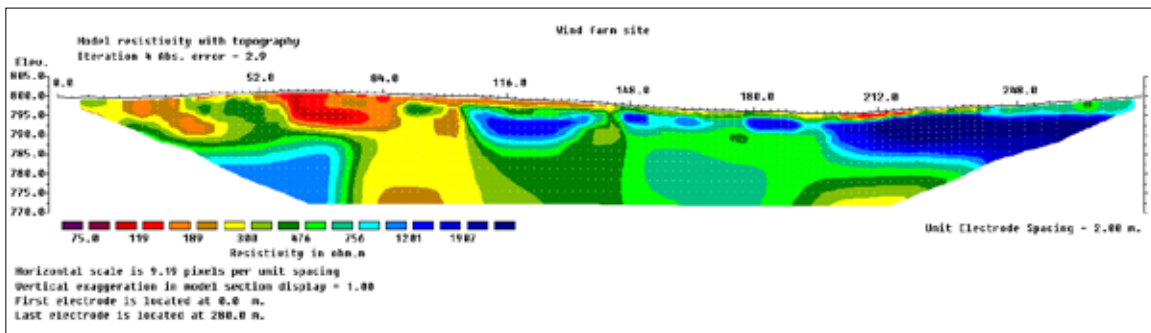


Figure 51. ERT profile from southwest to northeast at the Kluane First Nation wind energy project site (see Figures 1 and 50 for location). The profile is 280 m long with a maximum penetration depth of 25 m. The boundary between frozen and unfrozen materials is interpreted to be at about 300 ohm m (between the yellow and green shades). WF_Bh1 was at 150 m along the profile and WF_Bh2 at about 80 m, but located 10 m away from the line of the ERT profile.

Borehole *WF_Bh1* is located in a forested area at 150 m along the ERT profile. The permafrost table was encountered at a depth of 1.1 m. A thin organic layer (40 cm thick) composed of organic matter and tephra overlies sand, silty sand, and sandy silt layers (220 cm thick all total), which in turn overlies gravel that extends to the base of the borehole. Ice contents were noted as being low to moderate (45-60% by volume) and present a wide range of cryostructures varying from porous visible and invisible, to microlenticular; most of the ice content and settlement potential is linked to lenticular structures visible in a thin, 10 cm layer at the bottom of the borehole. However, there is thaw potential averaging approximately 10%, so that thaw of the top 1.5 m of the permafrost would result in at least 15 cm of settlement (not taking into account subsequent soil consolidation). The complete borehole log is shown in Appendix A7, and grain size analysis results are shown in Appendix C.

Borehole *WF_Bh2* is located at approximately 80 m along the ERT profile, in a recently deforested area (the trees had been cut 2 weeks prior to the survey), approximately 10 m away from the ERT profile. The top layer (47 cm thick) is a mix of silt, sand, organic matter and tephra that cover a layer of silty sand (present from 47 to 62 cm). From 62 cm to the bottom of the borehole (at 365 cm), a diamicton (silty sand with gravel) was observed. The permafrost table was documented at a depth of 207 cm where the samples were plastic and had a frozen core. It is likely that the drilling generated enough heat to partially melt the ice in the samples. The complete borehole log is shown in Appendix A8, and grain size analysis results are shown in Appendix C.

There is a lack of concurrence between *WF_Bh2*, which demonstrated the presence of permafrost, and the ERT profile. At 80 m along the ERT profile, resistivities of less than 200 ohm m were measured, indicating unfrozen conditions. The explanation lies in the positioning of *WF_Bh2*, which is about 10 m away from the ERT transect. This demonstrates that discontinuities in permafrost conditions that exist along the length of the transect, may also exist perpendicular to it, and permafrost conditions are spatially heterogeneous.

Along GPR profile GPR 32, the signal reached ~1.7 m depth (Figure 52), which is shallower than the depth of the permafrost (~207 cm) identified in *WF_Bh2*. The GPR transect parallels the ERT survey between 40-80 m.

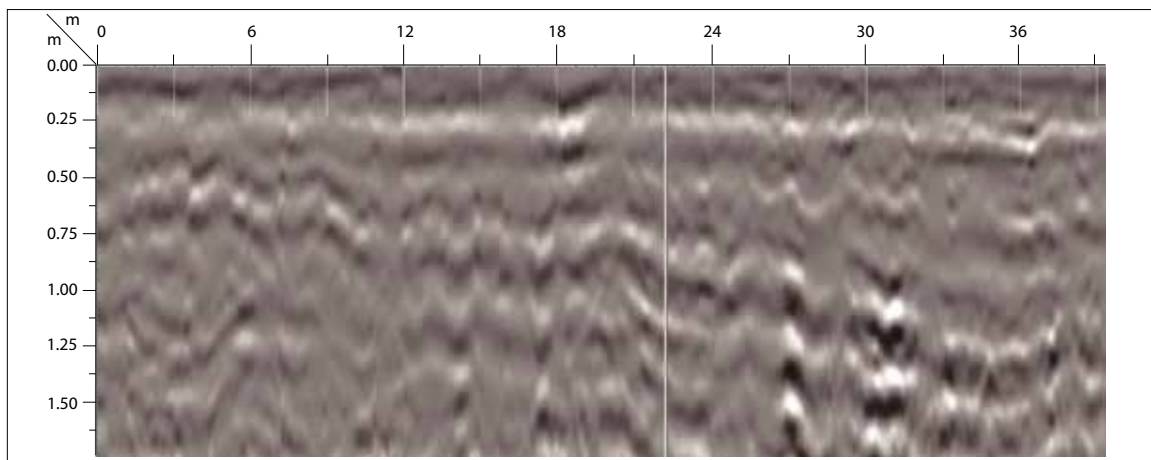


Figure 52. GPR profile from the wind energy project site. The GPR signal did not penetrate to permafrost which was noted at a depth of 207 cm.

The conclusion to be drawn from this site is that permafrost conditions are complex and vary locally, and moderately ice-rich sites tend to be adjacent to zones of unfrozen terrain. A thorough site investigation would be required to delineate non-permafrost zones, including additional drilling, and the use of parallel ERT surveys which could give a three-dimensional view of conditions across the site.

DESTRUCTION BAY TOWNSITE

The surficial geology in the Destruction Bay subdivision is characterized by a thin veneer of eolian silt and sand overlying fluvial fan sediments of sandy gravel and a compact glacial diamict unit. The fan sediments are thickest close to the highway and nearer to the lakeshore. The middle of the subdivision is at a slightly higher elevation than the surrounding area, and gravelly fan sediments are thinner or absent in many spots. The fan sediments overlay a compact glacial diamict that demonstrates some streamlined morphology where it outcrops at surface. Water-well records from the community indicate that this unit is extensive and continues at depth. It is likely that the diamict unit acts as a low-permeability barrier to drainage in the subdivision and is probably subject to permafrost conditions. Also of note at this site, the unit between the highway and waypoint 050 (mapped as szEv.eOv\sgFf.zdMb-X on the accompanying map “*Surficial Geology of Burwash Landing and Destruction Bay*”; Kennedy, 2013) was very poorly drained when we visited the site. Standing water was present along both sides of the road, and new construction on a lot showed that most of the ground was saturated and organic-rich.

Heginbottom and Radburn (1992) classify the unit that includes this site as part of the intermediate discontinuous permafrost zone having low to high ground ice contents (see Figure 29).

To examine permafrost conditions at this study site in more detail, a 160 m-long ERT profile was completed and a permafrost borehole (*DB_Bh1*) was drilled (Figure 53). The ERT profile was conducted from northeast to southwest, beginning at an undeveloped plot populated by tall spruce trees and a mossy groundcover, and transitioning at 104 m along the profile into a FireSmart area (Figure 54). The ground surface at this site undulates slightly and rises by about 3 m over the profile’s length. The profile demonstrates a near-surface low resistivity layer (values <300 ohm m) overlying a higher resistivity layer that has values exceeding 3000 ohm m. These layers are interpreted as representing the active layer and the underlying permafrost. In the first half of the profile, the permafrost clearly extends to greater than the maximum penetration depth of 25 m. Beneath the FireSmart area, it is most likely that the permafrost also extends to 25 m, but if the boundary between frozen and unfrozen soils is around 500 ohm m, it is possible that the base of permafrost is starting to be imaged at a depth of about 15-20 m. The active layer was not always imaged in the other ERT profiles, so the almost-complete continuity displayed for the active layer at this site suggests that its thickness is greater than elsewhere, likely because of the coarse substrate. Based on results from borehole *DB_Bh1*, described below, the active layer is likely to exceed 1.2 m across the entire profile.

Permafrost borehole *DB_Bh1* is located in the forested area at 0 m along the ERT the profile. The first layer (0-25 cm depth) is composed of sandy silt mixed with organic matter and tephra. The second layer (25-78 cm depth) is composed of sandy silt. The deepest layer (78-117 cm depth) is a diamicton (silty sand with gravel). No permafrost was found in the borehole. The complete borehole log is shown in Appendix A9, and grain size analysis results are shown in Appendix C.



Figure 53. Map illustrating detailed site investigations for the Destruction Bay townsite. Refer to Figure 1 for site location.

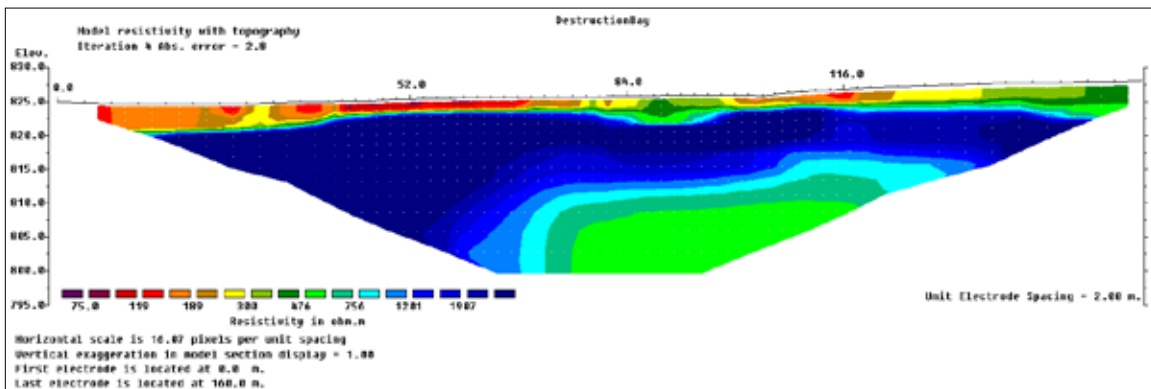


Figure 54. ERT profile northeast to southwest at Destruction Bay (see Figures 1 and 53 for location). The profile is 160 m long with a maximum penetration depth of 25 m. The boundary between frozen and unfrozen materials is interpreted to be at about 300 ohm m (between the yellow and green shades). DB_Bh1 was at 0 m along the profile.

PERMAFROST SENSITIVITY TO ENVIRONMENTAL CHANGE

When mapping hazards in permafrost environments, numerous factors have to be taken into consideration and the entire area under investigation must be studied as a whole. The ground thermal regime of permafrost is influenced by surface conditions and the complex interactions of geophysical factors such as hydrography, topography, vegetation, soil texture and ground ice content (Jorgensen and Osterkamp, 2005). As a result, variations in climate or terrain conditions can both have a great impact on permafrost stability. Higher surface temperatures, variations in depth of snow cover, the presence of infrastructure, and fire disturbances are good examples of changes that can play, at various scales, a major role on permafrost degradation. Additionally, since it is closely linked to local factors, permafrost response to environmental change can be spatially and temporally heterogeneous and can respond differently to geomorphological processes. Therefore, permafrost landscapes will have a dynamic response to environmental change and must be considered with a holistic approach.

Because permafrost stability is essentially maintained by the bonding between ice and the ground particles, when ice melts cohesion is lost and soil stability is diminished (French, 2007). Following an increase in air temperature, the active layer is expected to deepen as the ice contained in the upper part of permafrost (right below the bottom of the active layer) melts, allowing water to flow into soil pores. If the volumetric water content of the ground is lower than the volume of soil pores, the ground is not saturated. Thawing of this type of ground results in moderate surface settlement, which is essentially due to the loss of volume when ground ice melts and soil consolidates. If the volumetric water content of the ground is equal to, or slightly above the volume of soil pores when frozen, the soil is saturated. Thawing of this type of ground results in wet surface conditions, and the soil is unable to consolidate much due to the presence of water in the pore spaces. On sloping terrain, these soil conditions are conducive to subsurface flow, essentially due the loss of volume upon ground ice melting and soil consolidation. If the volumetric water content of the ground is higher than the volume of soil pores, the ground is super-saturated and contains excess ice in its frozen state. Thawing of this type of ground results in severe surface settlement; in this case, it is due the loss of volume when ground ice melts and the soil becomes saturated and eventually begins to drain (Nelson et al., 2002). In flat and gently sloping areas, water ponding is frequent, and on slopes, the release of water builds excess pore water pressure in the soil pores which is conducive to mass movements. Depending on the nature of the soil material and the amount of ground ice, thaw settlement can be significant enough to represent a hazard for development. In terms of permafrost-related hazards, this process represents the principal challenge for planning and development in permafrost environments.

To assess permafrost stability for land-planning purposes, an estimation of the maximum thaw depth that could be reached under the changing climatic conditions is essential, mainly to evaluate the potential deformation that the soil may undergo in the future (Instanes, 2003). The rate and type of deformation is closely linked to the type of surficial deposits present, the ground ice content and how it is distributed in the ground, the ground temperature, and the soil hydrological regime. Recognizing the importance of soil dynamics in evaluating permafrost sensitivity to environmental change, the characteristics and vulnerabilities of the major soil types identified in the study region have been characterized below.

SENSITIVITY OF LOCAL PERMAFROST SOIL TYPES

ORGANIC COVER

Generally occurring at the top of the soil column, the organic cover (i.e., peat) has a very low thermal conductivity when drained and prevents atmospheric heat accumulating in underlying sediment beds (and hence affecting permafrost). The thicker the organic cover, the cooler the permafrost is kept. Under a thick organic mat, the active layer stays thin and colder permafrost may develop. The high porosity of peat allows it to retain an incredible amount of water or ice. Regardless of the presence of a visible cryostructure, peat appears perfectly solid when frozen but becomes highly compressible when thawed. If compression is applied, porosity and hydraulic conductivity decrease while thermal conductivity increases. Since it is one of the most significant drivers for ground ice sustainability, by removing or by compacting the organic cover, degradation of the underlying permafrost may be initiated due the changes in its thermal regime. Additionally, high hydraulic conductivity in areas of groundwater flow can lead to preferential flow paths and discharge areas. When a flow pattern is disturbed by removal or compaction of the organic cover, water accumulation may trigger further localized permafrost degradation by heat advection through groundwater.

UNITS 1 AND 2

Where surficial hydrologic and thermal regimes allow, coarse silt and fine sand may contain a great amount of excess ice in various forms, because they are two materials that present a noticeable ice segregation and settlement potential (Darrow et al., 2008). The potentially over-saturated state of these materials upon thawing can lead directly to a decrease of the ground's bearing capacity. Under natural conditions (i.e., no disturbance, intact organic cover), this degradation will likely happen slowly, by progressively turning ice into water (Dyke and Egginton, 1988). The rate of consolidation will equal the pace of thaw only if hydraulic conductivity is high enough to accommodate the meltwater; otherwise, oversaturation will occur.

UNIT 3

Unit 3 (buried under 1-3 m of eolian and organic deposits) is of an unknown thickness. Because its nature is only partially understood, no precise estimation can be made regarding depth to bedrock. When excluding the coarse particles from this unit, the fine sediments it contains should have a notable segregation potential. The few cryostructures analyzed support this hypothesis (despite exhibiting low ice content; Table 2). Comparable research in Beaver Creek, Yukon, demonstrates that excess ice content decreases with depth in epigenetic permafrost (Stephani et al., 2010). In the finer fraction of Unit 3, over-saturation may occur with thawing when hydraulic conductivity is too low to allow instant consolidation. Such conditions are capable of presenting a mass movement hazard. The unit's potentially oversaturated state under thaw conditions could lead to a decrease in bearing capacity. Despite a high hydraulic conductivity, the good thermal conductivity of this material could result in a thick, relatively well-drained active layer. Even with a well-drained surface, the moisture level at depth can be elevated due to the poor hydraulic conductivity of the frozen material. Where permafrost is present, and there is a lack of effective organic cover, ground temperatures are likely to be higher, and a lower tolerance to any increases in surface temperature will result in faster permafrost degradation.

IMPLICATIONS FOR PERMAFROST IN THE STUDY AREA

Based on the information provided above, and a synthesis of results from the case study investigations, characteristics and implications of environmental change on permafrost in the Burwash Landing and Destruction Bay areas can be projected.

Where permafrost is present, it nearly always extends to the base of the ERT profiles and therefore is thicker than 25 m, with the exceptions of the wind energy project site and the empty lot in Destruction Bay. At the wind energy project site, the ERT profile illustrates the base of permafrost at a depth of 15-20 m, while at the empty lot in Burwash Landing, it is unclear whether any permafrost is present within the shallow ERT profile.

Permafrost in the study area is variably sensitive to changes in surface conditions. FireSmart cutting, like that along the Burwash Landing fire break, left the active layer and permafrost largely unaffected. In other cases, clearing resulted in increased thaw depths and either a very deep active layer or a talik (e.g., the developed area of the Copper Joe subdivision). Greater levels of disturbance can result in deep thaw and the development of taliks that extend to depths of several metres (typically 5-8 m). This development of taliks took place at the Burwash Landing fire break, following a fire in the undeveloped areas of the Copper Joe subdivision, beneath trails or roads in the study area (like those through the Burwash Landing fire break and in the undeveloped areas of the Copper Joe subdivision), and possibly below the empty lot site in Burwash Landing.

At relatively flat sites, lateral changes in permafrost relate primarily to the degree of surface disturbance. At the wind energy project site, however, changes in permafrost conditions relate to topography and the type of sediments present. The permafrost at this site is discontinuous along the profile, as well as perpendicular to it, suggesting complex patterns of distribution at comparable sites. Construction at the wind energy project site should be preceded by careful evaluation of permafrost conditions which may change significantly over short distances.

Borehole logs and previous mapping by Heginbottom and Radburn (1992) indicate that ground ice contents in the study area are generally low to moderate, although ice contents are potentially higher immediately beneath the active layer in the eolian cover. The thickness of permafrost and its sensitivity to disturbance, however, mean that structures built on permafrost with moderate ice content - and subsequently inducing permafrost thaw - may settle slowly and differentially for many years. Considering the fine-grained content of the deeper gravel layer, moderate to ice-rich zones can be encountered in the stratigraphy at depth. This should be taken into account in the design phase of new infrastructure.

None of the boreholes penetrated taliks into the underlying permafrost so it is not known whether the permafrost contains significant amounts of ground ice. It is also not clear whether taliks detected by the ERT profiles are becoming deeper, are stable, or are gradually freezing back. Since disturbance causes these taliks to form and disturbance is almost inevitable during construction activities, it is recommended that a borehole and associated instrumentation be installed at one or two of the talik sites in order to assess the impact of these changes. This monitoring would help determine whether deliberate clearing to induce active thawing of sites in advance of construction would be an appropriate measure. Given that future climate warming will make it harder to preserve permafrost, a technique that uses thawing to prepare land for construction, if feasible, would become progressively easier to use in the future.

It is also important to consider the role fire plays in the distribution and nature of permafrost in the Burwash Landing and Destruction Bay areas. In permafrost areas, forest fires can have a great impact not only on forest ecosystems and wildlife but also on the permafrost thermal

regime. As vegetation is burned, the organic cover that insulates the ground can be lost, resulting in the potential deepening of the active layer. In 1999, an extensive forest fire swept through the Burwash Landing area, forcing the evacuation of residents and destroying several buildings. In total, a little over 3000 hectares was burned (Hirsch, 1999). Fire disturbance mapping was conducted to delineate the burned area within the study area boundary (Figure 55). (It is important to note that fire disturbance mapping did not delineate all areas burned in recent decades; instead, the focus was placed on the areas that were not only burned in the recent past, but that were also still exhibiting low, to moderately low vegetation cover, because of the impact the combination of these conditions can have on permafrost. It is highly likely that a fair amount of the area located southwest of the mapped area, towards the mountains, was also burned, but is not included in Figure 55.)

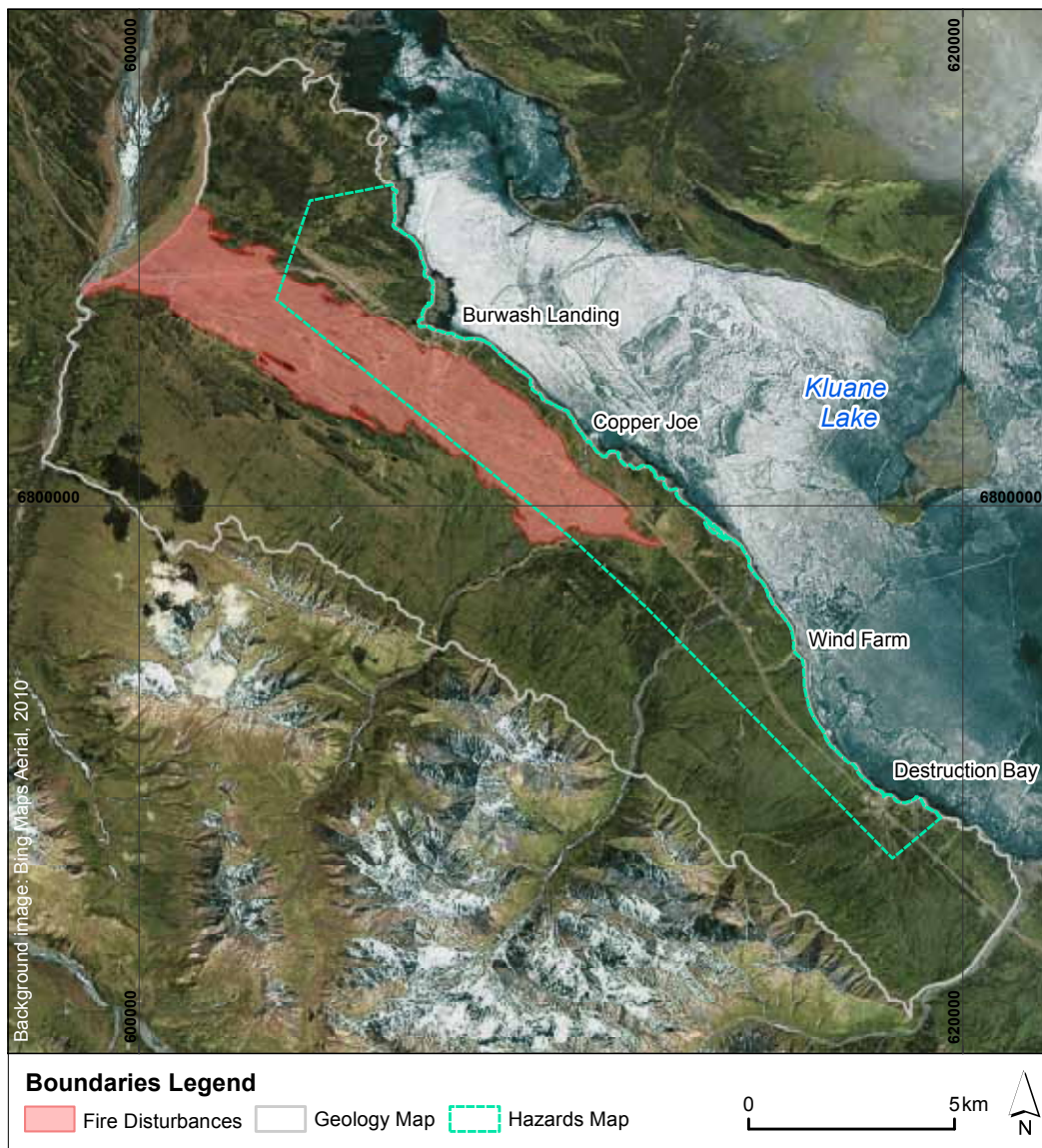


Figure 55. Map delineating the main area disturbed by fire in the Burwash Landing area in 1990.

The fire disturbance map is important, because it indicates permafrost areas in the study region that may be more stable than unburned areas over the next 20-25 years. Permafrost in burned areas is likely to be less sensitive to environmental change because of the following: (1) the upper ice-rich part of the permafrost has already thawed and settled; (2) heat propagation at depth will be slower due to the time delay in heat propagation; and (3) the layers at depth are likely to contain less ice (based on sediment type) than the upper part of the permafrost.

PROJECTED CLIMATE CHANGES IN THE STUDY AREA

Projections of changes in mean annual air temperature (MAAT) were prepared for this report based on annual air temperature modelling, which was enhanced to reflect heterogeneity in the local landscape (specifically, mountainous terrain). The approach used to prepare these projections is described in detail in Appendix D. Generally, projections were prepared based on a series of model scenarios provided by the Scenarios Network for Arctic and Alaska Planning (SNAP, 2012), which incorporates scenarios developed for the Intergovernmental Panel on Climate Change (IPCC, 2007). IPCC scenarios used in the development of the models presented here were B1, A1B and A2, which represent a broad range of potential climate conditions (whereby B1 is the most modest, and A2 is the most severe). Projections were backcast to the period 1950-1979, to provide historical context; projections are also provided for the years 2020, 2050 and 2080.

Figures depicting scenario results are presented in Appendix D1-10, while overall model results are presented in Table 4. The B1 scenario predicts the lowest amount of warming by 2080, due to the nature of the scenario. In the vicinity of the communities, temperatures under this scenario fall between -1.25 and -2.5°C, and the largest changes are predicted in the lowest elevation areas. Significant changes in temperature are seen in the areas directly above treeline – this feature is evident in all scenarios applied. Under the A1B scenario, significantly more warming is seen in comparison with B1. The model also predicts the most overall warming by the 2050 time period. By the end of the 2080 time period, temperatures in the communities are modelled to be between 0 and -1.25°C. Comparable temperatures are seen as a result of modelling using the A2 scenario; however, under the B1 scenario, more overall area is classified as falling between this temperature range, representing the most overall warming of all scenarios. Under both the A1B and A2 scenarios, significant changes are also seen above treeline and into the mountain glacial terrain, which have implications for glacial area and volume. In general, the Burwash Landing and Destruction Bay areas will likely react to changes in air temperature in distinct ways, both above and below treeline, as the result of the heterogeneous nature of landscape in the region.

PROJECTED CLIMATE CHANGE IMPLICATIONS FOR SURFICIAL GEOLOGY

Under the projected climate scenarios presented in this report, risks associated with surficial materials are variable. The primary risks to surficial materials are related to the presence of permafrost in soils. With projected reductions in permafrost within the map area, there is potential for an increase in mass movement events high in drainages that flow into the study area. This may generate an increase in debris flows or flooding events in the study area. While difficult to predict, changes in permafrost may also affect surface and groundwater drainage so that areas that presently have shallow water tables may become wetter or drier (depending on slope), and well-drained areas may become wetter. Additionally, increases in regional moisture delivery could affect stream and lake levels which, in turn, can influence erosion on stream banks and lake shores in the map area.

Table 4. Results of modelled temperature changes for the Burwash Landing area under B1, A1B and A2 climate scenarios, backcast for the 1950-1979 period and forecast for the 2020s, 2050s and 2080s. See Appendix D for details.

Projection Surface	Temperature (°C)		
	Mean	Min	Max
1950 - 1979	-7.74	-21.47	-4.30
B1 2020s	-6.26	-20.00	-2.83
B1 2050s	-5.73	-19.50	-2.30
B1 2080s	-4.79	-18.57	-1.42
A1B 2020s	-6.29	-20.04	-2.87
A1B 2050s	-5.12	-18.89	-1.73
A1B 2080s	-3.80	-17.63	-0.44
A2 2020s	-6.38	-20.13	-2.95
A2 2050s	-5.43	-19.20	-2.02
A2 2080s	-3.57	-17.40	-0.20

PROJECTED CLIMATE CHANGE IMPLICATIONS FOR PERMAFROST

The regional permafrost probability model for the Burwash Landing and Destruction Bay area (presented in *Regional Geological and Permafrost Conditions*, above) can be perturbed by altering the mean annual air temperature (MAAT) to predict the probability of permafrost occurrence in the study area under differing degrees of warming. Scenario temperature changes in this report are indicated in degrees Kelvin (K) in order to avoid confusion with MAATs, which are stated in degrees Celsius. A range of MAAT increases from +1 K to +5 K were investigated based on IPCC and ACIA predictions for the upcoming century. A scenario approach was favoured over applying Global or Regional Climate Model predictions which suffer from inadequate representation of the topography in the Yukon (see Burn, 1994).

The goal of imposing climate change scenarios on the regional permafrost probability model is to examine the sensitivity of the permafrost model response over the long term to changes in MAAT. It is important to note that modelling is done for equilibrium conditions and therefore does not take into account the rate at which the change in climate might occur, nor the lag times associated with permafrost thaw.

Increases in MAAT were simulated in the spatial model by uniformly decreasing the values of equivalent elevation in the transformed DEM (Janke, 2005; Bonnaventure and Lewkowicz, 2011; Lewkowicz and Bonnaventure, 2011), and then running the model to produce an altered basal temperature of snow surface. This affects the predicted permafrost probabilities that are calibrated with the non-linear logistic regression coefficients determined for 1971-2000 climate normal conditions. An increase of 1 K is represented by a decrease in the equivalent elevation surface of 154 m. Even though the change is uniformly applied across the region, it results in differential responses that depend on the surface lapse rates below treeline. This methodology has the advantage of preserving all elements of the spatial model for a given area such as aspect, shading and slope, as well as the specific relationships that exist between changes in elevation and basal temperature of snow values. Although other environmental factors, such as snow and vegetation, significantly influence permafrost distribution in the discontinuous zones (e.g., Smith and Riseborough, 2002) and are expected to alter in the future (e.g., IPCC, 2007), the model cannot take such changes into account, as they are not part of the input variables.

The results of the perturbed permafrost probability modelling show that a relatively small increase in air temperature (+1 K) is likely to have a significant impact on permafrost probability in the region (Figure 56; compare with Figure 35). In the areas adjacent to the Alaska Highway, probabilities decline from 0.5-0.6 to between 0.2 and 0.4. In other words, about half of the permafrost currently in this area is expected to degrade over the long term. A further increase of 1 K reduces the permafrost probability near Kluane Lake to between 0.1 and 0.2 (Figure 57), and with a MAAT increase of +3 K, all this terrain becomes part of the isolated patches of permafrost (probabilities less than 0.1; Figure 58). There is little additional change in permafrost probabilities close to the lake as the MAAT increases further because there is so little permafrost remaining (Figures 59 and 60).

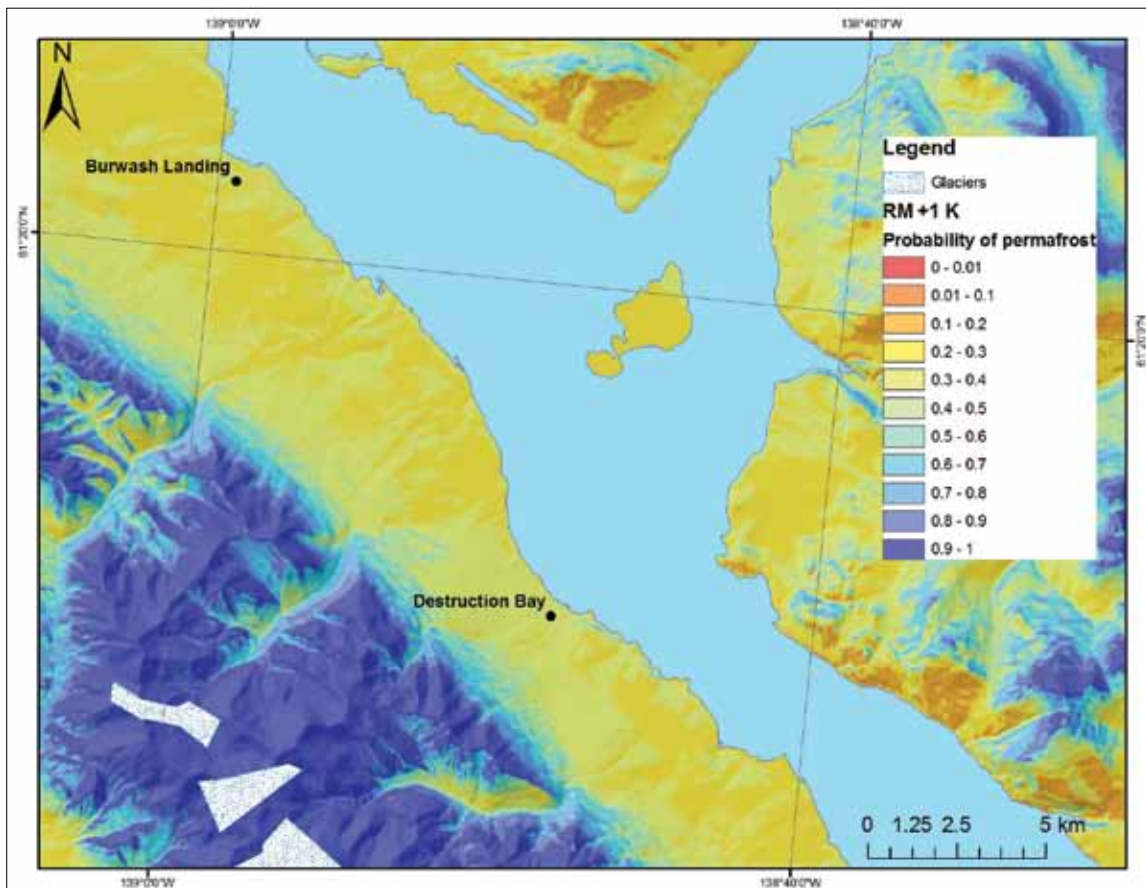


Figure 56. Permafrost probability for the area around Burwash Landing and Destruction Bay depicting an increase in MAAT of +1 K. Note that glacier extent is highly generalized.

The pattern of permafrost loss is different in the Kluane Range to the southwest of Burwash Landing and Destruction Bay. There is a strong topographic influence on probabilities which therefore increase at high elevations above tree line. With increasing MAATs, the area of high probability decreases, but even for the +5 K change, there are small areas of probability greater than 0.9 on the highest peaks (Figure 60). This loss of permafrost may happen with shorter lag times than in the lowlands because rocks are less likely to have a significant ice content (see Figure 29) and so there is little to no latent heat to satisfy as the ground thaws. In addition, the lack of a substantial buffering layer of vegetation and organic mat means that the ground is likely to react more quickly to changes in air temperature than at sites below tree line.

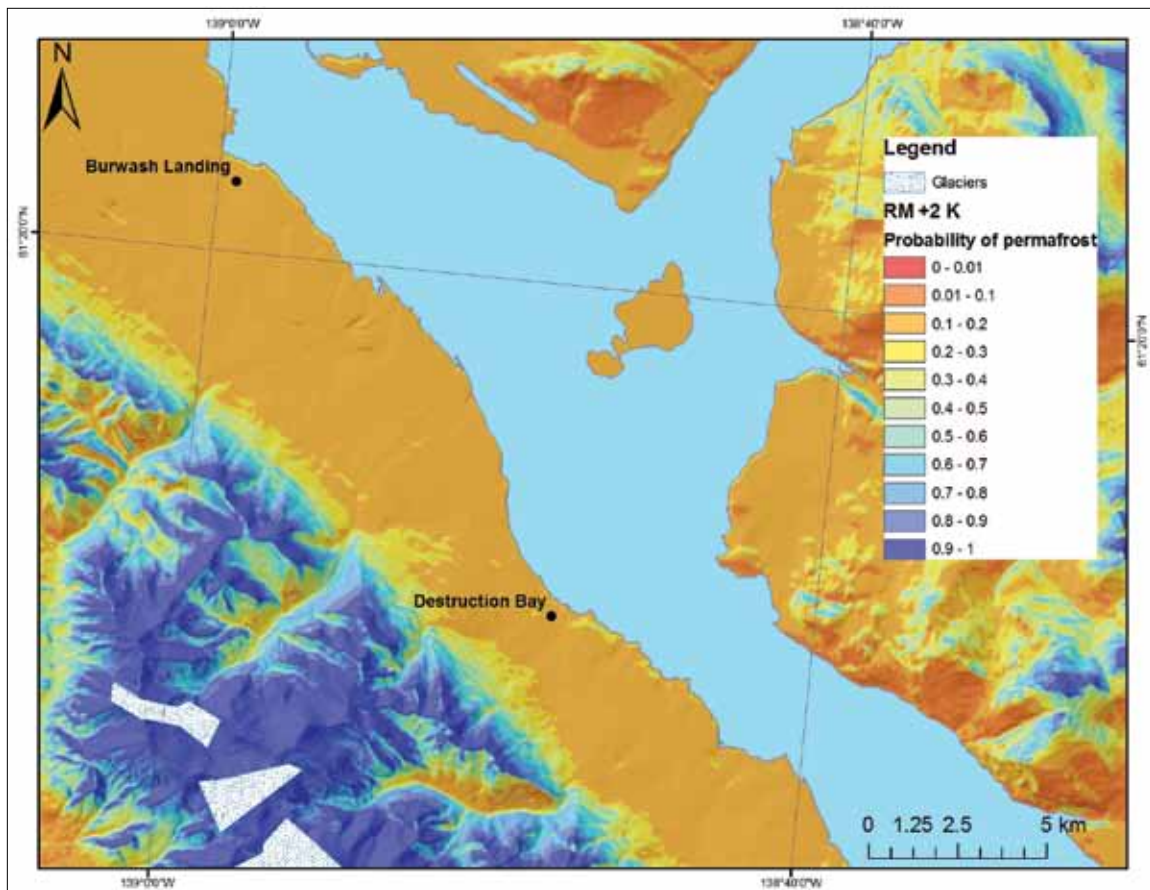


Figure 57. Permafrost probability for the area around Burwash Landing and Destruction Bay depicting an increase in MAAT of +2 K. Note that glacier extent is highly generalized.

The permafrost probability modelling indicates that 50-60% of the terrain in the vicinity of the communities is currently underlain by permafrost and that a rise in temperatures of only 1 K (equivalent to 1°C) in mean annual air temperature would have a very significant impact over the long term, potentially halving the amount of permafrost. A further increase of 1 K would halve again the remaining permafrost. These changes would affect terrain with temperatures close to 0°C first, followed by the colder sites, but overall there would be widespread impact. Increasing permafrost temperature close to the thawing point will increase the unfrozen content of the ground and therefore lead to a decrease of the ground bearing capacity which can cause shifting of infrastructure.

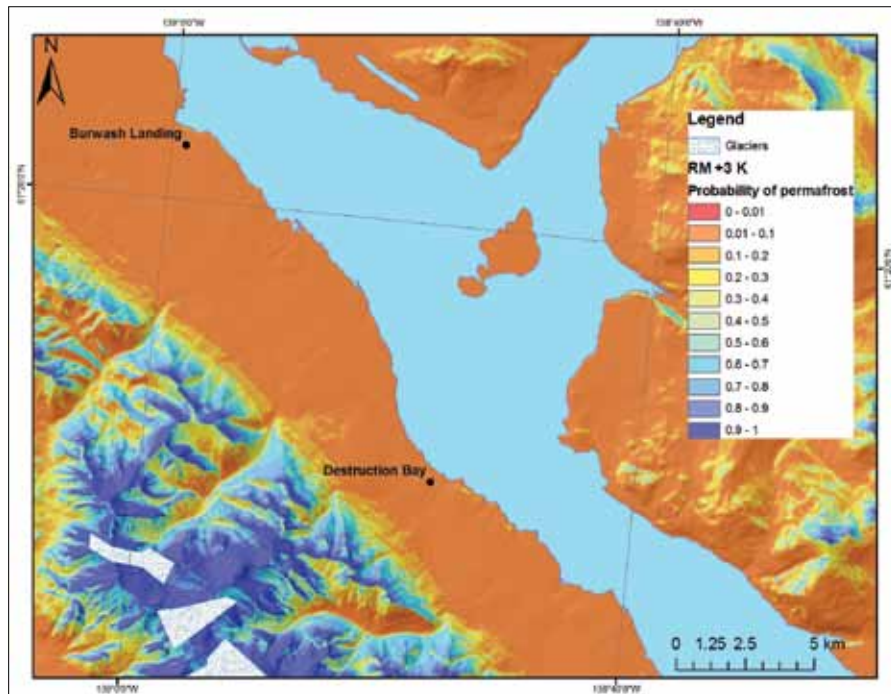


Figure 58. Permafrost probability for the area around Burwash Landing and Destruction Bay depicting an increase in MAAT of +3 K. Note that glacier extent is highly generalized.

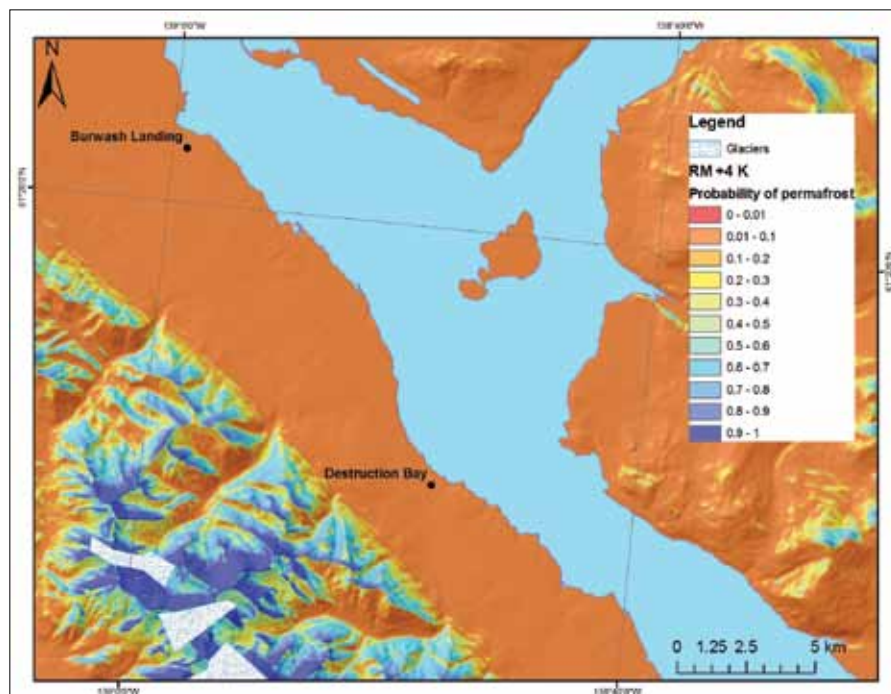


Figure 59. Permafrost probability for the area around Burwash Landing and Destruction Bay depicting an increase in MAAT of +4 K. Note that glacier extent is highly generalized.

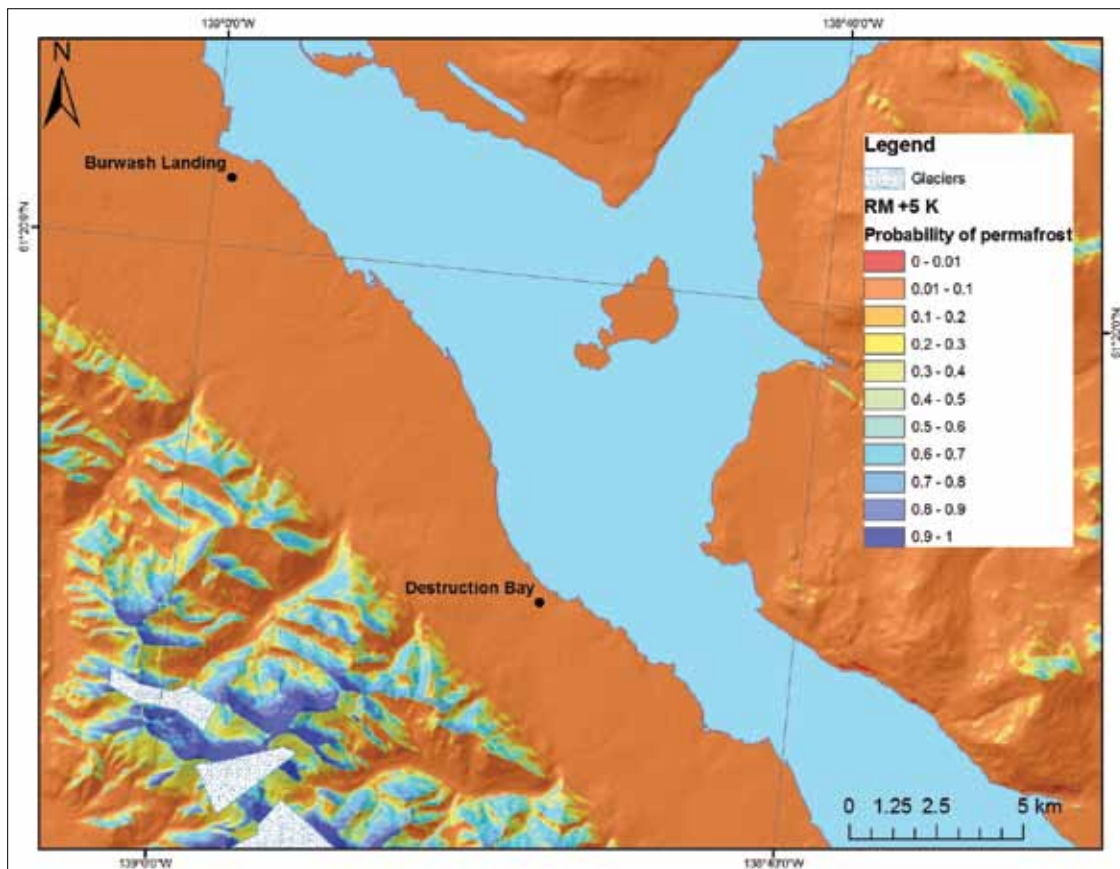


Figure 60. Permafrost probability for the area around Burwash Landing and Destruction Bay depicting an increase in MAAT of +5 K. Note that glacier extent is highly generalized.

HAZARDS CLASSIFICATION

Results from study site characterizations, case study investigations, laboratory analyses, climate projections and contemporary and future permafrost probability modelling in the Burwash Landing and Destruction Bay regions were used to identify current and future landscape hazards for the study area. The combined properties of surficial material type, landform shape and slope, local hydrology, climate regime, and permafrost conditions have been used to arrive at a set of hazard rankings that can be used to assess the potential stability of landscape units in the study region. The following four classes of hazard risk were developed:

- **Green:** no risk of permafrost degradation, **no** risk of geologic hazards.
- **Yellow:** moderate risk of permafrost degradation (i.e., moderate thaw settlement) **or** moderate risk of geologic hazards.
- **Orange:** moderate to high risk of permafrost degradation (i.e., moderate thaw settlement on flat terrain, poor drainage, and slow mass movement on slopes due to high pore water pressure) **and** moderate risk of geologic hazards.
- **Red:** moderate to high risk of permafrost degradation (i.e., high thaw settlement, water ponding, and slow to rapid mass movement on slopes due to excess pore water pressure) **and/or** high risk of geologic hazards.

In classifying polygons, we have taken a precautionary approach and applied a category of higher risk where we are not confident in lower categories. However, every polygon will contain zones of lower and higher risk than the overall polygon classification. It is for this reason that this map should serve only as an initial guide for planning purposes. Any development will still require detailed site investigations. It is also important to note that hazard rankings are based on general observations of surface materials, drainage, slope angle, vegetation and the presence of permafrost landforms, as well as subsurface information provided by ERT and GPR profiles, drilling and probing of permafrost, and textural analyses of surficial and borehole samples. This has resulted in a projected risk ranking that will require geotechnical and/or engineering analyses to quantify.

Results of hazards classification for the map area (outlined on Figure 1) are presented in Figure 61 (see a larger print version of this map in back pocket). Appendix E details the hazard classification assigned to each numbered polygon in the map area, and outlines its associated hazard(s). General results are summarized below.

As the case study investigations described in this report demonstrate, permafrost in the study area is highly heterogeneous and spatially variable. It represents the most prevalent hazard encountered throughout the map area. Nearly all polygons exhibit this hazard, with the exception of a limited number of units that are located in areas of high risk for flooding (e.g., polygons 12, 47, 62 and 103). As a result of the extensive and predominant nature of permafrost in the study region, no polygons in the hazards map area were classified as green (i.e., as having no risk of permafrost degradation or geological hazards).

The majority of polygons in the study area (~80%) are classified as either yellow or orange. Most polygons affected by the region's 1999 forest fire (e.g., polygons 114, 128 and 130) were classified as yellow, because areas within the fire disturbance limits (see Figure 55) are most likely underlain by permafrost with a deeper active layer and warmer thermal profile than surrounding non-burned areas. However, organic parcels within the burned area (e.g., polygons 123, 132 and 148) were classified as red, reflecting their poor drainage capacity. The few remaining polygons classified as yellow that are not located within the fire disturbance limits represent either old inactive fluvial terraces potentially susceptible to large-scale floods (e.g., polygons 43, 50 and 69), or units composed of well-drained morainal material (e.g., polygons 56, 60, 66 and 79).

Half of the map area has been classified as orange (i.e., as having moderate to high risk of permafrost degradation and moderate risk of geological hazards). The predominant hazard exhibited by these polygons is related to the presence of permafrost. Additionally, most of these units are composed in part of finer material (e.g., morainal units), which gives them an elevated probability of containing ice in excess of the soil porosity, thus increasing their susceptibility to significant thaw settlement.

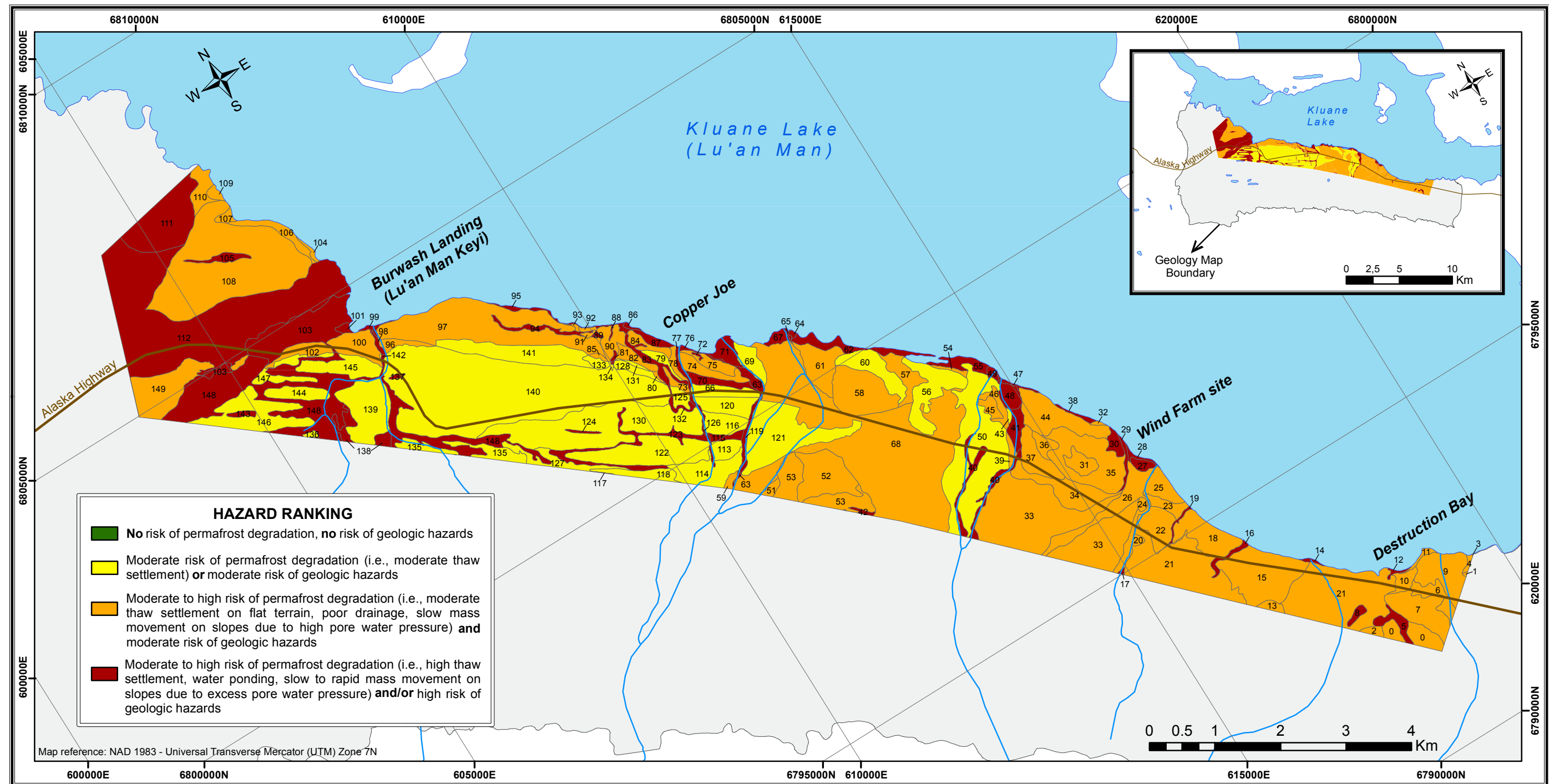


Figure 61. Map depicting results of hazards classification for the Burwash Landing and Destruction Bay areas (see Figure 1 for location of map boundary). Specific hazards associated with each numbered polygon are listed in Appendix E.

BLANK PAGE

Polygons ranked as red (i.e., as having moderate to high risk of permafrost degradation and high risk of geological hazards) constitute 20% of the map area, and are relatively small and scattered. This class encompasses all the organic and lacustrine units in the map area. It also includes all active fluvial units, because their active states render them inappropriate for development. Most polygons presenting a risk of seasonal flooding or poor drainage were also classified as red. However, this class excludes a few beach landforms that were either very steep (e.g., polygons 104, 107 and 109) or at a relatively high elevation (e.g., polygon 11). These four units were classified as orange, because only very large floods could represent a hazard risk. Polygons classified as red represent poor choices for development.

It is important to note that, because no polygons in the study area have been classified as green, any development in the Burwash Landing and Destruction Bay areas will take place on ground containing some percentage of permafrost. To assist in planning and development activities in the area, Appendix F details considerations and potential development options for construction on permafrost.

GENERATING ACTION FROM SCIENCE

The knowledge and data generated by the Burwash Landing and Destruction Bay hazards mapping project can be used to inform planning and policy development and establish a baseline from which future science can be generated. It is the hope of the authors that the information contained herein informs planning and decision-making processes in the Burwash Landing and Destruction Bay areas.

This project has contributed to the assessment of vulnerability for the Burwash Landing and Destruction Bay areas. In particular, this project has characterized the local landscape and assessed local hazards, while advancing our understanding of potential climate change impacts in the region. This information may serve as a basis for evaluating how community infrastructure, security and well-being may be influenced by climate variability, and how the community might take action to respond. By integrating variability into decision-making through multiple scenarios, robust and responsive adaptation strategies can be developed. In this way, the science of hazard assessment is an important foundation from which to build action.

BLANK PAGE

REFERENCES

- ASTM Standard C29 – 09, 2000. Standard Test Method Bulk Density (“Unit Weight”) and Voids in Aggregate. West Conshohocken, PA, ASTM International.
- ASTM Standard D422 – 63, 2000. Standard Test Method for Particle-Size Analysis of Soils. West Conshohocken, PA, ASTM International.
- ASTM Standard D854 – 10, 2000. Standard Test Methods for Specific Gravity of Soil Solids by Water Pycnometer. West Conshohocken, PA, ASTM International.
- ASTM Standard D4318 – 00, 2000. Standard Test Methods for Liquid Limit, Plastic Limit, and Plasticity Index of Soils. West Conshohocken, PA, ASTM International.
- ASTM Standard D5334 – 08, 2000. Standard Test Method for Determination of Thermal Conductivity of Soil and Soft Rock by Thermal Needle Probe Procedure. West Conshohocken, PA, ASTM International.
- Berg, E.E. and Henry, J.D., 2003. The history of spruce bark beetle outbreak in the Kluane region as determined from the dendrochronology of selected forest stands. Parks Canada Report, 48 p.
- Bonnaventure, P.P. and Lewkowicz, A.G., 2011. Modelling climate change effects on the spatial distribution of mountain permafrost at three sites in northwest Canada. *Climatic Change*, vol. 105, issue 1-2, p. 293-312, doi:10.1007/s10584-010-9818-5.
- Bonnaventure, P.P., Lewkowicz, A.G., Kremer, M. and Sawada, M., 2012. A regional permafrost probability model for the southern Yukon and northern British Columbia, Canada. *Permafrost and Periglacial Processes*, vol. 23, p. 52-68, doi:10.1002/ppp.1733.
- Borns Jr., H.W. and Goldthwait, R.P., 1966. Late-Pleistocene fluctuations of Kaskawulsh Glacier. *American Journal of Science*, vol. 269, p. 600-619.
- Bostock, H.S., 1969. Kluane Lake, Yukon Territory, its drainage and allied problems. Geological Survey of Canada, Paper 69-28, p. 36-65.
- Brahney, J., Clague, J.J., Menounos, B. and Edwards, T.W.D., 2010. Late Holocene paleohydrology of Kluane Lake, Yukon Territory, Canada. *Journal of Paleolimnology*, vol. 44, p. 873-885.
- Brahney, J., Clague, J.J., Menounos, B. and Edwards, T.W.D., 2008a. Geochemical reconstruction of late Holocene drainage and mixing in Kluane Lake, Yukon Territory. *Journal of Paleolimnology*, vol. 40, p. 489-505.
- Brahney, J., Clague, J.J., Menounos, B. and Edwards, T.W.D., 2008b. Timing and cause of water level fluctuations in Kluane Lake, Yukon Territory, over the past 5000 years. *Quaternary Research*, vol. 70, p. 213-227.
- Burn, C.R., 1994. Permafrost, tectonics, and past and future regional climate change, Yukon and adjacent Northwest Territories. *Canadian Journal of Earth Sciences*, vol. 31, p. 182-191.
- Campbell, R.B. and Dodds, C.J., 1982. Geology, Kluane Lake map area (115F and G). Geological Survey of Canada Open File 829.
- Clague, J.J., Luckman, B.H., Van Dorp, R.D., Gilbert, R., Froese, D., Jensen, B.J.L. and Reyes, A.V., 2006. Rapid changes in the level of Kluane Lake in Yukon Territory over the last millennium. *Quaternary Research*, vol. 66, p. 342-355.

- Clague, J.J., 1981. Landslides at the south end of Kluane Lake, Yukon Territory. *Canadian Journal of Earth Sciences*, vol. 18, p. 959-971.
- Clague, J.J., 1979. The Denali Fault System in southwestern Yukon Territory – A geologic hazard? *Geological Survey of Canada Paper 79-1A*, p. 169-178.
- Cobbett, R.N., 2011. Timing and Kinematics of the Duke River fault: Insights into the evolution of the Insular Terrane, Southwest Yukon. cIRcle: UBC's Digital Repository: Electronic Theses and Dissertations (ETDs) 2008+ <http://hdl.handle.net/2429/38156>
- Conyers, L., 2004. *Ground-Penetrating Radar for Archaeology*. AltaMira Press, Walnut Creek, California, 209 p.
- Cutter, S.L., 1996. Vulnerability to environmental hazards. *Progress in Human Geography*, vol. 20, p. 529-539.
- Darcy, H., 1856. *Les fontaines publiques de la ville de Dijon*. Dalmont, Paris, 647 p. & atlas.
- Darrow, M.M., Huang, S.L., Shur, Y. and Akagawa, S., 2008. Improvements in frost heave laboratory testing of fine-grained soils. *Journal of Cold Regions Engineering*, vol. 22, p. 65-78.
- Denton, G.H. and Stuiver, M., 1966. Neoglacial chronology, northeastern St. Elias Mountains, Canada. *American Journal of Science*, vol. 264, p. 577-599.
- Denton, G. H. and Stuiver, M., 1967. Late Pleistocene glacial stratigraphy and chronology, northeastern Saint Elias Mountains, Canada. *Geological Society of America Bulletin*, vol. 78, p. 485-510.
- Duk-Rodkin, A., 1999. *Glacial Limits Map of Yukon*, Yukon Geological Survey, Geoscience Map, 1999-2; GSC Open File 3694.
- Dyke, L. and Egginton, P.A., 1988. Till behavior and its relationship to active-layer hydrology, District of Keewatin, Northwest Territories. *Canadian Geotechnical Journal*, vol. 25, p. 167-172.
- Environment Canada, 2013. *Canadian Climate Normals 1971-2000*. Environment Canada, Ottawa, Ontario, http://www.climate.weatheroffice.gc.ca/climate_normals/index_e.html
- Etzelmüller, B., Farbrót, H., Guomundsson, A. and Humlum, O., 2007. The regional distribution of mountain permafrost in Iceland. *Permafrost and Periglacial Processes*, vol. 18, p. 185-199.
- Ford, J.D., 2008. Emerging trends in climate change policy: the role of adaptation. *International Public Policy Review*, vol. 3, p. 5-16.
- Ford, J.D., Smit, B., Wandel, J., Allurut, M., Shappa, K., Ittusarjuat, H. and Qrunnut, K., 2008. Climate change in the Arctic: current and future vulnerability in two Inuit communities in Canada. *The Geographical Journal*, vol. 174, p. 45-62.
- Ford, J.D. and Smit, B., 2004. A framework for assessing the vulnerability of communities in the Canadian Arctic to risks associated with climate change. *Arctic*, vol. 57, p. 389-400.
- Foy, N., Copland, L., Zdanowicz, C., Demuth, M. and Hopkinson, C., 2011. Recent volume and area changes of Kaskawulsh Glacier, Yukon, Canada. *Journal of Glaciology*, vol. 57, p. 515-525.
- French, H.M., 2007. *The Periglacial Environment*, 3rd edition. John Wiley and Sons, West Sussex, England, 478 p.

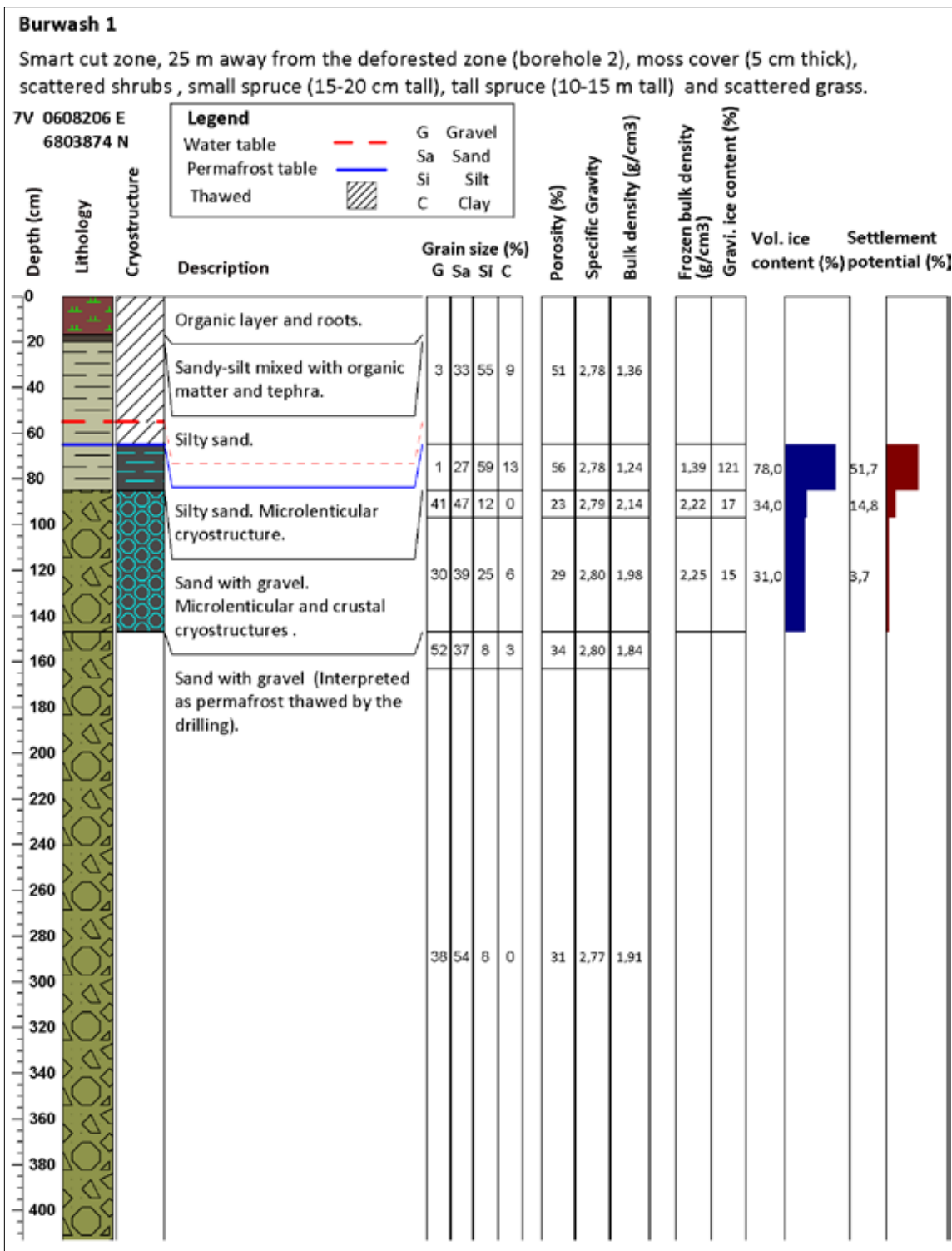
- Geomatics Yukon, 2011. Fire History Datasets. Wildland Fire Management, Community Services, Yukon Government, <http://www.geomatics Yukon.ca/data/datasets>
- Global Terrestrial Network on Permafrost, 2013, <http://www.gtnp.org/>
- Grandmont, K., Cardille, J.A., Fortier, D. and Gibéryen, T., 2012. Assessing land suitability for residential development in permafrost regions: a multi-criteria approach to land-use planning in Northern Quebec, Canada. *Journal of Environmental Assessment Policy and Management*, vol. 14, doi:10.1142/S146433321250032.
- Hauck, C., Isaksen, K., Vonder Mühll, D. and Sollid, J.L., 2004. Geophysical surveys designed to delineate the altitudinal limit of mountain permafrost: an example from Jotunheimen, Norway. *Permafrost and Periglacial Processes*, vol. 15, p. 191-205, doi:10.1002/ppp.493.
- Heginbottom, J.A., Dubreuil, M.A. and Harker, P.T., 1995. Permafrost Map of Canada. *In: The National Atlas of Canada, 5th Edition, (1978-1995)*, published by Natural Resources Canada, sheet MRC 4177, 1:7 500 000 scale.
- Heginbottom, J. A. and Radburn, L.K., 1992. Permafrost and ground ice conditions of Northwest Canada. Geological Survey of Canada, Map 1691A, scale 1:1 000 000.
- Hilbich, C., Hauck, C., Hoelzle, M., Scherler, M., Schudel, L., Voelksch, I., Vonder Muehll, D. and Maüsbacher, R., 2008. Monitoring mountain permafrost evolution using electrical resistivity tomography: a 7-year study of seasonal, annual, and long-term variations at Schilthorn, Swiss Alps. *Journal of Geophysical Research-Earth Surface*, vol. 113, doi:10.1029/2007JF000799.
- Hilbich, C., Marescot, L., Hauck, C., Loke, M.H. and Maüsbacher, R., 2009. Applicability of electrical resistivity tomography monitoring to coarse blocky and ice-rich permafrost landforms. *Permafrost and Periglacial Processes*, vol. 20, p. 269-284, doi:10.1002/ppp.652.
- Hirsch, K.G., 1999. Canada's wildland-urban interface: challenges and solutions. (Zones périurbaines du Canada: défis et solutions.) Natural Resources Canada, Canadian Forest Service, Northern Forestry Centre, Edmonton, AB, 8 p.
- Huntington, H. and Weller, G., 2005. Chapter 1: An Introduction to the Arctic Climate Impact Assessment. *In: Arctic Climate Impact Assessment Scientific Report*, C. Symo, L. Arris and B. Heal (eds.), Cambridge University Press, p. 1-20.
- Huscroft, C.A., Lipovsky, P.S. and Bond, J.D., 2004. A regional characterization of landslides in the Alaska Highway corridor, Yukon. Yukon Geological Survey, Open File 2004-18, 65 p., report and CD-ROM.
- Instanes, A., 2003. Climate change and possible impact on Arctic infrastructure. *Proceedings of the Eighth International Conference on Permafrost, Zürich, Switzerland*, p. 461-466.
- IPCC, 2007. <http://www.ipcc.ch/ipccreports/assessments-reports.htm>
- Janke, J.R., 2005. Modelling past and future alpine permafrost distribution in the Colorado Front Range. *Earth Surface Processes and Landforms*, vol. 30, p. 1495-1508, doi: 10.1002/esp.1205.
- Janowicz, R., 2008. Apparent recent trends in hydrologic response in permafrost regions of northwest Canada. *Hydrology Research*, vol. 39, p. 267-275.
- Jorgenson, M.T. and Osterkamp, T.E., 2005. Response of boreal ecosystems to varying modes of permafrost degradation. *Canadian Journal of Forest Research*, vol. 35, p. 2100-2111, doi:10.1139/x05-153.

- Kennedy, K.E., 2013. Surficial geology of Burwash Landing and Destruction Bay (parts of NTS 115G/2, 6 and 7). Yukon Geological Survey, Open File 2013-14.
- Kneisel, C., Hauck, C. and Vonder Mühll, D., 2000. Permafrost below the timberline confirmed and characterized by geoelectrical resistivity measurements, Bever Valley, eastern Swiss Alps. *Permafrost and Periglacial Processes*, vol. 11, p. 295-304, doi:10.1002/1099-1530(200012)11:4<295::AID-PPP353>3.0.CO;2-L.
- Kneisel, C., Hauck, C., Fortier, R. and Moorman, B., 2008. Advances in geophysical methods for permafrost investigations. *Permafrost and Periglacial Processes*, vol. 19, p. 157-178.
- Koch, J., Clague, J.J. and Blais-Stevens, A., *in press*. Debris flow chronology and potential hazard along the Alaska Highway in southwest Yukon Territory. *Environmental and Engineering Geoscience*. Submitted February 4, 2013.
- Lewkowicz, A.G. and Bonnaventure, P.P., 2011. Equivalent elevation: a method to incorporate variable lapse rates into mountain permafrost modeling. *Permafrost and Periglacial Processes*, vol. 22, p. 153-162.
- Lewkowicz, A.G. and Ednie, M., 2004. Probability mapping of mountain permafrost using the BTS method, Wolf Creek, Yukon Territory, Canada. *Permafrost and Periglacial Processes*, vol. 15, p. 67-80.
- Lewkowicz, A.G., Etzelmüller, B.E. and Smith, S.L., 2011. Characteristics of discontinuous permafrost from ground temperature measurements and electrical resistivity tomography, southern Yukon, Canada. *Permafrost and Periglacial Processes*, vol. 22, p. 320-342.
- Lipovsky, P.S., Seitz, G.J., Haeussler, P.J., Crone, A.J., Schwartz, D.P., Clague, J.J., Mazzotti, S. and Cobbett, R., 2009. Neotectonics investigations in southwestern Yukon. CANQUA-CGRG Biennial Meeting. May 3-8, 2009. Simon Fraser University, Burnaby Campus, Burnaby, British Columbia. Programme and Abstracts Volume, p. 123.
- Loke, M.H. and Barker, R.D., 1996. Rapid leastsquares inversion of apparent resistivity pseudosections using a quasi-Newton method. *Geophysical Prospecting*, vol. 44, p. 131-152, doi:10.1111/j.1365-2478.1996.tb00142.x
- Loke, M.H., Acworth, I. and Dahlin, T., 2003. A comparison of smooth and blocky inversion methods in 2D electrical imaging surveys. *Exploration Geophysics*, vol. 34, p. 182-187.
- Miceli, C., 2012. Seasonal cycling in electrical resistivities at ten thin permafrost sites, southern Yukon and northern British Columbia. Unpublished M.Sc. thesis, Department of Geography, University of Ottawa, ON, 201 p.
- Murton, J.B. and French, H.M., 1994. Cryostructures in permafrost, Tuktoyaktuk coastlands, western arctic Canada. *Canadian Journal of Earth Sciences*, vol. 31, no. 4, p. 737-747.
- NCE (Northern Climate Exchange), 2011. Mayo Landscape Hazards: Geological Mapping for Climate Change Adaptation Planning. Yukon Research Centre, Yukon College, Whitehorse, YT, 64 p.
- Nakicenovic, N., Davidson, O., Davis, G., Grübler, A., Kram, T., La Rovere, E.L., Metz, B., Morita, T., Pepper, W., Pitcher, H., Sankovski, A., Shukla, P., Swart, R., Watson, R. and Dadi, Z., 2000. Emissions Scenarios: A Special Report of Working Group III of Intergovernmental Panel on Climate Change. Intergovernmental Panel on Climate Change, Geneva, Switzerland, 27 p.
- Nelson, F.E., Anisimov, O.A. and Shiklomanov, N.I., 2002. Climate change and hazard zonation in the circum-Arctic permafrost regions. *Natural Hazards*, vol. 26, p. 203-225.

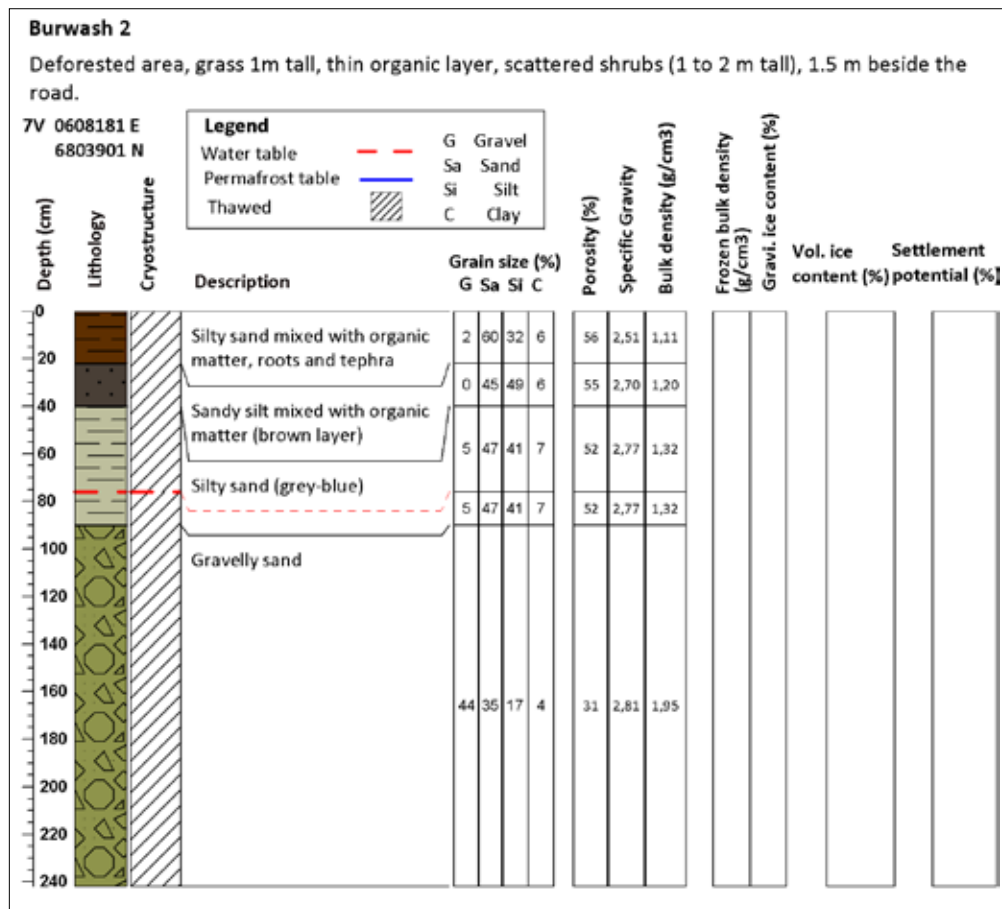
- Page, A., 2009. A topographic and photogrammetric study of rock glaciers in the southern Yukon Territory. Unpublished M.Sc. thesis, Department of Geography, University of Ottawa, 160 p.
- Rampton, V.N., 1969. Pleistocene geology of the Snag-Klutan area, southwestern Yukon, Canada. Ph.D. thesis, University of Minnesota, Duluth, Minnesota.
- Rampton, V.N., 1980a. Surficial geology and geomorphology, Burwash Landing, Yukon Territory. Geological Survey of Canada. Geological Survey of Canada Map 6-1978, NTS 115G/06, 07, 10, 11, 1:100 000 scale.
- Rampton, V.N., 1980b. Surficial geology and geomorphology, Congdon Creek, Yukon Territory. Geological Survey of Canada Map 8-1978, NTS 115B/15, 16 & 115G 01,02, 1:100 000 scale.
- Rampton, V.N., 1980c. Surficial geology and geomorphology, Generic River, Yukon Territory. Geological Survey of Canada Map 7-1978, NTS 115F NE & 115G/12, 13, 1:100 000 scale.
- Rampton, V.N., 1980d. Surficial geology and geomorphology, Koidern Mountain, Yukon Territory. Geological Survey of Canada Map 5-1978, NTS 115K SE, 1:100 000 scale.
- Rampton, V.N., 1980e. Surficial geology and geomorphology, Mirror Creek, Yukon Territory. Geological Survey of Canada Map 4-1978, NTS 115K NE, 1:100 000 scale.
- Rampton, V.N., 1981. Surficial materials and landforms of Kluane National Park, Yukon Territory. Geological Survey of Canada, Paper 79-24, 37 p. (includes maps 13-1979 and 14-1979).
- Rampton, V.N. and Paradis, S., 1981a. Surficial geology and geomorphology Taye Lake, Yukon Territory. Geological Survey of Canada Map 14-1981, 1:100 000 scale.
- Rampton, V.N. and Paradis, S., 1981b. Surficial geology and geomorphology of Pine Kake, Yukon Territory. Geological Survey of Canada Map 16-1981, 1:100 000 scale.
- Rampton, V.N. and Shearer, J.M., 1978. The geology and limnology of Kluane Lake, Yukon Territory, I preliminary assessment. Geological Survey of Canada Open File 527 prepared for Terrain Sciences Division Geological Survey of Canada, Terrain Analysis and Mapping Services Ltd., Stittsville, ON, 61 p.
- Reyes, A.V., Luckman, B.H., Smith, D.J., Clague, J.J. and Van Dorp, R.D., 2006. Tree-ring dates for the maximum Little Ice Age advance of Kaskawulsh Glacier, St. Elias Mountains, Canada. *Arctic*, vol. 59, p. 14-20.
- Sawada, M. and Johnson, P.G., 2000. Hydrometeorology, suspended sediment and conductivity in a large glacierized basin, Slims River, Yukon Territory, Canada (1993-94). *Arctic*, vol. 53, p. 101-117.
- Seitz, G.J., Haeussler, P.J., Crone, A.J., Lipovsky, P. and Schwartz, D.P., 2008. Eastern Denali Fault slip rate and paleoseismic history, Kluane Lake area, Yukon Territory, Canada. AGU Fall Meeting, San Francisco, CA, December 15-19, 2008, poster T53B-1947.
- Smith, M.W. and Riseborough, D.W., 2002. Climate and the limits of permafrost: a zonal analysis. *Permafrost and Periglacial Processes*, vol. 13, p. 1-15.
- Smith, C.A.S., Mickle, J.C. and Roots, C.F. 2004. Ecoregions of the Yukon Territory – Biophysical Properties of Yukon Landscapes. PARC Technical Bulletin 04-01. Summerland, British Columbia: Agriculture and Agri-Food Canada, 313 p.
- SNAP (Scenarios Network for Alaska and Arctic Planning), 2012. www.snap.uaf.edu

- Stephani, E., Fortier, D. and Shur, Y., 2010. Applications of cryofacies approach to frozen ground engineering – Case study of a road test site along the Alaska Highway (Beaver Creek, Yukon, Canada). GEO2010: 63rd Canadian Geotechnical Conference and 6th Canadian Permafrost Conference, Calgary, Canada.
- Thomalla, F., Downing, T., Spanger-Seigfried, E., Han, G. and Rockström, J., 2006. Reducing hazard vulnerability: towards a common approach between disaster risk reduction and climate adaptation. *Disasters*, vol. 30, p. 39-48.
- Wahl, H.E., Fraser, D.B., Harvey, R.C. and Maxwell, J.B., 1987. *Climate of Yukon*. Climatological Studies Number 40. Ottawa, Ontario: Atmospheric Environment Service, Environment Canada, 233 p.
- Yukon Bureau of Statistics, 2012. Information Sheet #58.41 – June 2012: Population Report. Government of Yukon Executive Council Office Bureau of Statistics, Whitehorse, Yukon, 4 p.
- Yukon Bureau of Statistics, 2009. Information Sheet #C06-12 – July 2009: Housing and Shelter Costs. Government of Yukon Executive Council Office Bureau of Statistics, Whitehorse, Yukon, 4 p.
- Yukon Bureau of Statistics, 2008. Information Sheet #C06-08 – April 2008: Aboriginal Data. Government of Yukon Executive Council Office Bureau of Statistics, Whitehorse, Yukon, 4 p.
- Yukon Bureau of Statistics, 2007. Information Sheet #C06-01 – March 2007: Population and Dwelling Counts. Government of Yukon Executive Council Office Bureau of Statistics, Whitehorse, Yukon, 4 p.
- Yukon Community Profiles, 2004. Kluane First Nation – Communities of Burwash Landing and Destruction Bay, <http://www.yukoncommunities.yk.ca/communities/burwash-destruction/>

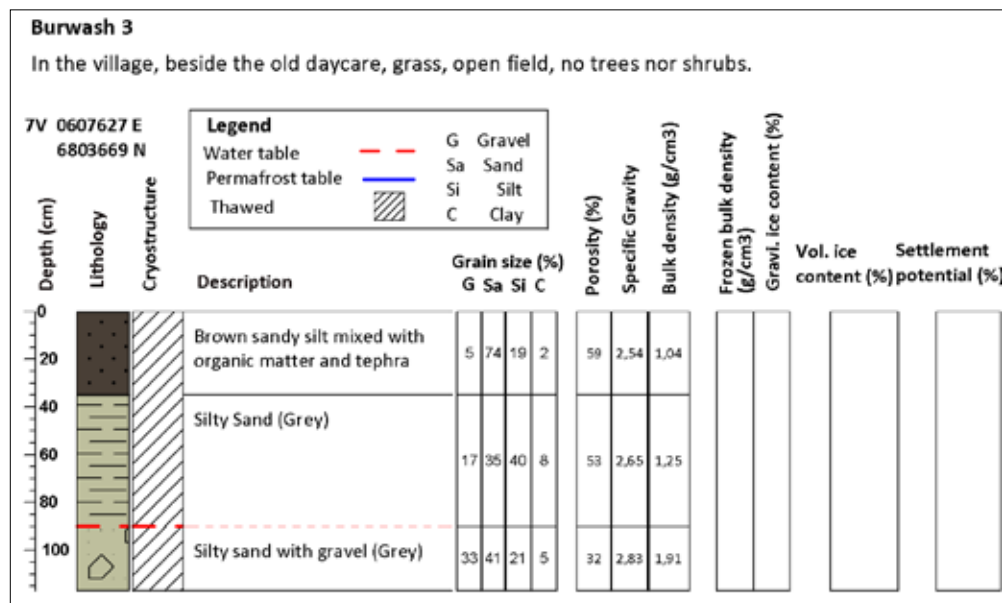
APPENDIX A - BOREHOLE LOG DESCRIPTIONS



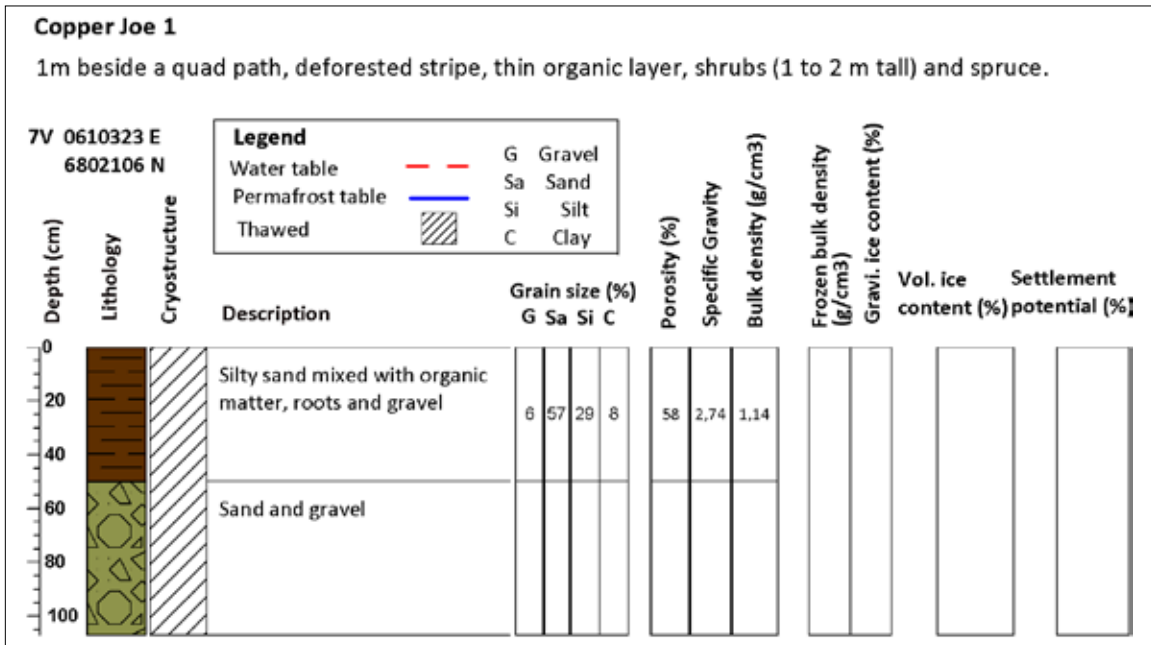
Appendix A1 – Borehole log for borehole BW_Bh1 in Burwash Landing (see Figure 1 and Figure 36 for location).



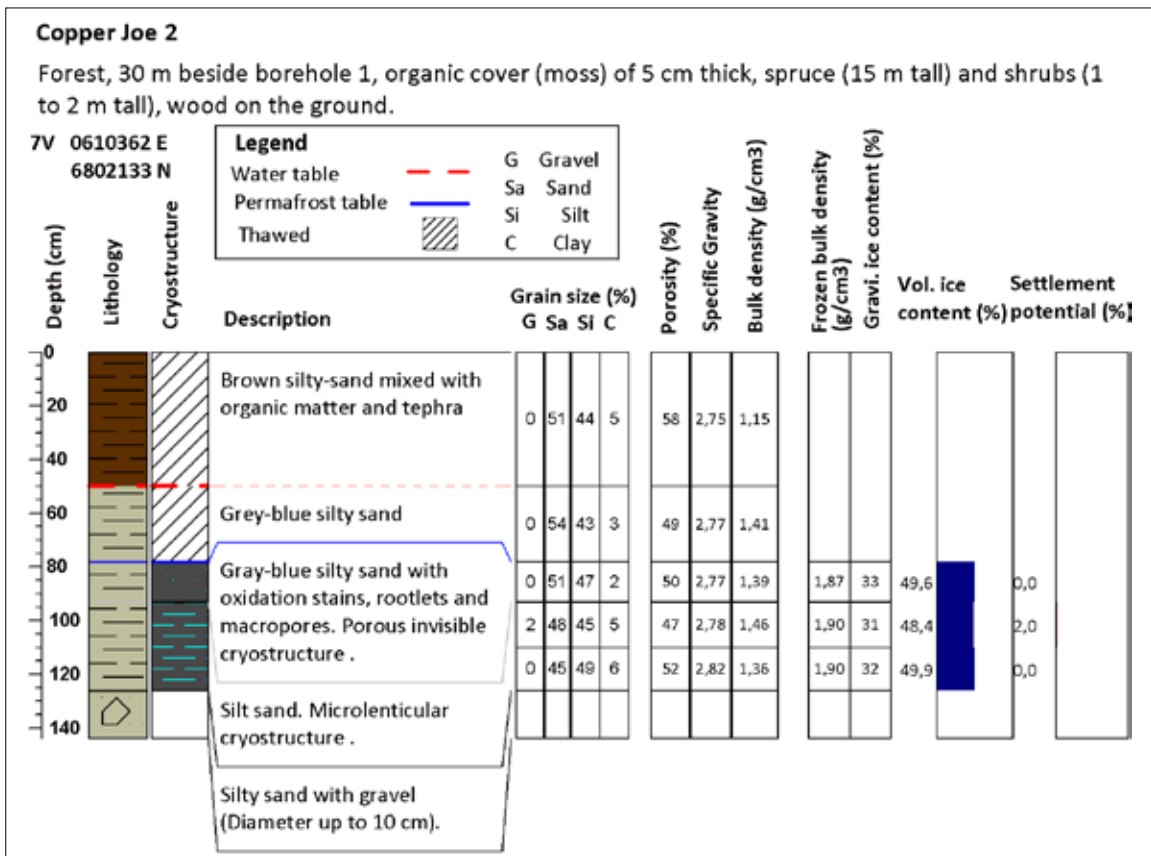
Appendix A2 – Borehole log for borehole BW_Bh2 in Burwash Landing (see Figure 1 and Figure 36 for location).



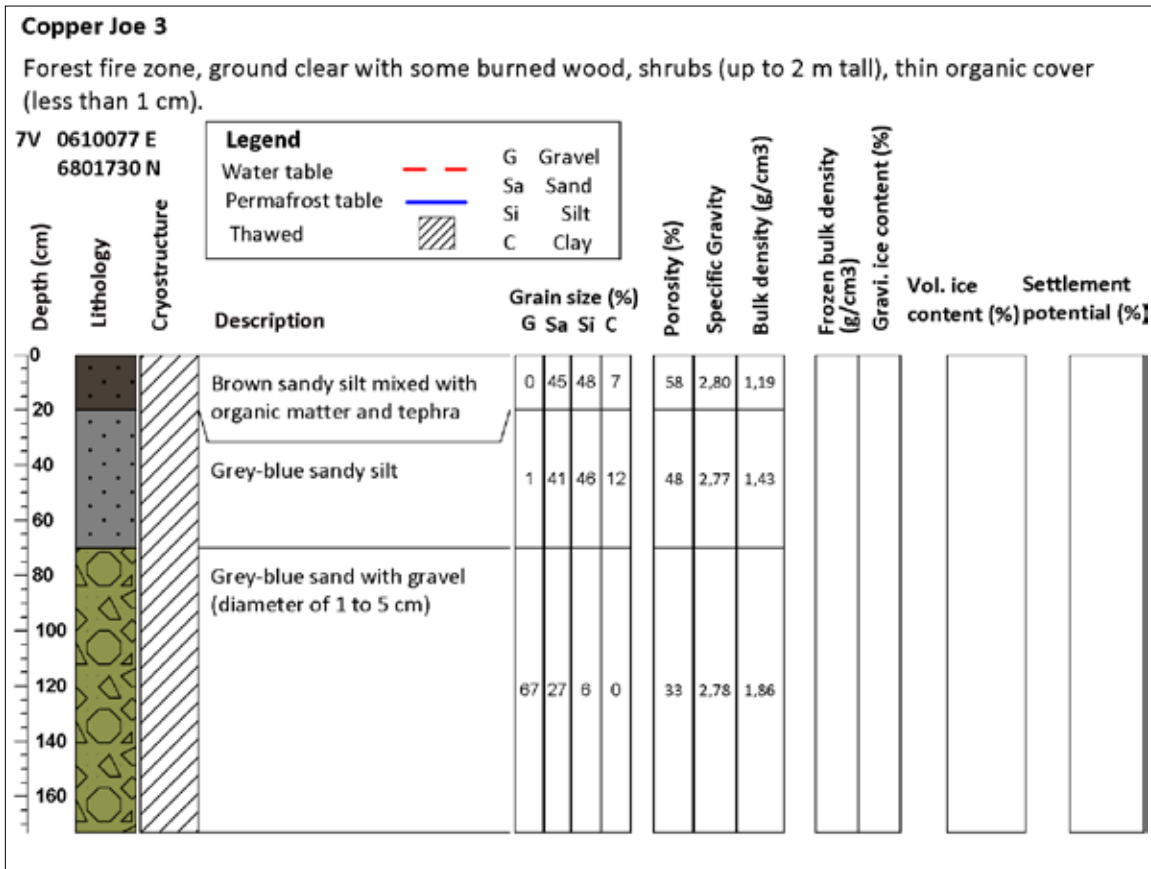
Appendix A3 – Borehole log for borehole BW_Bh3 in Burwash Landing (see Figure 1 and Figure 36 for location).



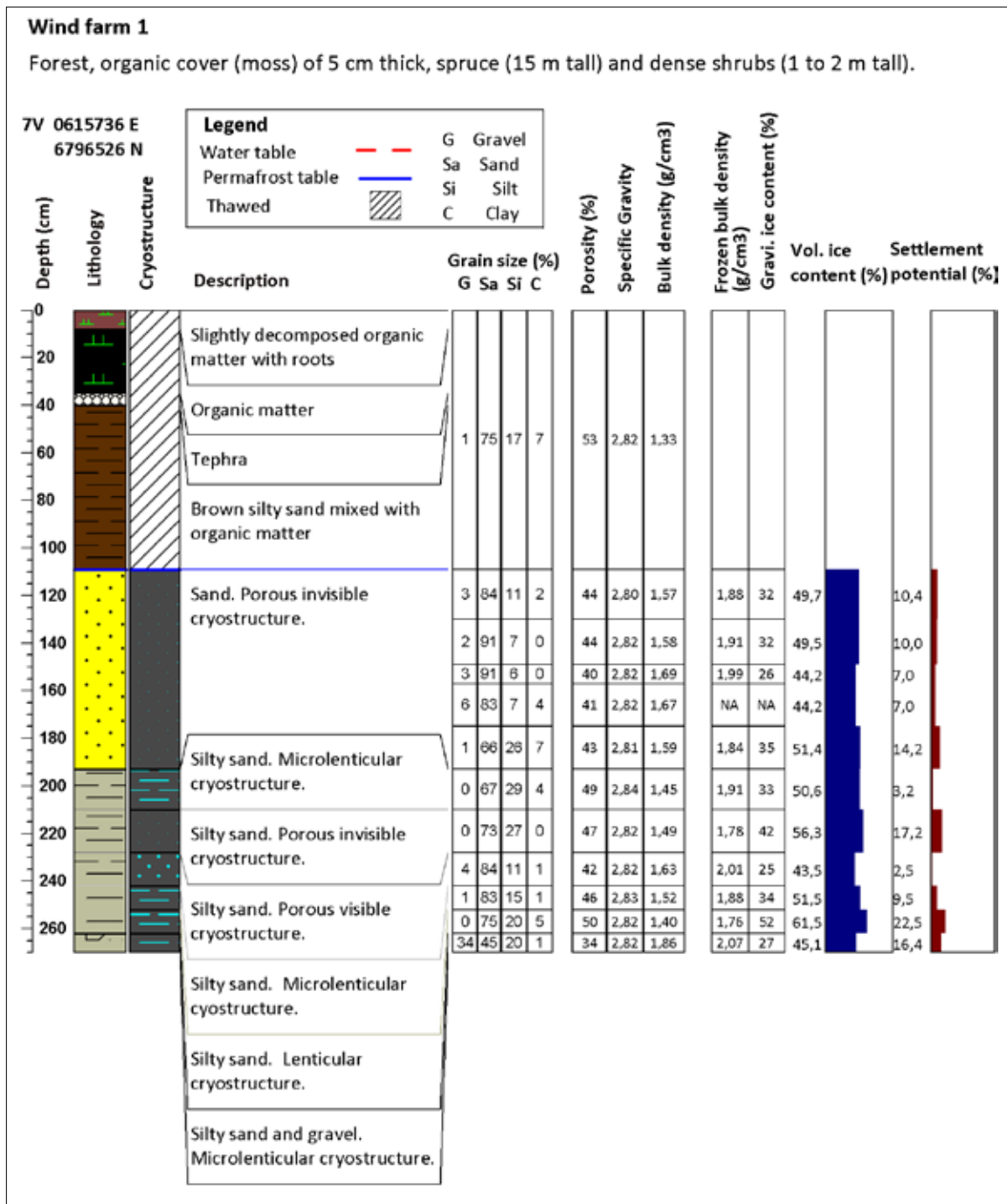
Appendix A4 – Borehole log for borehole CJ_Bh1 in Copper Joe subdivision (see Figure 1 and Figure 44 for location).



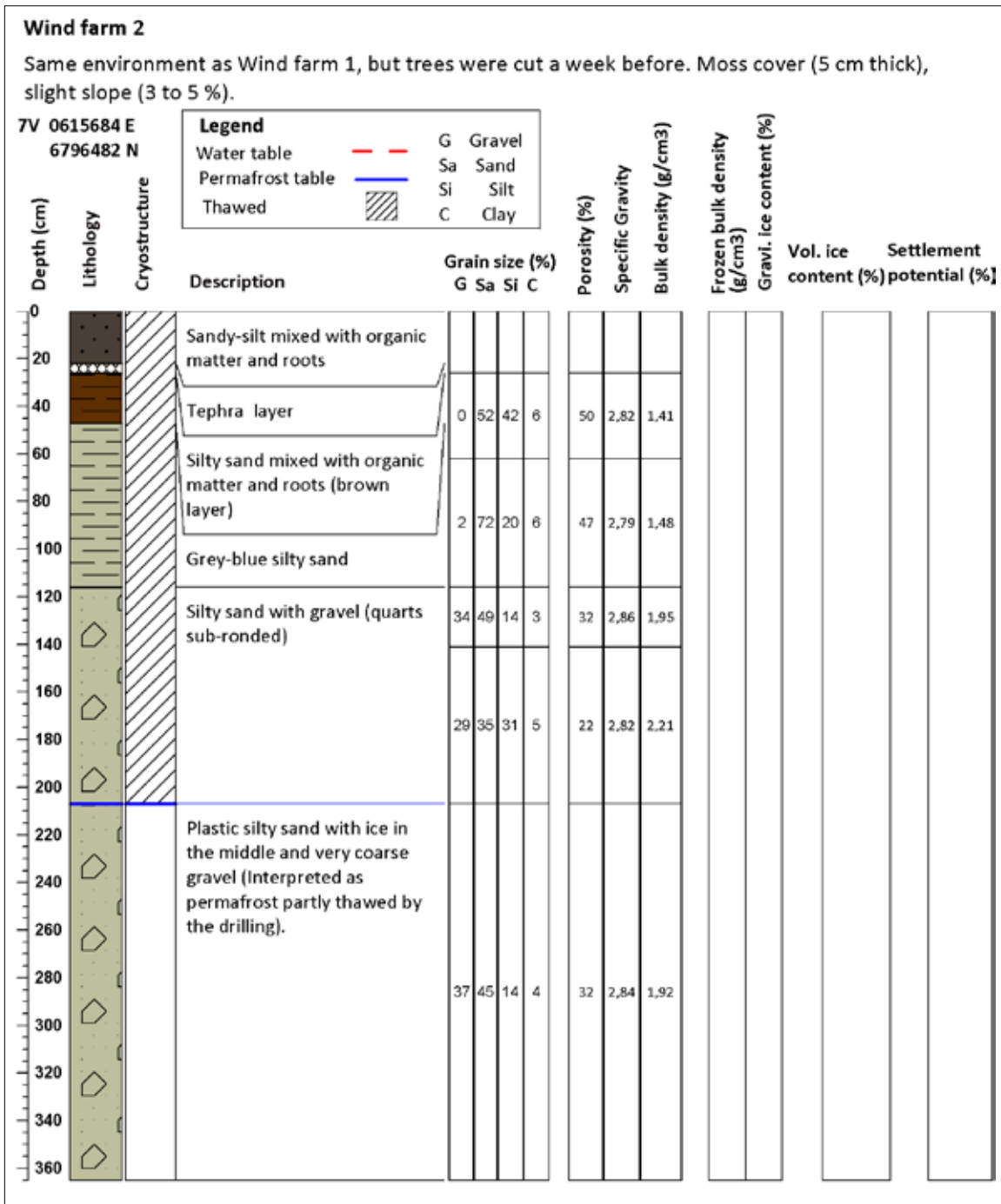
Appendix A5 – Borehole log for borehole CJ_Bh2 in Copper Joe subdivision (see Figure 1 and Figure 44 for location).



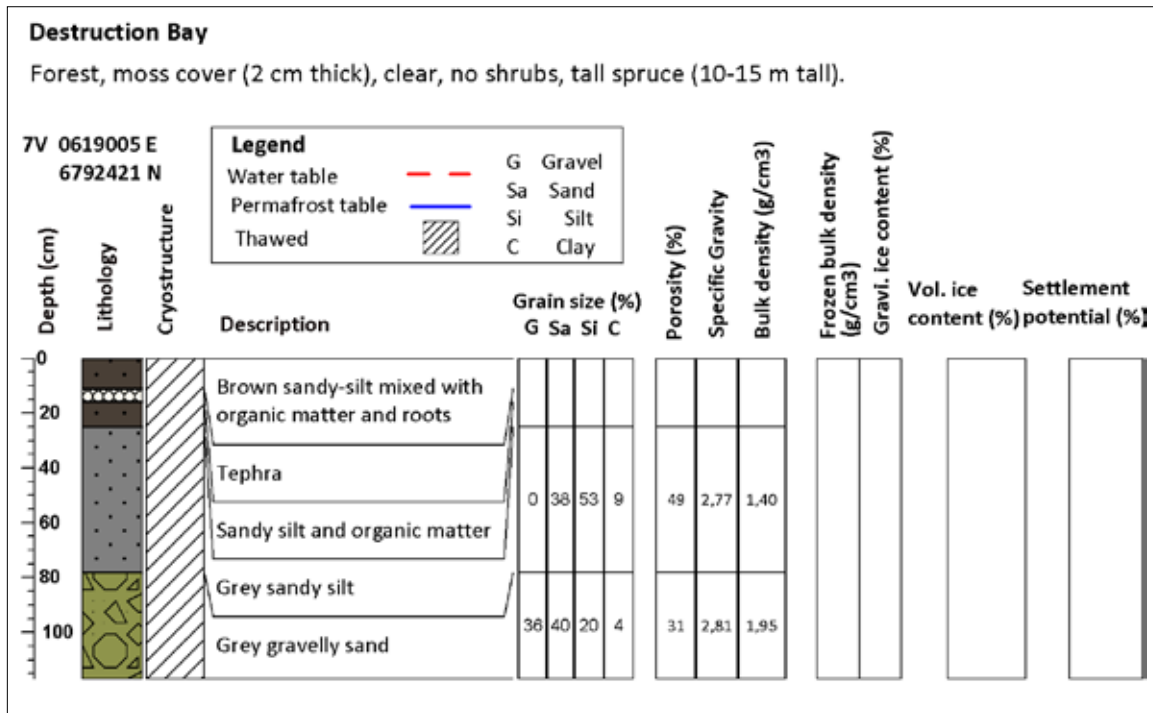
Appendix A6 – Borehole log for borehole CJ_Bh3 in Copper Joe subdivision (see Figure 1 and Figure 44 for location).



Appendix A7 – Borehole log for borehole WF_Bh1 at the Kluane First Nation wind energy project site (see Figure 1 and Figure 50 for location).



Appendix A8 – Borehole log for borehole WF_Bh2 at the Kluane First Nation wind energy project site (see Figure 1 and Figure 50 for location).



Appendix A9 – Borehole log for borehole DB_Bh1 Destruction Bay (see Figure 1 and Figure 53 for location).

BLANK PAGE

APPENDIX B - TEXTURE RESULTS FOR SURFICIAL DEPOSITS

Table B1. Textural data for surficial materials in the study area, samples 1 to 7, inclusive. Locations of individual samples are provided on accompanying map "Surficial Geology of Burwash Landing and Destruction Bay" (Kennedy, 2013).

	1	2	3	4	5	6	7
SAMPLE LOCATION:	6804617 E; 601948 N	6804971 E; 603620 N	6804971 E; 603620 N	6804653 E; 605694 N	6806161 E; 606118 N	6804529 E; 606697 N	6804860 E; 606855 N
ANALYST AND DATE:	MS/LPR, 12/12/2012	MS/LPR, 12/12/2012	MS/LPR, 12/12/2012	MS/LPR, 12/12/2012	MS/LPR, 12/12/2012	MS/LPR, 12/12/2012	MS/LPR, 12/12/2012
SIEVING ERROR:	0.0%	0.0%	0.0%	0.0%	0.0%	0.0%	0.0%
SAMPLE TYPE:	Trimodal, Poorly Sorted	Bimodal, Very Poorly Sorted	Polymodal, Very Poorly Sorted	Polymodal, Very Poorly Sorted	Trimodal, Very Poorly Sorted	Unimodal, Moderately Well Sorted	Trimodal, Poorly Sorted
TEXTURAL GROUP:	Gravel	Muddy Sandy Gravel	Slightly Gravelly Sandy Mud	Gravelly Muddy Sand	Slightly Gravelly Muddy Sand	Sand	Gravelly Sand
SEDIMENT NAME:	Coarse Gravel	Clayey Sandy Medium Gravel	Slightly Fine Gravelly Very Fine Sandy Very Coarse Silt	Very Fine Gravelly Very Coarse Silty Very Fine Sand	Slightly Very Fine Gravelly Very Coarse Silty Very Fine Sand	Moderately Well Sorted Medium Sand	Very Fine Gravelly Very Fine Sand
% GRAVEL:	85.4%	77.7%	2.3%	29.3%	3.4%	0.0%	9.4%
% SAND:	12.7%	20.1%	41.4%	41.4%	55.0%	98.2%	88.5%
% MUD:	1.8%	2.3%	56.3%	29.4%	41.6%	1.8%	2.0%
% V COARSE GRAVEL:	0.0%	24.7%	0.0%	0.0%	0.0%	0.0%	0.0%
% COARSE GRAVEL:	32.2%	10.0%	0.0%	6.3%	0.0%	0.0%	0.0%
% MEDIUM GRAVEL:	17.8%	29.4%	0.0%	3.5%	0.0%	0.0%	0.0%
% FINE GRAVEL:	25.1%	7.9%	2.2%	9.6%	1.1%	0.0%	3.4%
% V FINE GRAVEL:	10.3%	5.7%	0.1%	9.9%	2.3%	0.0%	6.0%
% V COARSE SAND:	4.3%	4.5%	0.2%	7.6%	1.9%	0.2%	6.9%
% COARSE SAND:	3.9%	6.2%	1.3%	9.0%	7.7%	2.7%	13.4%
% MEDIUM SAND:	2.4%	5.9%	15.7%	6.5%	20.7%	67.3%	33.4%
% FINE SAND:	1.2%	3.1%	0.0%	0.0%	0.0%	26.7%	0.0%
% V FINE SAND:	1.0%	0.4%	24.1%	18.4%	24.7%	1.3%	34.9%
% V COARSE SILT:	0.0%	0.0%	20.8%	17.5%	22.4%	0.0%	1.9%
% COARSE SILT:	0.0%	0.0%	12.5%	7.3%	8.3%	0.0%	0.2%
% MEDIUM SILT:	0.0%	0.0%	11.8%	1.7%	3.5%	0.0%	0.0%
% FINE SILT:	0.0%	0.0%	3.2%	0.7%	0.9%	0.0%	0.0%
% V FINE SILT:	0.0%	0.0%	3.2%	0.7%	0.9%	0.0%	0.0%
% CLAY:	1.8%	2.2%	4.8%	1.5%	5.5%	1.8%	0.0%

Table B2. Textural data for surficial materials in the study area, samples 12 to 15, inclusive; sample 15C; and samples 16 and 17. Locations of individual samples are provided on accompanying map “*Surficial Geology of Burwash Landing and Destruction Bay*” (Kennedy, 2013).

	12	13	14	15	15C	16	17
SAMPLE LOCATION:	6800434 E; 610593 N	6800434 E; 610593 N	6800434 E; 610593 N	6801447 E; 610590 N	6801447 E; 610590 N	6800478 E; 609329 N	6795133 E; 611978 N
ANALYST AND DATE:	MS/LPR, 12/12/2012	MS/LPR, 12/12/2012	MS/LPR, 12/12/2012	MS/LPR, 12/12/2012	MS/LPR, 12/12/2012	MS/LPR, 12/12/2012	MS/LPR, 12/12/2012
SIEVING ERROR:	0.0%	0.0%	0.0%	0.0%	0.0%	0.0%	0.0%
SAMPLE TYPE:	Polymodal, Extremely Poorly Sorted	Trimodal, Very Poorly Sorted	Bimodal, Very Poorly Sorted	Polymodal, Extremely Poorly Sorted	Polymodal, Very Poorly Sorted	Polymodal, Very Poorly Sorted	Polymodal, Very Poorly Sorted
TEXTURAL GROUP:	Muddy Sandy Gravel	Gravel	Gravel	Muddy Sandy Gravel	Muddy Sandy Gravel	Muddy Sandy Gravel	Muddy Sandy Gravel
SEDIMENT NAME:	Coarse Silty Sandy Fine Gravel	Very Coarse Gravel	Medium Gravel	Fine Silty Sandy Fine Gravel	Very Coarse Silty Sandy Fine Gravel	Coarse Silty Sandy Very Fine Gravel	Clayey Sandy Coarse Gravel
% GRAVEL:	39.3%	84.4%	80.5%	44.6%	44.6%	47.7%	68.3%
% SAND:	33.7%	15.2%	19.3%	34.8%	38.1%	35.7%	25.6%
% MUD:	27.1%	0.4%	0.2%	20.6%	17.3%	16.5%	6.1%
% V COARSE GRAVEL:	0.0%	29.9%	20.6%	0.0%	0.0%	0.0%	0.0%
% COARSE GRAVEL:	7.7%	11.7%	6.1%	9.5%	9.5%	8.9%	20.2%
% MEDIUM GRAVEL:	4.3%	24.2%	33.2%	5.3%	5.3%	4.9%	11.2%
% FINE GRAVEL:	16.4%	10.8%	11.3%	17.1%	17.1%	14.3%	18.0%
% V FINE GRAVEL:	10.9%	7.7%	9.3%	12.8%	12.8%	19.6%	18.8%
% V COARSE SAND:	8.3%	5.9%	7.6%	14.8%	14.8%	12.5%	9.6%
% COARSE SAND:	6.4%	4.9%	6.3%	5.7%	5.7%	9.1%	6.0%
% MEDIUM SAND:	5.1%	2.8%	3.9%	6.1%	6.1%	5.3%	4.1%
% FINE SAND:	0.0%	1.1%	0.7%	0.0%	0.0%	0.0%	3.1%
% V FINE SAND:	13.9%	0.5%	0.8%	8.2%	11.5%	8.8%	2.8%
% V COARSE SILT:	5.2%	0.0%	0.0%	0.9%	5.3%	3.8%	0.0%
% COARSE SILT:	5.8%	0.0%	0.0%	0.9%	3.6%	4.4%	0.0%
% MEDIUM SILT:	3.9%	0.0%	0.0%	0.9%	2.1%	1.4%	0.0%
% FINE SILT:	2.5%	0.0%	0.0%	6.8%	0.9%	1.8%	0.0%
% V FINE SILT:	2.4%	0.0%	0.0%	6.6%	0.9%	1.7%	0.0%
% CLAY:	7.3%	0.4%	0.2%	4.6%	4.6%	3.5%	6.1%

Table B3. Textural data for surficial materials in the study area, samples 18 to 24, inclusive. Locations of individual samples are provided on accompanying map “*Surficial Geology of Burwash Landing and Destruction Bay*” (Kennedy, 2013).

	18	19	20	21	22	23	24
SAMPLE LOCATION:	6769820 E; 612985 N	6798349 E; 613903 N	6798349 E; 613903 N	6797107 E; 615531 N	6797340 E; 615350 N	6797521 E; 614727 N	6798644 E; 613308 N
ANALYST AND DATE:	MS/LPR, 12/12/2012	MS/LPR, 12/12/2012	MS/LPR, 12/12/2012	MS/LPR, 12/12/2012	MS/LPR, 12/12/2012	MS/LPR, 12/12/2012	MS/LPR, 12/12/2012
SIEVING ERROR:	0.0%	0.0%	0.0%	0.0%	0.0%	0.0%	0.0%
SAMPLE TYPE:	Trimodal, Poorly Sorted	Bimodal, Poorly Sorted	Polymodal, Very Poorly Sorted	Trimodal, Very Poorly Sorted	Polymodal, Very Poorly Sorted	Trimodal, Very Poorly Sorted	Trimodal, Poorly Sorted
TEXTURAL GROUP:	Gravel	Slightly Gravelly Sandy Mud	Muddy Sandy Gravel	Slightly Gravelly Sandy Mud	Gravelly Muddy Sand	Sandy Gravel	Gravel
SEDIMENT NAME:	Coarse Gravel	Slightly Very Fine Gravelly Very Fine Sandy Very Coarse Silt	Very Coarse Silty Sandy Coarse Gravel	Slightly Very Fine Gravelly Very Fine Sandy Very Coarse Silt	Very Fine Gravelly Very Coarse Silty Very Fine Sand	Sandy Coarse Gravel	Fine Gravel
% GRAVEL:	80.5%	0.3%	70.1%	0.2%	21.3%	70.3%	80.9%
% SAND:	19.2%	40.9%	26.9%	40.5%	48.6%	28.0%	17.4%
% MUD:	0.3%	58.8%	3.1%	59.2%	30.1%	1.7%	1.7%
% V COARSE GRAVEL:	0.0%	0.0%	0.0%	0.0%	0.0%	0.0%	0.0%
% COARSE GRAVEL:	35.3%	0.0%	29.8%	0.0%	4.5%	25.9%	22.7%
% MEDIUM GRAVEL:	19.5%	0.0%	16.5%	0.0%	2.5%	14.3%	12.6%
% FINE GRAVEL:	15.5%	0.0%	15.7%	0.0%	7.0%	16.7%	27.7%
% V FINE GRAVEL:	10.2%	0.3%	8.0%	0.2%	7.2%	13.3%	17.9%
% V COARSE SAND:	7.0%	0.9%	4.8%	0.4%	5.0%	10.6%	8.0%
% COARSE SAND:	6.5%	1.7%	4.8%	1.1%	8.9%	8.3%	4.4%
% MEDIUM SAND:	4.1%	1.7%	5.5%	16.5%	6.8%	4.1%	2.3%
% FINE SAND:	1.3%	0.0%	0.0%	0.0%	0.0%	3.6%	1.4%
% V FINE SAND:	0.3%	36.6%	11.7%	22.5%	27.9%	1.5%	1.4%
% V COARSE SILT:	0.0%	35.0%	1.5%	31.6%	11.9%	0.0%	0.0%
% COARSE SILT:	0.0%	14.6%	0.7%	12.8%	3.3%	0.0%	0.0%
% MEDIUM SILT:	0.0%	3.5%	0.3%	4.4%	3.3%	0.0%	0.0%
% FINE SILT:	0.0%	1.3%	0.1%	2.5%	1.7%	0.0%	0.0%
% V FINE SILT:	0.0%	1.3%	0.1%	2.4%	1.7%	0.0%	0.0%
% CLAY:	0.3%	3.0%	0.4%	5.5%	8.1%	1.7%	1.7%

Table B4. Textural data for surficial materials in the study area, samples 25 to 31, inclusive. Locations of individual samples are provided on accompanying map “*Surficial Geology of Burwash Landing and Destruction Bay*” (Kennedy, 2013).

	25	26	27	28	29	30	31
SAMPLE LOCATION:	6796561 E; 615875 N	6796319 E; 615649 N	6796319 E; 615649 N	6796319 E; 615649 N	6802062 E; 610467 N	6802312 E; 610247 N	6803104 E; 608974 N
ANALYST AND DATE:	MS/LPR, 12/12/2012	MS/LPR, 12/12/2012	MS/LPR, 12/12/2012	MS/LPR, 12/12/2012	MS/LPR, 12/12/2012	MS/LPR, 12/12/2012	MS/LPR, 12/12/2012
SIEVING ERROR:	0.0%	0.0%	0.0%	0.0%	0.0%	0.0%	0.0%
SAMPLE TYPE:	Trimodal, Very Poorly Sorted	Polymodal, Very Poorly Sorted	Polymodal, Very Poorly Sorted	Trimodal, Very Poorly Sorted	Trimodal, Very Poorly Sorted	Polymodal, Poorly Sorted	Polymodal, Very Poorly Sorted
TEXTURAL GROUP:	Sandy Gravel	Gravelly Muddy Sand	Muddy Sandy Gravel	Slightly Gravelly Muddy Sand	Slightly Gravelly Sandy Mud	Slightly Gravelly Sandy Mud	Muddy Sandy Gravel
SEDIMENT NAME:	Sandy Coarse Gravel	Fine Gravelly Very Coarse Silty Very Fine Sand	Very Coarse Silty Sandy Coarse Gravel	Slightly Very Fine Gravelly Very Coarse Silty Coarse Sand	Slightly Very Fine Gravelly Very Fine Sandy Very Coarse Silt	Slightly Very Fine Gravelly Very Fine Sandy Very Coarse Silt	Very Coarse Silty Sandy Fine Gravel
% GRAVEL:	48.9%	26.7%	56.4%	2.5%	0.3%	3.4%	42.0%
% SAND:	50.7%	40.3%	35.1%	85.6%	45.7%	35.6%	40.7%
% MUD:	0.4%	33.0%	8.4%	12.0%	54.0%	61.0%	17.3%
% V COARSE GRAVEL:	0.0%	0.0%	0.0%	0.0%	0.0%	0.0%	0.0%
% COARSE GRAVEL:	18.7%	4.3%	18.8%	0.0%	0.0%	0.0%	7.5%
% MEDIUM GRAVEL:	10.3%	2.4%	10.4%	0.0%	0.0%	0.0%	4.1%
% FINE GRAVEL:	13.5%	11.2%	16.2%	0.0%	0.1%	0.0%	19.0%
% V FINE GRAVEL:	6.3%	8.8%	11.0%	2.5%	0.2%	3.4%	11.4%
% V COARSE SAND:	15.6%	5.9%	8.6%	15.9%	0.3%	0.9%	7.6%
% COARSE SAND:	29.8%	6.6%	9.3%	26.2%	1.6%	1.5%	9.9%
% MEDIUM SAND:	5.0%	8.2%	7.6%	26.1%	2.3%	0.4%	9.1%
% FINE SAND:	0.2%	0.0%	0.0%	0.0%	0.0%	0.0%	0.0%
% V FINE SAND:	0.1%	19.6%	9.6%	17.3%	41.3%	32.8%	14.1%
% V COARSE SILT:	0.0%	10.1%	3.7%	4.5%	25.0%	33.6%	7.0%
% COARSE SILT:	0.0%	8.3%	1.5%	2.0%	9.5%	15.8%	3.3%
% MEDIUM SILT:	0.0%	5.8%	1.0%	0.8%	4.7%	6.9%	2.1%
% FINE SILT:	0.0%	2.6%	0.5%	0.6%	1.9%	1.9%	1.1%
% V FINE SILT:	0.0%	2.6%	0.5%	0.6%	1.9%	1.8%	1.1%
% CLAY:	0.4%	3.6%	1.2%	3.4%	11.0%	1.1%	2.9%

Table B5. Textural data for surficial materials in the study area, samples 32 to 38, inclusive. Locations of individual samples are provided on accompanying map "Surficial Geology of Burwash Landing and Destruction Bay" (Kennedy, 2013).

	32	33	34	35	36	37	38
SAMPLE LOCATION:	6792919 E; 616835 N	6793596 E; 617106 N	6793596 E; 617106 N	6792581 E; 619182 N	6792581 E; 619182 N	6792200 E; 619865 N	6806789 E; 601705 N
ANALYST AND DATE:	MS/LPR, 12/12/2012	MS/LPR, 12/12/2012	MS/LPR, 12/12/2012	MS/LPR, 12/12/2012	MS/LPR, 12/12/2012	MS/LPR, 12/12/2012	MS/LPR, 12/12/2012
SIEVING ERROR:	0.0%	0.0%	0.0%	0.0%	0.0%	0.0%	0.0%
SAMPLE TYPE:	Polymodal, Very Poorly Sorted	Polymodal, Extremely Poorly Sorted	Polymodal, Very Poorly Sorted	Polymodal, Very Poorly Sorted	Polymodal, Extremely Poorly Sorted	Bimodal, Very Poorly Sorted	Bimodal, Poorly Sorted
TEXTURAL GROUP:	Sandy Gravel	Gravelly Mud	Gravelly Muddy Sand	Muddy Sandy Gravel	Gravelly Mud	Muddy Sandy Gravel	Slightly Gravelly Muddy Sand
SEDIMENT NAME:	Sandy Fine Gravel	Very Fine Gravelly Mud	Very Fine Gravelly Clayey Coarse Sand	Very Coarse Silty Sandy Fine Gravel	Medium Gravelly Coarse Silt	Very Coarse Silty Sandy Medium Gravel	Slightly Very Fine Gravelly Very Coarse Silty Very Fine Sand
% GRAVEL:	67.4%	16.6%	21.6%	51.2%	15.1%	54.8%	0.3%
% SAND:	30.5%	40.6%	67.6%	42.6%	37.0%	39.2%	74.3%
% MUD:	2.1%	42.8%	10.8%	6.2%	47.9%	6.1%	25.3%
% V COARSE GRAVEL:	0.0%	0.0%	0.0%	0.0%	0.0%	7.3%	0.0%
% COARSE GRAVEL:	18.0%	0.9%	0.0%	9.5%	0.0%	4.0%	0.0%
% MEDIUM GRAVEL:	10.0%	0.5%	0.0%	5.3%	6.7%	21.4%	0.0%
% FINE GRAVEL:	24.8%	7.2%	4.6%	23.2%	3.1%	10.7%	0.1%
% V FINE GRAVEL:	14.6%	8.0%	17.0%	13.2%	5.2%	11.4%	0.3%
% V COARSE SAND:	8.1%	5.1%	16.5%	9.0%	5.3%	7.9%	0.3%
% COARSE SAND:	7.5%	6.0%	16.9%	10.7%	5.2%	12.4%	0.4%
% MEDIUM SAND:	7.5%	7.6%	13.7%	9.3%	6.1%	10.9%	5.2%
% FINE SAND:	5.0%	11.3%	10.6%	0.0%	0.0%	0.0%	0.0%
% V FINE SAND:	2.4%	10.5%	9.9%	13.7%	20.4%	8.0%	68.4%
% V COARSE SILT:	0.0%	10.0%	0.0%	3.5%	9.1%	3.0%	13.6%
% COARSE SILT:	0.0%	8.6%	0.0%	0.9%	9.7%	1.0%	6.2%
% MEDIUM SILT:	0.0%	3.5%	0.0%	0.5%	8.7%	0.5%	4.5%
% FINE SILT:	0.0%	2.6%	0.0%	0.3%	4.1%	0.2%	0.6%
% V FINE SILT:	0.0%	2.6%	0.1%	0.3%	4.1%	0.2%	0.5%
% CLAY:	2.1%	15.6%	10.7%	0.7%	12.2%	1.2%	0.0%

BLANK PAGE

APPENDIX C - GRAIN SIZE ANALYSIS OF PERMAFROST BOREHOLE SAMPLES

Table C1. Sieve and hydrometric analysis computed with Gradistat software. Results from lab analyses of samples collected from permafrost boreholes at case study sites (see Figures 1, 36, 44, 50 and 53 for locations). Data from frozen core sections are presented in italics. D50 = median grain size.

Identification		Grain-size analysis					Material description	
PointID	Lab#	Depth	Gravel	Sand	Silt (or mud)	Clay	D50	Sediment name
		cm	%				mm	
BW_Bh1	D2b	0-65	3.18%	33.22%	54.97%	8.63%	0.05	Slightly Fine Gravelly Very Fine Sandy Very Coarse Silt
	<i>D3</i>	<i>75-85</i>	<i>1.19%</i>	<i>27.08%</i>	<i>58.87%</i>	<i>12.86%</i>	<i>0.04</i>	<i>Slightly Very Fine Gravelly Very Fine Sandy Very Coarse Silt</i>
	<i>D4</i>	<i>92-97</i>	<i>41.17%</i>	<i>47.02%</i>	<i>11.81%</i>	<i>N/A</i>	<i>1.12</i>	<i>Very Coarse Silty Sandy Very Fine Gravel</i>
	<i>D5</i>	<i>127-135</i>	<i>30.19%</i>	<i>39.46%</i>	<i>24.61%</i>	<i>5.74%</i>	<i>0.24</i>	<i>Very Coarse Silty Sandy Very Fine Gravel</i>
	D6	163	52.17%	37.14%	8.24%	2.45%	2.16	Very Coarse Silty Sandy Very Fine Gravel
	D7	406	38.00%	53.74%	8.26%	N/A	1.13	Very Coarse Silty Sandy Very Fine Gravel
BW_Bh2	E1	0-22	1.98%	60.28%	31.53%	6.21%	0.11	Slightly Very Fine Gravelly Very Coarse Silty Medium Sand
	E2	22-30	0.24%	44.55%	48.85%	6.36%	0.06	Slightly Very Fine Gravelly Very Fine Sandy Very Coarse Silt
	E3	40-90	4.99%	47.28%	40.53%	7.20%	0.07	Slightly Very Fine Gravelly Very Fine Sandy Very Coarse Silt
	E4	90-104	44.42%	34.92%	16.75%	3.91%	1.22	Very Coarse Silty Sandy Fine Gravel
BW_Bh3	L1	0-35	4.61%	74.52%	18.66%	2.21%	0.14	Slightly Very Fine Gravelly Very Coarse Silty Fine Sand
	L2	35-90	16.48%	35.26%	40.18%	8.07%	0.07	Very Fine Gravelly Very Coarse Silt
	L3	1-90	33.26%	40.73%	20.72%	5.29%	0.34	Very Coarse Silty Sandy Very Fine Gravel
CJ_Bh1	A1	0-50	5.55%	57.48%	29.32%	7.65%	0.14	Very Fine Gravelly Very Coarse Silty Coarse Sand
CJ_Bh2	B1	0-50	0.40%	50.48%	44.46%	4.66%	0.07	Slightly Very Fine Gravelly Very Coarse Silty Very Fine Sand
	B2	50-78	0.16%	53.99%	42.48%	3.37%	0.07	Slightly Very Fine Gravelly Very Coarse Silty Very Fine Sand
	<i>B3</i>	<i>78-93</i>	<i>0.00%</i>	<i>51.60%</i>	<i>46.61%</i>	<i>1.78%</i>	<i>0.07</i>	<i>Slightly Very Fine Gravelly Very Coarse Silty Very Fine Sand</i>
	<i>B4</i>	<i>93-107</i>	<i>1.79%</i>	<i>48.50%</i>	<i>44.80%</i>	<i>4.91%</i>	<i>0.06</i>	<i>Slightly Very Fine Gravelly Very Fine Sandy Very Coarse Silt</i>
	<i>B5</i>	<i>112-126</i>	<i>0.10%</i>	<i>44.79%</i>	<i>49.47%</i>	<i>5.64%</i>	<i>0.06</i>	<i>Slightly Very Fine Gravelly Very Fine Sandy Very Coarse Silt</i>
CJ_Bh3	C3	0-50	0.48%	44.84%	48.19%	6.50%	0.06	Slightly Very Fine Gravelly Very Fine Sandy Very Coarse Silt
	C4	50-70	0.86%	40.97%	46.07%	12.10%	0.05	Slightly Very Fine Gravelly Very Fine Sandy Very Coarse Silt
	C5	130-144	67.41%	26.64%	5.95%	N/A	4.97	Very Coarse Silty Sandy Fine Gravel
WF_Bh1	<i>F1</i>	<i>40-109</i>	<i>0.68%</i>	<i>74.79%</i>	<i>16.78%</i>	<i>7.75%</i>	<i>0.16</i>	<i>Slightly Very Fine Gravelly Very Coarse Silty Very Fine Sand</i>
	<i>F2</i>	<i>110-130</i>	<i>2.62%</i>	<i>83.74%</i>	<i>11.35%</i>	<i>2.29%</i>	<i>0.32</i>	<i>Slightly Very Fine Gravelly Very Coarse Silty Medium Sand</i>
	<i>F3</i>	<i>132-149</i>	<i>2.03%</i>	<i>90.69%</i>	<i>7.29%</i>	<i>N/A</i>	<i>0.34</i>	<i>Slightly Very Fine Gravelly Medium Sand</i>
	<i>F4</i>	<i>149-157</i>	<i>2.74%</i>	<i>90.65%</i>	<i>6.61%</i>	<i>N/A</i>	<i>0.36</i>	<i>Slightly Very Fine Gravelly Medium Sand</i>
	<i>F5</i>	<i>168-175</i>	<i>5.81%</i>	<i>82.54%</i>	<i>7.22%</i>	<i>4.43%</i>	<i>0.22</i>	<i>Very Fine Gravelly Muddy Fine Sand</i>
	<i>F6</i>	<i>175-193</i>	<i>0.54%</i>	<i>66.41%</i>	<i>26.48%</i>	<i>6.56%</i>	<i>0.14</i>	<i>Slightly Very Fine Gravelly Very Coarse Silty Fine Sand</i>
	<i>F7</i>	<i>193-210</i>	<i>0.34%</i>	<i>66.84%</i>	<i>28.57%</i>	<i>4.25%</i>	<i>0.12</i>	<i>Slightly Very Fine Gravelly Very Coarse Silty Fine Sand</i>
	<i>F8</i>	<i>210-228</i>	<i>0.19%</i>	<i>72.91%</i>	<i>26.90%</i>	<i>0.00%</i>	<i>0.12</i>	<i>Slightly Very Fine Gravelly Very Coarse Silty Very Fine Sand</i>
	<i>F9</i>	<i>228-242</i>	<i>4.34%</i>	<i>84.24%</i>	<i>10.77%</i>	<i>0.64%</i>	<i>0.43</i>	<i>Slightly Very Fine Gravelly Very Coarse Silty Coarse Sand</i>
	<i>F10</i>	<i>242-252</i>	<i>0.72%</i>	<i>83.26%</i>	<i>15.18%</i>	<i>0.84%</i>	<i>0.18</i>	<i>Slightly Very Fine Gravelly Very Coarse Silty Fine Sand</i>
	<i>F11Top</i>	<i>252-262</i>	<i>0.00%</i>	<i>74.70%</i>	<i>20.13%</i>	<i>5.18%</i>	<i>0.12</i>	<i>Very Coarse Silty Fine Sand</i>
<i>F11Bot</i>	<i>262-270</i>	<i>34.22%</i>	<i>44.79%</i>	<i>20.08%</i>	<i>0.91%</i>	<i>0.32</i>	<i>Very Coarse Silty Sandy Very Fine Gravel</i>	

Table C1, continued. Sieve and hydrometric analysis computed with Gradistat software. Results from lab analyses of samples collected from permafrost boreholes at case study sites (see Figures 1, 36, 44, 50 and 53 for locations). Data from frozen core sections are presented in italics. D50 = median grain size.

Identification		Grain-size analysis					Material description	
PointID	Lab#	Depth	Gravel	Sand	Silt (or mud)	Clay	D50	Sediment name
		cm	%			mm		
WF_Bh2	G1	26-47	0.03%	52.07%	41.61%	6.29%	0.07	Slightly Very Fine Gravelly Very Coarse Silty Fine Sand
	G2	62-116	2.04%	72.24%	19.39%	6.33%	0.20	Slightly Very Fine Gravelly Very Coarse Silty Medium Sand
	G3	116-141	33.49%	48.80%	14.40%	3.31%	0.75	Very Coarse Silty Sandy Very Fine Gravel
	G4	299-311	29.19%	34.62%	30.63%	5.56%	0.18	Very Fine Gravelly Very Coarse Silt
	G5	353-365	36.95%	45.19%	13.74%	4.12%	0.86	Very Coarse Silty Sandy Very Fine Gravel
DB_Bh1	H1	25-64	0.16%	38.37%	52.85%	8.61%	0.05	Slightly Very Fine Gravelly Fine Sandy Very Coarse Silt
	H2	78-91	35.61%	39.88%	20.53%	3.99%	0.73	Very Coarse Silty Sandy Very Fine Gravel

APPENDIX D - CLIMATE PROJECTIONS

Projections of changes in mean annual air temperature (MAAT) were prepared for this report based on annual air temperature modelling, and were enhanced to reflect heterogeneity in the local landscape (specifically, mountainous terrain). This represents a significant increase in the understanding of MAAT. This approach incorporated specific topographical features in the study region (e.g., mountains) and knowledge about related area-specific surface lapse rates (SLRs) at fine resolution (30 x 30 m). To develop these enhanced air temperature models and predictions, current MAAT modeling was conducted. Work drew on data from clusters of previously established air temperature monitoring stations in Yukon. Each monitoring station consisted of a radiation shield mounted at 1.5-1.6 m on a metal pole. An Onset Hobo Pro data-logger (accuracy $\pm 0.2^{\circ}\text{C}$), equipped with an external thermistor, was used to monitor air temperature inside the screen. In order to predict MAAT across the region, a 3rd order polynomial trend surface of annual SLR values below treeline was generated (Lewkowicz and Bonnaventure, 2011). This surface was then combined with a 4th order polynomial trend surface of treeline elevations, which was separately developed from sampling topographic maps and Google Earth images to limit the application of the SLR values to terrain below treeline. Above this level, it was assumed that standard environmental lapse rates of $-6.5^{\circ}\text{C}/\text{km}$ prevail. In addition, a 3rd order polynomial trend surface of projected sea level temperature was generated from the long-term records of 18 climate stations in the region (Environment Canada, 2013), which had been reduced to sea level (e.g., Etzelmuller et al., 2007) by applying the projected SLR value for each station based on its continentality (Lewkowicz and Bonnaventure, 2011). The projected sea level temperature surface was then readjusted using a digital elevation model at 30 x 30 m resolution, the SLR grid for elevations up to treeline, and the standard environmental lapse rate from treeline upwards. The result was a gridded model of MAAT for the region based on elevation with the measured variability in SLR taken into account but not including aspect or localized topographic effects on cold-air pooling.

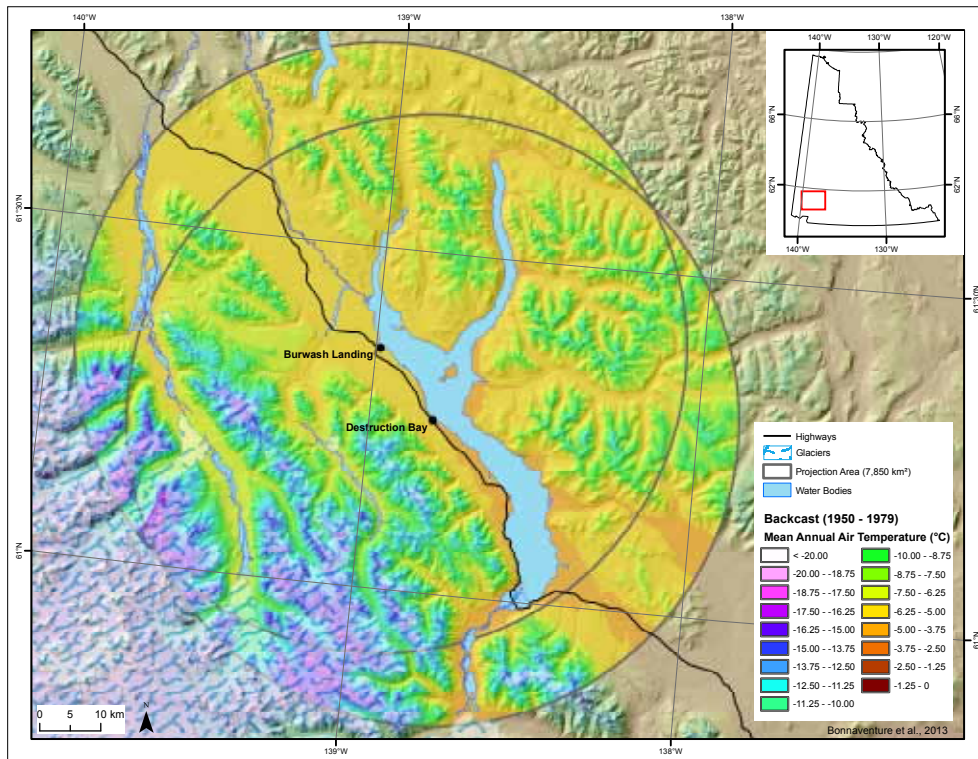
The basis for developing projections of MAAT incorporating the SLRs (also called perturbed MAAT models) involved using statistically downscaled GCM data obtained from the Scenarios Network for Arctic and Alaska Planning at the University of Alaska Fairbanks (SNAP, 2012; www.snap.uaf.edu). The SNAP dataset contains multiple GCM scenarios for mean annual air temperatures, as well as modelled average temperature surfaces for past climate normals (e.g., 1980-2009). The data used to obtain the perturbed MAAT models included the 2 km-resolution projection surfaces provided by SNAP for the IPCC scenarios of A1B, A2 and B1. These particular scenarios were chosen for this application because they represent the most commonly used scenarios in GCM modelling and represent a broad range of potential climate conditions. To develop each scenario, SNAP drew on data from five separate models, thereby ensuring the greatest range of predictions within each scenario. Perturbed MAAT models were developed by examining difference (and thus change) between what the SNAP model predicted for the current climate (i.e., the 1980-2009 climate normal) and each of the three scenarios for the years 2020, 2050 and 2080. In addition, a backcasted model was also produced which examined the difference between current climate (1980-2009) and the climate normal from 1950-1979. Hence, modelling efforts examined the predicted difference between each time slice for each scenario and adjusted the previously created MAAT model accordingly. In order to incorporate the data from the 2 x 2 km grid cells for each SNAP model, the cell size was resampled to 30 x 30 m. This effectively provided a broad geographic basis for sample change at a territorial scale (macroclimate), which could then be topographically corrected to site specific SLRs in the Burwash and Destruction Bay study area. The differences between the predicted SNAP models were then added (forecasting) or subtracted (backcasting) to the current MAAT model using

raster calculator in ArcGIS® 10.1 (ESRI, USA). The results of these models provide significantly more information about the variable nature of spatial climate in geographically mountainous areas than the raw GCM data itself, which typically displays high levels of inaccuracies in the mountainous regions of Yukon.

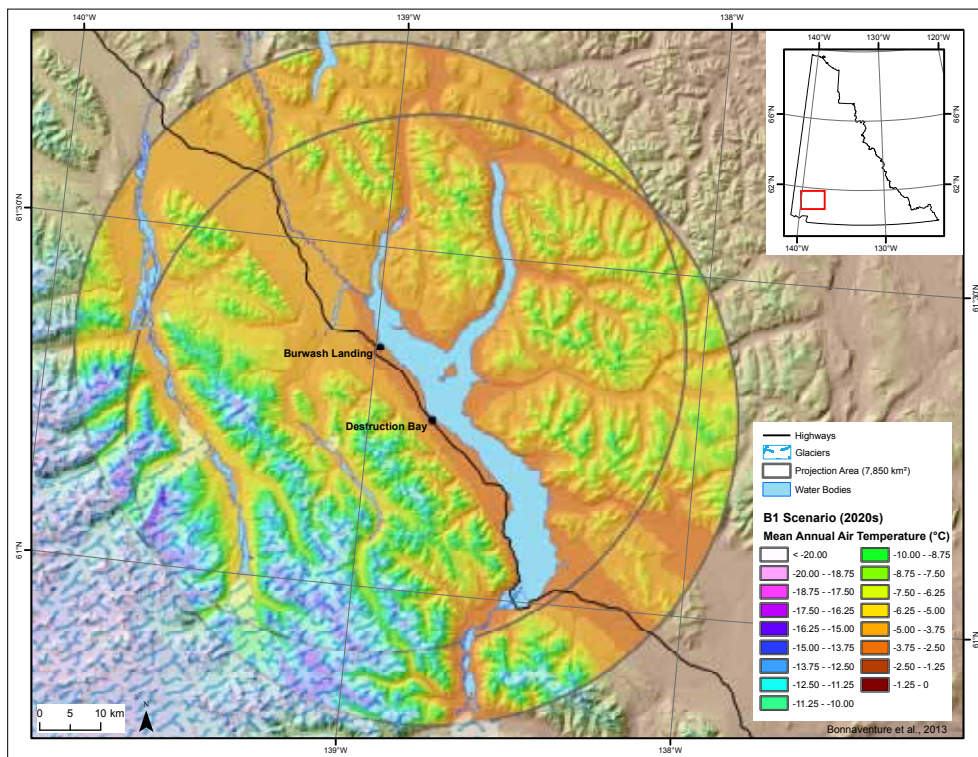
Current (i.e., 1980-2009) MAAT results in the area of Burwash Landing and Destruction Bay fall within the range of -2.5 to -3.75°C, and temperatures were found to be colder in the backcasted model along the Alaska Highway by about 1°C. There is little spatial difference with respect to temperature between the two communities for the current time period. A characteristic of temperature trends in this area is a distinctive difference in spatial trends with elevation below treeline compared to above treeline. Treeline in this area is around 1400 m a.s.l.; below this elevation, SLRs are relatively gentle (<-6.5°C/km). However, at elevations above treeline, they are normal (-6.5°C/km). This controls the rate at which temperature changes with respect to elevation and as a result, only small changes are noted with elevation below treeline. Both the SLRs and treeline remain constant through all time periods in the modelling which is a necessary limitation of the modeling approach. The coldest temperatures in these areas are seen in the regions above treeline where mountain glaciers are present, adjacent to the communities and west of Kluane Lake.

Results are presented in figures Appendix D1-10, below. Modelled results using the B1 scenario predict the lowest amount of warming by 2080, due to the nature of the scenario. In the vicinity of the communities, MAATs under this scenario fall between -1.25 and -2.5°C, and the greatest changes are predicted to occur in the lowest elevation areas. Significant changes in temperature are forecasted in the areas directly above treeline – this feature is evident in all scenarios applied. Under the A1B scenario, significantly more warming is noted when compared with the B1 scenario. The model also predicts the most overall warming by the 2050 time period. By the end of the 2080 time period, temperatures in the communities are modelled to be between 0 and -1.25°C. Comparable temperatures are predicted as a result of modelling using the A2 scenario; however, under the B1 scenario, more area overall is classified as falling between this temperature range, representing the most overall warming of all scenarios. Under both the A1B and A2 scenarios, significant changes are also predicted above treeline and into the glacial terrain, which have implications for area and volume of the glaciers. In general, the Burwash Landing and Destruction Bay areas will likely be affected by changes in air temperature in distinct ways both above and below treeline, due to the heterogeneous nature of the landscape in the region.

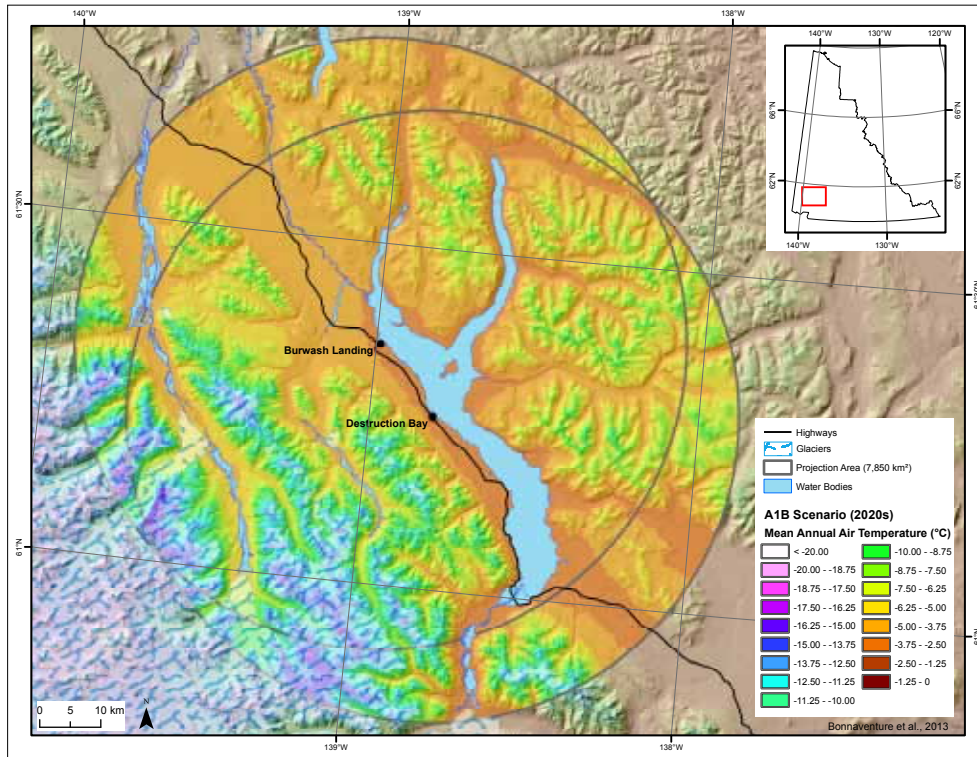
Note that additional climate projections, based on data provided by SNAP (2012), are available by contacting the Northern Climate ExChange (Yukon Research Centre, Yukon College). Projections are available for mean annual and seasonal temperature and precipitation, as well as freeze and thaw dates and growing degree days, for the A1B and B1 scenarios, for the 2020s and 2050s, as well as the 1960-1990 time period.



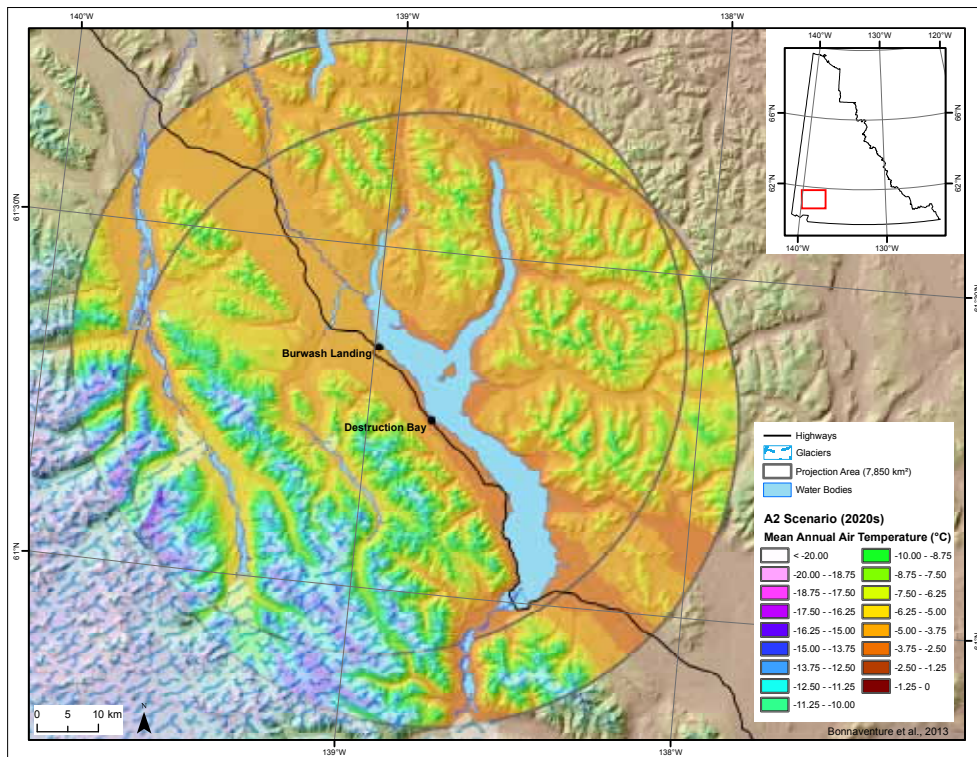
Appendix D1 – Mean annual air temperature for the Burwash Landing area, backcasted for the 1950-1979 period.



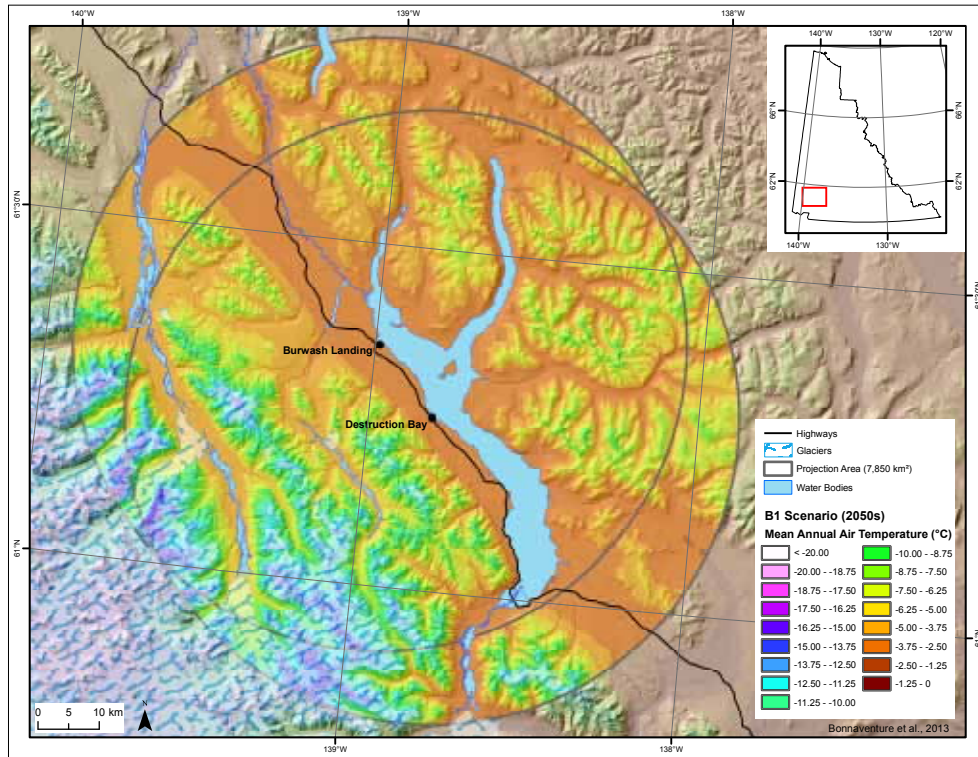
Appendix D2 – Mean annual air temperature for the Burwash Landing area for 2020, projected using the B1 scenario.



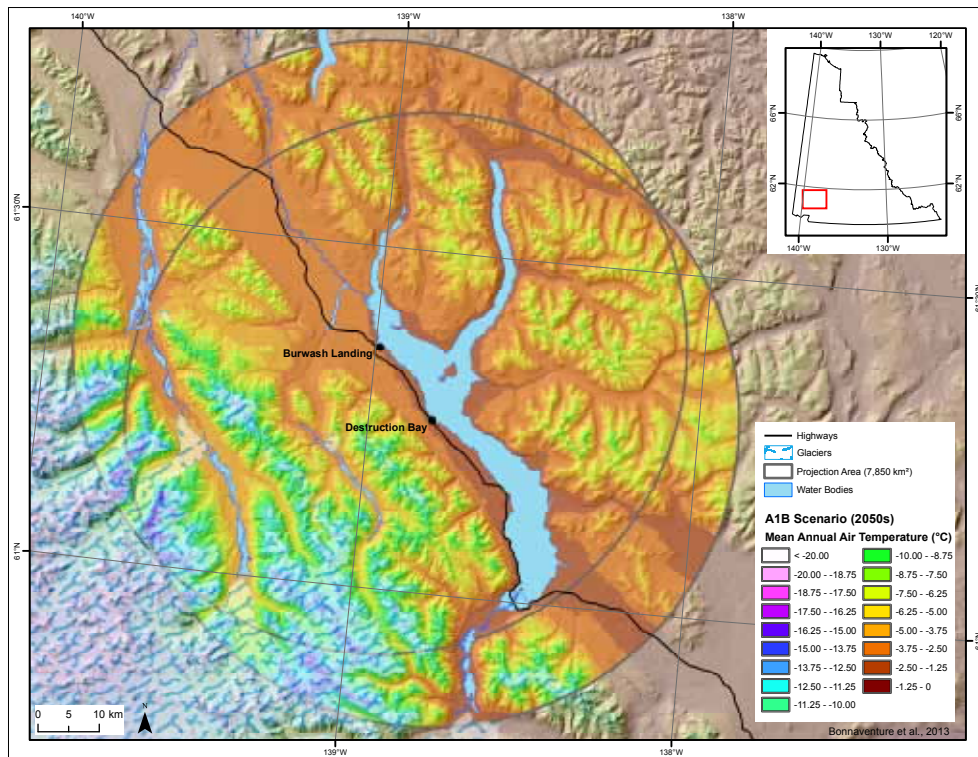
Appendix D3 – Mean annual air temperature for the Burwash Landing area for 2020, projected using the A1B scenario.



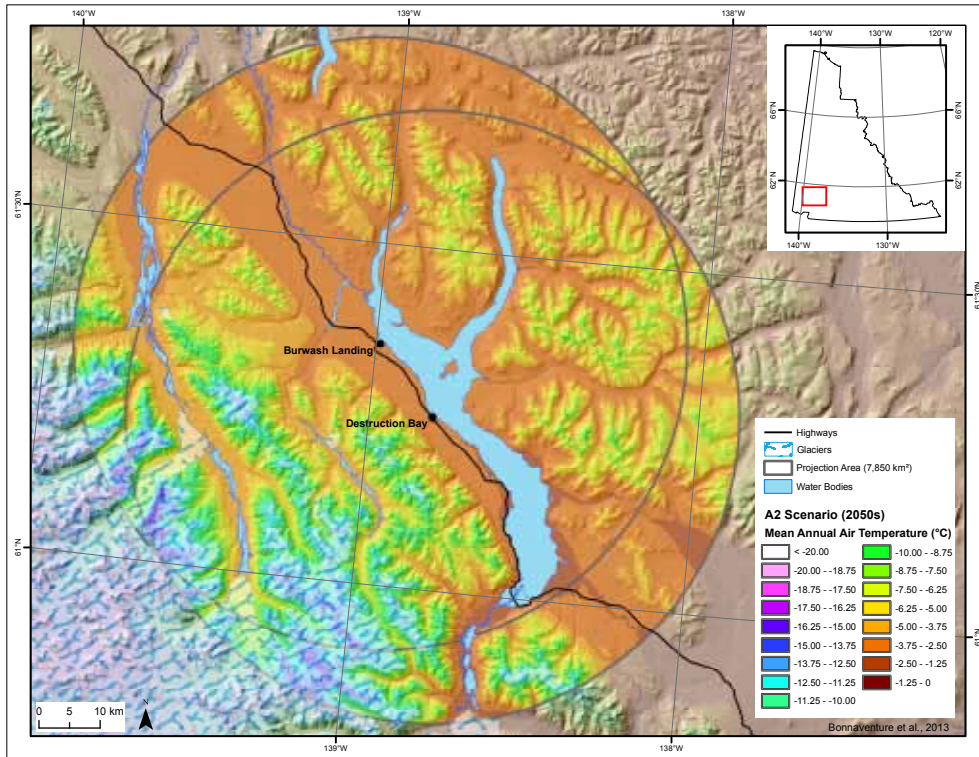
Appendix D4 – Mean annual air temperature for the Burwash Landing area for 2020, projected using the A2 scenario.



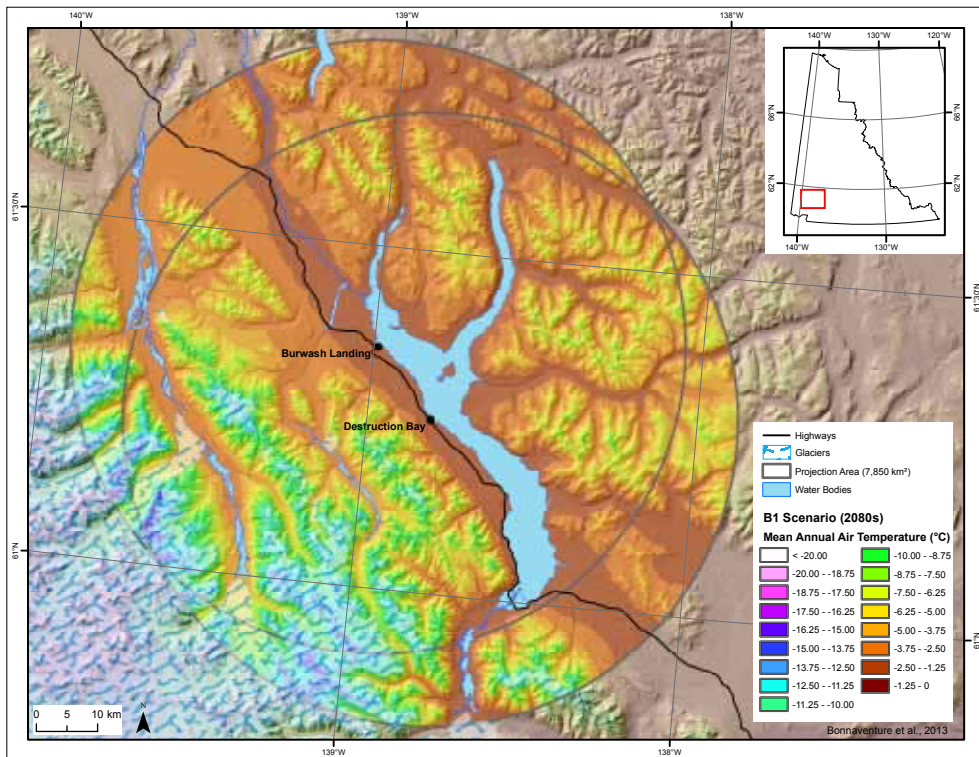
Appendix D5 – Mean annual air temperature for the Burwash Landing area for 2050, projected using the B1 scenario.



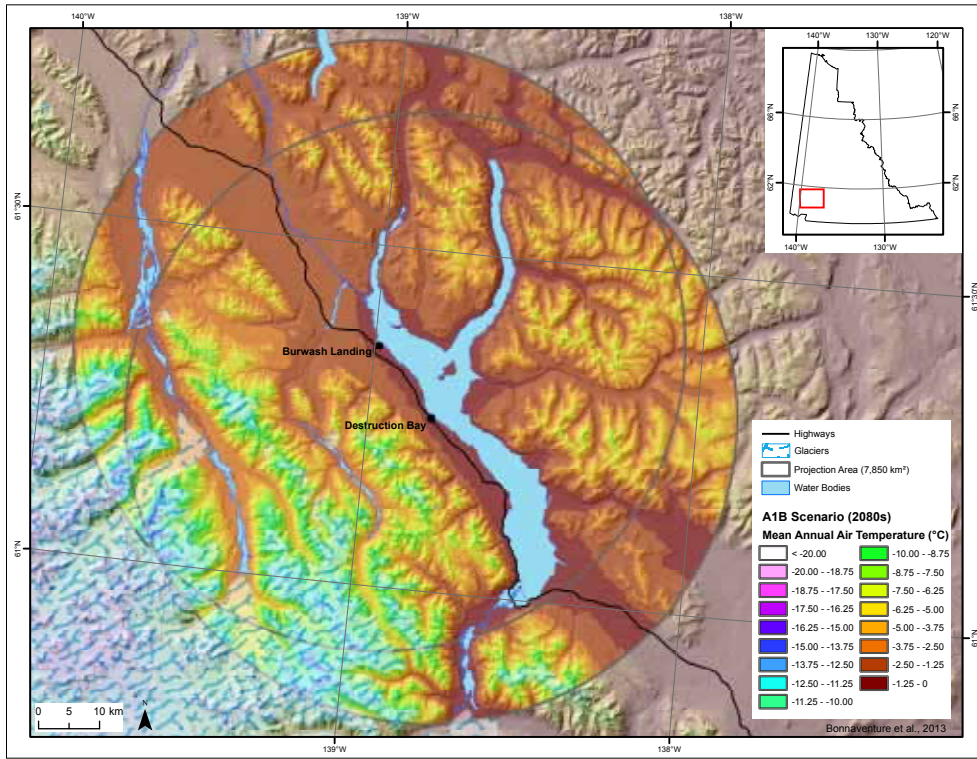
Appendix D6 – Mean annual air temperature for the Burwash Landing area for 2050, projected using the A1B scenario.



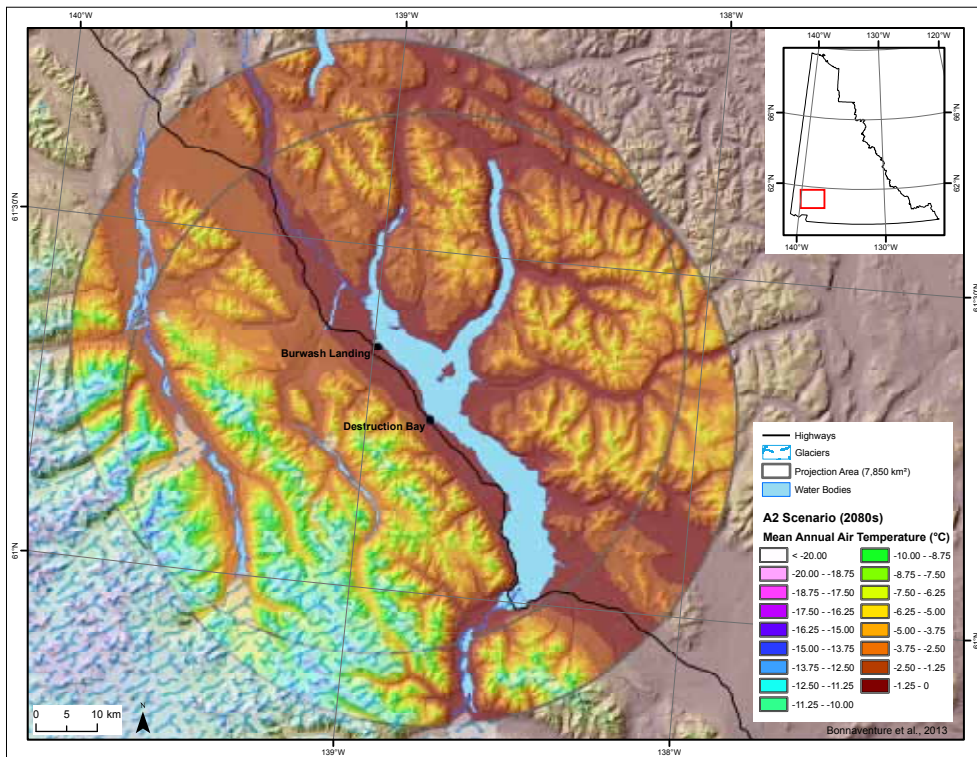
Appendix D7 – Mean annual air temperature for the Burwash Landing area for 2050, projected using the A2 scenario.



Appendix D8 – Mean annual air temperature for the Burwash Landing area for 2080, projected using the B1 scenario.



Appendix D9 – Mean annual air temperature for the Burwash Landing area for 2080, projected using the A1B scenario.



Appendix D10 – Mean annual air temperature for the Burwash Landing area for 2080, projected using the A2 scenario.

BLANK PAGE

APPENDIX E - HAZARDS MAP POLYGON DESCRIPTIONS

Table E1. Hazard classification results for polygons labelled on Figure 61 (see larger print version of this map in back pocket); *denotes those polygons located within the fire disturbances limits (see Figure 55 in body of report).

Polygon number	Surficial geology	Hazard ranking	Hazard description
0	Colluvium (C)	orange	permafrost
1	Glaciofluvial (FG)	orange	permafrost
2	Morainal (M)	orange	permafrost
3	Glaciofluvial (FG)	orange	permafrost
4	Fluvial (F)	orange	permafrost
5	Organic (O)	red	poor drainage; permafrost
6	Fluvial (F)	orange	poor drainage; permafrost
7	Fluvial (F)	orange	permafrost
8	Organic (O)	red	poor drainage; permafrost
9	Fluvial (F)	orange	permafrost
10	Fluvial (F)	orange	poor drainage; permafrost
11	Eolian (E)	orange	flooding; erosion
12	Fluvial Active (FA)	red	flooding
13	Morainal (M)	orange	permafrost
14	Fluvial (F)	red	flooding
15	Fluvial (F)	orange	permafrost
16	Eolian (E)	red	poor drainage; permafrost
17	Morainal (M)	red	poor drainage; permafrost
18	Eolian (E)	orange	permafrost
19	Eolian (E)	red	poor drainage; permafrost
20	Morainal (M)	orange	permafrost
21	Fluvial (F)	orange	permafrost
22	Fluvial (F)	orange	permafrost
23	Glaciofluvial (FG)	orange	permafrost
24	Morainal (M)	orange	permafrost
25	Eolian (E)	orange	permafrost
26	Fluvial (F)	orange	poor drainage; permafrost
27	Fluvial (F)	red	flooding; shallow water table
28	Lacustrine (L)	red	flooding; erosion
29	Colluvium (C)	red	erosion
30	Eolian (E)	red	permafrost
31	Glaciofluvial (FG)	orange	permafrost
32	Eolian (E)	orange	permafrost
33	Fluvial (F)	orange	permafrost
34	Fluvial (F)	orange	poor drainage; permafrost

Table E1, *continued*. Hazard classification results for polygons labelled on Figure 61 (see larger print version of this map in back pocket); *denotes those polygons located within the fire disturbances limits (see Figure 55 in body of report).

Polygon number	Surficial geology	Hazard ranking	Hazard description
35	Eolian (E)	orange	permafrost
36	Fluvial (F)	orange	permafrost
37	Morainal (M)	orange	permafrost
38	Lacustrine (L)	red	flooding; erosion
39	Fluvial (F)	orange	permafrost
40	Fluvial Active (FA)	red	flooding; permafrost
41	Fluvial (F)	red	flooding; permafrost
42	Organic (O)	red	poor drainage; permafrost
43	Fluvial (F)	yellow	flooding; permafrost
44	Morainal (M)	orange	permafrost
45	Eolian (E)	orange	permafrost
46	Eolian (E)	orange	permafrost
47	Lacustrine (L)	red	flooding
48	Fluvial Active (FA)	red	flooding; permafrost
49	Fluvial (F)	red	flooding; permafrost
50	Fluvial (F)	yellow	flooding; permafrost
51	Fluvial (F)	orange	permafrost
52	Eolian (E)	orange	permafrost
53	Morainal (M)	orange	permafrost
54	Colluvium (C)	orange	permafrost
55	Lacustrine (L)	red	flooding
56	Morainal (M)	yellow	permafrost
57	Eolian (E)	orange	permafrost
58	Eolian (E)	orange	permafrost
59	Fluvial (F)	orange	permafrost
60	Morainal (M)	yellow	permafrost
61	Eolian (E)	orange	permafrost
62	Eolian (E)	red	flooding
63	Fluvial Active (FA)	red	flooding; permafrost
64	Fluvial (F)	red	flooding
65	Fluvial Active (FA)	red	flooding
66	Morainal (M)	yellow	permafrost
67	Eolian (E)	red	flooding
68	Fluvial (F)	orange	permafrost
69	Fluvial (F)	yellow	flooding; permafrost
70	Organic (O)	red	poor drainage; permafrost
71	Fluvial Active (FA)	red	flooding
72	Organic (O)	red	poor drainage; permafrost

Table E1, continued. Hazard classification results for polygons labelled on Figure 61 (see larger print version of this map in back pocket); *denotes those polygons located within the fire disturbances limits (see Figure 55 in body of report).

Polygon number	Surficial geology	Hazard ranking	Hazard description
73	Morainal (M)	orange	permafrost
74	Morainal (M)	orange	permafrost
75	Eolian (E)	orange	permafrost
76	Eolian (E)	red	flooding
77	Fluvial Active (FA)	red	flooding
78	Fluvial (F)	orange	permafrost
79	Morainal (M)	yellow	permafrost
80	Eolian (E)	orange	permafrost
81	Organic (O)	red	poor drainage; permafrost
82	Eolian (E)	orange	permafrost
83	Organic (O)	red	poor drainage; permafrost
84	Eolian (E)	orange	permafrost
85	Eolian (E)	orange	permafrost
86	Eolian (E)	red	flooding
87	Eolian (E)	red	shallow water table; permafrost
88	Organic (O)	red	poor drainage; permafrost
89	Eolian (E)	red	poor drainage; permafrost
90	Eolian (E)	orange	permafrost
91	Glaciofluvial (FG)	orange	permafrost
92	Eolian (E)	orange	permafrost
93	Eolian (E)	orange	permafrost
94	Eolian (E)	red	poor drainage; permafrost
95	Eolian (E)	red	flooding
96	Morainal (M)	orange	permafrost
97	Morainal (M)	orange	permafrost
98	Fluvial (F)	red	poor drainage; permafrost
99	Lacustrine (L)	red	permafrost
100	Morainal (M)	orange	permafrost
101	Eolian (E)	red	shallow water table; permafrost
102	Morainal (M)	orange	permafrost
103	Organic (O)	red	poor drainage; flooding; shallow water table
104	Eolian (E)	orange	flooding
105	Organic (O)	red	poor drainage; permafrost
106	Eolian (E)	orange	permafrost
107	Eolian (E)	orange	flooding
108	Morainal (M)	orange	permafrost
109	Eolian (E)	orange	flooding

Table E1, *continued*. Hazard classification results for polygons labelled on Figure 61 (see larger print version of this map in back pocket); *denotes those polygons located within the fire disturbances limits (see Figure 55 in body of report).

Polygon number	Surficial geology	Hazard ranking	Hazard description
110	Eolian (E)	orange	permafrost
111	Eolian (E)	red	flooding; shallow water table; permafrost
112	Eolian (E)	red	shallow water table; permafrost
113	Morainal (M)	yellow	permafrost*
114	Fluvial (F)	yellow	permafrost*
115	Organic (O)	red	poor drainage; permafrost*
116	Morainal (M)	yellow	permafrost*
117	Organic (O)	red	poor drainage; permafrost*
118	Morainal (M)	yellow	permafrost*
119	Fluvial Active (FA)	red	flooding
120	Morainal (M)	yellow	permafrost*
121	Fluvial (F)	yellow	permafrost*
122	Morainal (M)	yellow	permafrost*
123	Organic (O)	red	poor drainage; permafrost*
124	Organic (O)	red	poor drainage; permafrost*
125	Morainal (M)	yellow	permafrost*
126	Fluvial Active (FA)	red	flooding
127	Fluvial (F)	yellow	permafrost*
128	Eolian (E)	yellow	permafrost*
129	Organic (O)	red	poor drainage; permafrost*
130	Morainal (M)	yellow	permafrost*
131	Eolian (E)	yellow	permafrost*
132	Organic (O)	red	poor drainage; permafrost*
133	Eolian (E)	yellow	permafrost*
134	Eolian (E)	yellow	permafrost*
135	Morainal (M)	yellow	permafrost*
136	Morainal (M)	yellow	permafrost*

Table E1, *continued*. Hazard classification results for polygons labelled on Figure 61 (see larger print version of this map in back pocket); *denotes those polygons located within the fire disturbances limits (see *Figure 55 in body of report*).

Polygon number	Surficial geology	Hazard ranking	Hazard description
137	Organic (O)	red	poor drainage; permafrost*
138	Morainal (M)	red	poor drainage; permafrost*
139	Morainal (M)	yellow	permafrost*
140	Morainal (M)	yellow	permafrost*
141	Morainal (M)	yellow	permafrost*
142	Fluvial (F)	red	poor drainage; permafrost*
143	Organic (O)	red	poor drainage; flooding; permafrost*
144	Morainal (M)	yellow	permafrost*
145	Morainal (M)	yellow	permafrost*
146	Morainal (M)	yellow	permafrost*
147	Morainal (M)	yellow	permafrost*
148	Organic (O)	red	poor drainage; flooding; shallow water table; permafrost*
149	Eolian (E)	orange	shallow water table; permafrost*

BLANK PAGE

APPENDIX F - SAFE HOME CONSTRUCTION ON PERMAFROST

SAFE HOME CONSTRUCTION ON PERMAFROST



*Report prepared for the Northern Climate ExChange and the
'Geological Mapping for Climate Change Adaptation Planning'
project*

Prepared by Julie Malenfant-Lepage and Benoît Loranger

*Northern Climate ExChange, Yukon College
(visiting researchers from Université Laval)*

March 2013

TABLE OF CONTENTS

INTRODUCTION	101
CONSTRUCTION ON PERMAFROST	101
Problems Related to House Construction on Permafrost	101
Types of Soils Affected by Thawing	102
INVESTIGATION	103
Frost-Probing.....	103
Drilling.....	103
Resistivity	104
FOUNDATIONS IN PERMAFROST	104
Foundation Design Data Requirements	104
Foundation Types.....	105
<i>Surface Pads</i>	105
<i>Deep Foundations</i>	108
<i>Foundations with Heat Exchangers</i>	109
CONCLUSIONS AND RECOMMENDATIONS	110
REFERENCES	111

INTRODUCTION

Residential construction in permafrost environments requires a good understanding of the nature of permafrost as well as the surficial geology. There are several techniques for building foundations on permafrost that have been proven in various parts of northern Canada and Alaska. This report aims to briefly present the different approaches applied in construction of new residential buildings. In some ways, it can be considered as an introductory guide for design and construction of foundations on permafrost. It is important to note, however, that this report is not prepared as an engineering design text.

This report on safe home construction in permafrost environments will provide an overview of problems related to house construction on permafrost, types of soils affected by thawing, preliminary investigation methodologies, foundation design data requirements, different types of foundations built in northern regions, and finally, recommendations that may be followed throughout the construction process.

CONSTRUCTION ON PERMAFROST

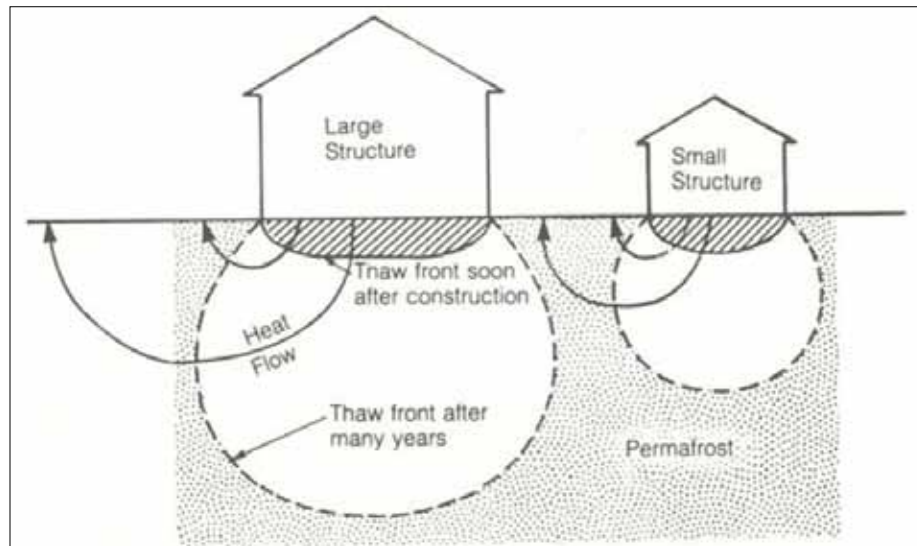
The best advice that could be given to an individual or to a contractor is to avoid building on permafrost terrain. If possible, it is always better to find a new site than to face the extra expense and maintenance involved in construction on permafrost. In many cases in northern Canada, including Yukon, this advice is unfortunately not possible to follow.

In continuous permafrost areas, the permafrost is always the controlling design parameter. In such circumstances, it is important to design and build in a way that will preserve the underlying permafrost. Stability and lifetime of the infrastructure depend directly on the success of this endeavour.

Discontinuous permafrost areas offer the greatest engineering challenge. It is very difficult to be sure that the site is not underlain by permafrost in such areas. Despite the costs associated with an analysis of a construction site by drilling, these analyses will never confidently ensure the presence or absence of permafrost. If the site is located in a thaw-stable area, more conventional and less expensive construction techniques can be used without great risk of destabilizing the ground. However, if the site is located in an area of ice-rich soil which is considered thaw-unstable, standard structural foundations may thaw the underlying permafrost and potentially lead to an eventual collapse of the structure. It is sometimes possible to remove or thaw the permafrost on a site before starting construction, but this is only possible in rare cases. The choice of a good structural foundation design which will preserve permafrost as well as respect the budget is the main challenge in discontinuous permafrost regions (Permafrost Technology Foundation, 2000).

PROBLEMS RELATED TO HOUSE CONSTRUCTION ON PERMAFROST

The most significant impact on permafrost usually occurs immediately beneath the house as heat is conducted downwards into the soil foundation. If a heated building is directly placed on permafrost, it will warm the ground throughout the entire year. Furthermore, site preparation and infrastructure construction impacts, including vegetation clearance, surface grading, and removal or compression of the organic layer, can increase heat intake by the ground surface. These ground disturbances usually result in an increase of the ground temperatures, deepening of the thaw depth, and subsequent thaw-settlements (Figure 1). In most cases, it will take several years for permafrost temperatures to reach a new equilibrium following construction.



Appendix F1. Cross section illustrating the evolution of permafrost degradation under house constructions (Barriault, 2012).

Building foundation failure does not necessarily occur in a short period of time. Sudden collapse is not a frequent phenomenon in the context of permafrost. In most cases, it takes time for the heat generated by a building to diffuse into the underlying permafrost. The length of time depends on several factors such as the thickness of the active layer (i.e., layer of soil that thaws and freezes annually), the soil type, the presence of water in the soil, as well as the amplitude of temperature change at the surface. However, once the process of warming is initiated, thawing of soil is often irreversible.

In permafrost environments, if buildings are left unattended, soil degradation will end up affecting the structure and will lead to the formation of cracks. Eventually, the building will no longer be functional and safe. Damage associated with permafrost degradation should be monitored and repaired as soon as possible to ensure viability of the structure. It is much cheaper and easier to ensure the viability of the structure if actions aimed at detection and repair of damages are initiated very early in the failure process. When thawing permafrost damage is left to run its course, the end result is total failure of the structure (Permafrost Technology Foundation, 2000)

It is also important to note that permafrost temperatures between -2°C and 0°C may not appear to be warming rapidly. A significant amount of transferred heat is mainly used to melt ground ice instead of warming the soil. Consequently, the strength of permafrost under the structure will be reduced significantly as the ground ice melts.

TYPES OF SOILS AFFECTED BY THAWING

In permafrost regions, coarse, granular soil and rocks without ice inclusions are typically the best material on which to construct a foundation. Upon thawing, these materials are stable and have good bearing capacity. (Bearing capacity refers to the load a soil can safely withstand, without significant compaction or displacement.) Foundation design in such soils should follow the current practice of moderate temperature regions.

Conversely, fine-grained soils, which are often ice-rich, have a low permeability and tend to be oversaturated after thawing. Pore-pressure generated during thawing may result in a significant

loss of shear strength. For fine-grained soils, foundation design in permafrost poses several challenges when attempting to control differential settlement of the soil that leads to the deformation of structures. The bearing capacity of fine-grained soils is largely a function of the amount and temperature of ground ice. As the amount of ground ice commonly varies across a construction site, bearing capacity may differ within a foundation, causing different portions of the structure to experience settlement at different rates. Furthermore, since ice-rich soils consolidate and discharge excess water as they thaw, variably distributed ground ice can result in the settlement of select portions of the ground, causing distortion in the structure above. These soils therefore do not offer good support for construction of buildings (Canadian Standard Association (CSA), 2010).

INVESTIGATION

The first step in construction on permafrost is a good preliminary site investigation carried out by qualified professionals such as geotechnical engineers, geophysicists or earth science specialists. The cost of the survey may initially seem disconcerting, but is more reasonable than costs associated with the selection and construction of an improper foundation type (Permafrost Technology Foundation, 2000). The objectives of the site investigation are to identify terrain units, determine relevant soil properties and identify areas of thaw-sensitive or unstable soils

FROST-PROBING

When the top of the permafrost is shallow and the active layer is relatively soft, frost-probing is an effective method for locating permafrost (Figure 2). This technique requires only a steel rod with a handle, which is pushed into the ground by hand. With this method, shallow permafrost can easily be detected, and its depth measured. Frost-probing is inexpensive, fast and very useful for preliminary site investigations.



Appendix F2. Frost-probing in Burwash area.

DRILLING

A very effective way to determine ground-ice conditions on a site level is to rely on drilling boreholes to collect samples of permafrost for geotechnical analysis. This provides specific information about soil characteristics and conditions at the subsurface at a specific location. A good borehole log will give useful information at varying depths, including the thickness of the

active layer, the soil or rock types, the ice content, the depth and characteristic of permafrost, the presence of massive ice bodies, and in some cases, the depth to bedrock.

The information derived from multiple boreholes in a given area can be extrapolated to obtain a spatial representation of ground conditions. It is very important to drill deep enough to obtain the appropriate information for each project. Generally speaking, the larger the building, the deeper the drilling must be. Permafrost drilling requires trained personnel with proper equipment; otherwise, results may be meaningless or even misleading.

RESISTIVITY

If a large area is being surveyed, a complimentary approach such as electrical resistivity surveys should be considered. A resistivity survey can be used to help extrapolate between boreholes. It is particularly useful for determining the thickness and extent of permafrost bodies and zones of unfrozen ground within permafrost. A resistivity survey is relatively fast and inexpensive and can save a lot of time and money by minimizing the number of boreholes needed for larger sites. Results obtained by drilling coupled with a resistivity survey allow a more substantial analysis of the subsurface conditions for the entire site.

FOUNDATIONS IN PERMAFROST

FOUNDATION DESIGN DATA REQUIREMENTS

The following list indicates principal factors and information requirements related to foundation design (Andersland and Ladanyi, 2004). This list is for large-scale projects and only needs to be fully applied in those cases. However, some elements are essential in the selection of the right type of foundation. It is good practice to gather as much information as possible about a site prior to beginning construction work.

1. Site data:
 - a. location
 - b. climate
 - c. physiography and geology
 - d. subsurface materials and their characteristics
 - e. thermal regime
 - f. hydrology and drainage
 - g. materials and construction
 - h. transportation facilities and access
 - i. construction cost factors
 - j. Availability of :
 - i. labor, skills, and knowledge
 - ii. construction equipment
 - iii. support facilities and equipment
2. Design policies, general criteria, and cost limitations

3. Technology (state of the art)
4. Facility technical data
 - a. size and design life (e.g., permanent versus temporary)
 - b. foundation loading
 - c. thermal conditions
 - d. movement and distortion

FOUNDATION TYPES

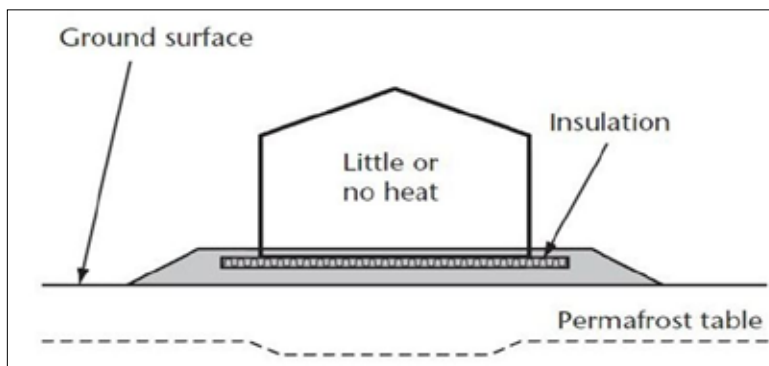
Good foundation construction in northern regions is essential to the ultimate longevity of a structure. Even the best house design could not survive a poorly constructed foundation. Proper foundation design will be the difference between a safe, stable structure with relatively low maintenance costs, and one with constant stability problems leading to a shorter lifespan. The selection of an appropriate foundation type generally depends on a soil's behaviour upon thawing. Foundations built on permafrost can be divided in three categories: (1) surface pads, (2) deep foundations, and (3) foundations with heat exchangers.

SURFACE PADS

The construction of a surface pad to preserve the temperature of the underlying permafrost is common in northern Canada. One of the primary advantages of using surface footings on a granular pad with a cold crawl space below is the ability to compensate for any differential settlement through jacking or shimming (CSA, 2010). According to Allard et al. (2010), houses built on properly designed, compacted granular foundations should not undergo significant thaw-settlements because the adjustment of the thermal profile to the new geometry leads to a rise of the permafrost into the active layer or even in the embankment itself. The active layer then becomes limited to the non-frost sensitive foundation, which ensures stability over cycles of freezing and thawing.

Unheated foundations

Unheated structures may be built directly on a pad (Figure 3), but only if they are well-ventilated, have insulation inserted between the structure and the pad, and remain unheated throughout their service life (CSA, 2010). Insulation will slow the rate at which heat enters the ground, but it does not eliminate heat exchange. Theoretically, it is possible to add enough layers of insulation to establish a new thermal balance between heat input from the area around the building and winter cooling, but this procedure is almost never performed because of the high costs associated with this approach.

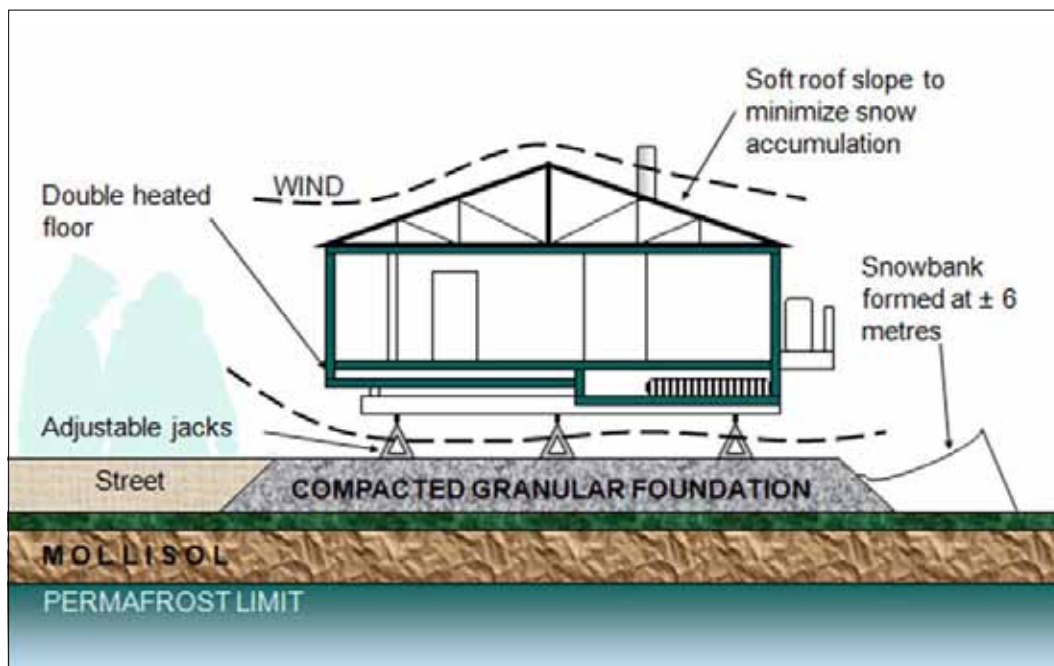


Appendix F3. Basic pad foundation design (CSA, 2010).

Several types of insulation can be considered in the construction of an unheated foundation. An insulative layer that is intended to be in contact with the soil must be able to withstand deterioration of its thermal properties and physical shape in the presence of soil moisture, soil chemicals, physical loading and other outside forces (Permafrost Technology Foundation, 2000).

Screw jack foundations

In the 1980s, the Société d’habitation du Québec developed a concept for house foundations to preserve permafrost. It involved buildings that are constructed on adjustable metal jacks over a compacted granular foundation (Figure 4). The granular foundation is laid directly on the ground surface without the removal of the vegetation cover. To date, this construction technique has been proven very effective for preserving permafrost (Gravel, 2012). The foundation must raise the building high enough to promote uninhibited air circulation beneath the building. It allows the wind to flow freely under the building, mainly to avoid snow accumulation that could increase the soil temperature (by insulation) under the foundation. Under these conditions, a snow bank will form approximately six metres away from the dwelling’s foundation. It is important that nothing be stored in the space between the floor and the soil so as to not interfere with the free air circulation during the winter months. Sufficient insulation should be placed under the floor of the structure so the energy loss from the bottom of the building is minimized and the floor inside the building is comfortable for residents.



Appendix F4. Foundation design that preserves permafrost, a concept developed by the Société d’Habitation du Québec in the 1980s (Gravel, 2012).

Once or twice a year, maintenance of a building on jacks needs to be performed in order to preserve the building’s stability. During the maintenance process, a screw in the middle of the jacks is used to raise or lower the height of the building (Figure 5). For a small single family house, it is common to use about 9 adjustable jacks which can withstand nearly 35 000 kg each (Gravel, 2012). It is important to ensure that the slope of the terrain around the building allow for the adequate drainage of surface water under the structure.

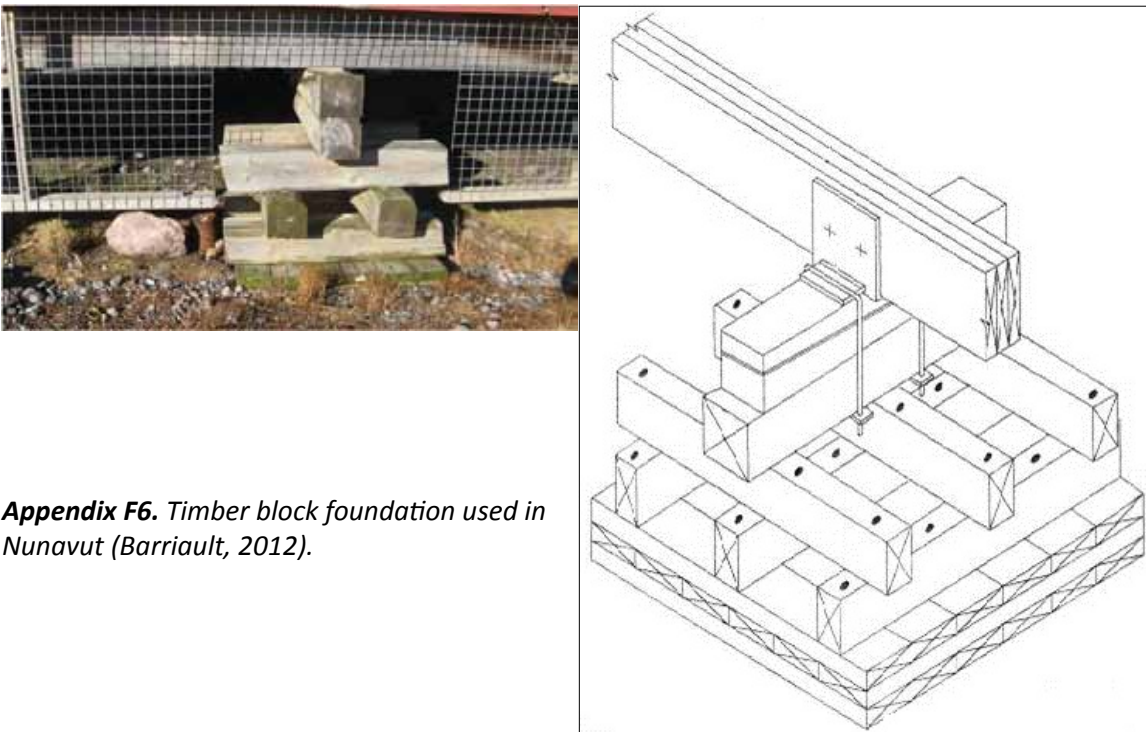


Appendix F5. Adjustable jack foundations (CSA, 2010; Gravel, 2012).

Timber block foundations

Timber block foundations (Figure 6) work on the same principle as the screw jack technique. However, screw jacks are not always easily obtainable and it can be more convenient to use timber block. Timber blocks need to be laterally stabilized with screws.

Maintenance operations are almost the same as for screw jack foundations, described above; however, the operator must use a hydraulic jack to lift the load of the building before shimming the timber blocks. Maintenance for this style of foundation is therefore more labour-intensive than for screw jack foundations.



Appendix F6. Timber block foundation used in Nunavut (Barriault, 2012).

Space frame foundations

Another surface foundation that has been proven successful in permafrost regions is the rigid three-dimensional truss-type foundation (Figure 7). This is a commercially available, pre-manufactured foundation that consists of metal tube members flattened on each end and connected by metal node pieces at the top and bottom to form approximately one-metre square cells. It is custom made to the building size for which it is to be used. It is assembled directly on site on a compacted granular foundation.

A screw at each structural node is used to level the building in the event of permafrost thaw underneath the building.



Appendix F7. Examples of space frame foundations in Nunavut (Barriault, 2012).

DEEP FOUNDATIONS

The majority of public housing, homeowner housing and commercial buildings in Nunavut is built on steel piles. Piles are long steel pipes driven into the ground to stabilize buildings into the permafrost or bedrock (Figure 8). This type of foundation requires less gravel, which can be a very expensive resource to produce and transport to northern communities. The use of steel piles can also allow for the construction of buildings on more difficult terrain compared with the types of terrain that are capable of accommodating granular foundations. The steel piles are more resilient to climate change than other foundation types when they are placed directly on bedrock.



Appendix F8. Housing built on steel piles (Gravel, 2012).

There are two fundamental pile types currently in use in the Canadian north: 1) adfreeze piles and 2) rock-socketed piles. Their design and applications are fundamentally different. Adfreeze piles are commonly installed where permafrost soils extend to substantial depths without encountering bedrock. These piles rely on the bond with the surrounding ground for their load-bearing capacity. The ground can be ice-rich, but should be below -3°C , and colder still if the soil is saline (CSA, 2010). Rock-socketed piles are used where bedrock occurs within a practical depth below the surface. These piles are designed to transfer the full load of a structure to the underlying bedrock. In Nunavut, rock-socketed piles are commonly used. Adfreeze piles have been either discontinued or are being driven deeper due to a thickening of the active layer (Barriault, 2012).

In response to ground warming, if the active layer above the permafrost deepens, foundation systems that rely on piles may experience accentuated frost heaving (Figure 9). This frost heaving occurs when a small part of each pile's surface is frozen to the surrounding soil year-round, while a larger part of the pile's surface is exposed to the lifting force exerted through soil expansion when the water in the active layer re-freezes in the autumn and winter (CSA, 2010). If piles are used in a frost sensitive soil and cannot be placed directly on bedrock, the piles must be equipped with anti-lift shafts to prevent the exertion of a vertical force by seasonal frost, which can distort the housing's structure. Various methods can prevent frost heaving when using pile jacking and a competent engineer should be consulted if this method is being considered.



Appendix F9. Examples of pile jacking and frost heaving in building structures, Nunavut (Barriault, 2012).

FOUNDATIONS WITH HEAT EXCHANGERS

Foundations enhanced with heat exchangers are now widespread in Canada's north. They are generally used where heated crawl spaces and warm first floors at finished grade are required. For such structures, systems are built to intercept heat that would otherwise flow into the ground and affect the underlying permafrost. Thermosyphons are the most widely-used heat exchangers (Figure 10). When designs using thermosyphons are being considered, detailed geothermal analyses are required. The inclusion of climate warming in the design process

requires careful consideration of the conditions of the site chosen for the design, particularly in winter when low temperatures drive heat removal (CSA, 2010).



Appendix F10. *Thermosyphons are an example of a foundation system that requires significant expertise to design, install, maintain, and monitor (Barriault, 2012).*

CONCLUSIONS AND RECOMMENDATIONS

Construction in permafrost environments is a process that requires many steps, including preliminary site investigation, drilling, data analysis, appropriate choice of foundation design, construction and maintenance. Several recommendations related to building on permafrost can be made, summarizing the contents of this report:

- Foundations need to be adapted to local permafrost and geomorphic conditions.
- The organic layer should not be removed before construction.
- The best available geotechnical norms and techniques should be applied for all construction.
- Even if all types of foundations can be constructed on bedrock, a geotechnical investigation should be completed before construction. Frost heaving in rock varies according to the characteristics of the substrate, including the presence or absence of fractures, the lithology, and structure.
- Compacted granular foundations should be built at least two years in advance of construction to allow the rise of permafrost and the stabilization of the soil (Allard et al., 2010).
- Permafrost thermal regime should be considered in the construction design while at the same time incorporating the anticipated climate warming effects in northern Canada.

It may also be appropriate, in some areas, to develop a municipal program with appropriate regulations to ensure yearly maintenance of houses and infrastructure (Allard et al., 2010).

It must be reiterated that this guide does not replace the necessary engineering design needed for building on permafrost. It is important to consult permafrost experts in order to get appropriate advice at the preliminary investigation stages, as well as through the construction and maintenance phases. Additionally, for detailed guidance with respect to roads and permafrost, the Transportation Association of Canada (TAC, 2010) guidelines for development and management of transportation infrastructure in permafrost regions should be consulted.

REFERENCES

- Allard, M., L'Hérault, E., Gybérien, T. and Barrette, C., 2010. Impact des changements climatiques sur la problématique de la fonte du pergélisol au village de Salluit (Nunavik), Rapport final, Center for Northern Studies, Université Laval, Quebec City, 69 p.
- Andersland, O.B. and Ladanyi, B., 2004. Frozen Ground Engineering, 2nd Edition. Wiley, Hoboken, NJ, 384 p.
- Barriault, A., 2012. Climatic Adaptations to Construction in Nunavut (Nunavut Housing Corporation), Northern Forum, Quebec City.
- CSA (Canadian Standards Association), 2010. Technical guide: Infrastructure in permafrost: A guideline for climate change adaptation, 1st edition, CSA Publication, 112 p.
- Gravel, J.-F., 2012. Impact of climate change on habitat development in Nunavik (Société d'habitation du Québec), Northern Forum, Quebec City.
- Permafrost Technology Foundation, 2000. Design Manual for New Foundations on Permafrost. PFE publications, 94 p.
- TAC (Transportation Association of Canada), 2010. Guidelines for Development and Management of Transportation Infrastructure in Permafrost Regions. R. McGregor, D. Hayley, D. Wilkins, E. Hoeve, E. Grozic, V. Roujanski, A. Jansen and G. Doré, (eds.), Transportation Association of Canada, 177 p.